

**Observational evidence of the large-scale environmental influence on dwarf galaxy
evolution**

A Thesis

Submitted to the Faculty

of

Drexel University

by

Kelly A. Douglass

in partial fulfillment of the

requirements for the degree

of

Doctor of Philosophy

July 2017



© Copyright 2017
Kelly A. Douglass. All Rights Reserved.

Dedications

Dedications

Acknowledgments

I would like to thank our collaborator Renyue Cen for his help in the interpretation of these results. I would also like to acknowledge Crystal Moorman for her help and support throughout this work. Finally, I would like to thank the referees (including Burcu Beygu) for their detailed comments and critique of my work.

Table of Contents

LIST OF TABLES	viii
LIST OF FIGURES	ix
ABSTRACT	xi
1. INTRODUCTION	1
2. METALLICITY OF DWARF GALAXIES	9
2.1 Introduction	9
2.2 Theory	13
2.2.1 Overview of Methods	13
2.2.2 [O III]	14
2.2.3 [O II]	15
2.2.4 [S II]	16
2.2.5 Direct T_e method	16
2.3 Data	17
2.3.1 Spectroscopic selection	18
2.3.2 Void classification	19
2.4 Results	19
2.4.1 Estimation of uncertainties and confirmation of our method	20
2.4.2 Results	20
2.4.3 Sources of systematic error	24
2.4.4 Comparison to previously published metallicity measurements	24
2.4.5 Mass-metallicity relation	25
2.4.6 SFR-metallicity relation	27
2.4.7 Color-metallicity relation	28
2.5 Discussion	31

2.5.1	Comparison to literature results	31
2.5.2	Large-scale environmental influence	31
2.5.3	Extreme low-metallicity galaxies	33
2.6	Conclusions	35
3.	N/O RATIO IN DWARF GALAXIES	36
3.1	Introduction	36
3.2	Theory	40
3.2.1	[N II]	40
3.2.2	Direct T_e method	40
3.3	Data	43
3.3.1	Spectroscopic selection	43
3.3.2	Void classification	44
3.4	Results	44
3.4.1	Estimation of uncertainties and comparison of N/O and N^+/O^+	45
3.4.2	Sources of systematic error	45
3.4.3	Galaxy abundances	46
3.4.4	N/O versus O/H	55
3.4.5	Mass–N/O relation	58
3.4.6	Color–N/O relation	59
3.4.7	(s)SFR–N/O relation	60
3.5	Discussion	61
3.5.1	Higher metallicities in void dwarf galaxies	62
3.5.2	Lower N/O ratios in void dwarf galaxies	63
3.5.3	N/O ratio for extremely low metallicity galaxies	64
3.6	Conclusions	64
4.	LARGE-SCALE ENVIRONMENTAL DEPENDENCE OF CHEMICAL ABUNDANCES IN DWARF GALAXIES AND IMPLICATIONS FOR CONNECTING STAR FORMATION AND HALO MASS	68
5.	SMALL-SCALE ENVIRONMENT	69

5.1	Introduction	69
5.2	Theory	70
5.2.1	Peculiar velocity	71
5.2.2	Sky separation in $h^{-1}\text{Mpc}$	71
5.2.3	Fractional virial radii	72
5.2.4	Absolute distance to nearest neighbor	72
5.3	Data	73
5.3.1	Various samples	73
5.3.2	Group catalog	74
5.4	Results	74
5.4.1	Parameter – distance relations	74
5.4.2	Linear fit parameters	81
5.4.3	Selection effects	81
5.4.4	Including redshift in the distance	89
5.5	Discussion	89
5.5.1	Comparison to literature results	90
5.6	Conclusions	91
6.	GREEN VALLEY GALAXIES	93
6.1	Introduction	93
6.2	Theory	94
6.3	Data	95
6.3.1	Optical data — SDSS	95
6.3.2	UV data — GALEX	96
6.4	Results	96
6.4.1	Properties of the Green Valley Galaxies	98
6.5	Discussion	102
6.5.1	Gas content indicators	103

6.5.2 Evidence of AGN feedback	103
6.6 Conclusions	105
7. CONCLUSION	106
7.1 Chemical abundances	106
7.2 Small-scale environment	108
7.3 GV galaxies	109
7.4 Future work	110
BIBLIOGRAPHY	112
APPENDIX A: DIRECT METHOD PHYSICS	117
A.1 Forbidden transitions	118
A.1.1 Time-dependent perturbation theory	118
A.2 Estimating the temperature	119
A.3 [S II]	121
APPENDIX B: SIMULATIONS	122
B.1 Dwarf galaxy formation and evolution	122
B.2 Environmental differences	123
VITA	125

List of Tables

2.1	Dwarf galaxy properties	22
2.2	Metallicity distribution of 135 dwarf galaxy sample	23
2.3	Extreme low-metallicity dwarf galaxies	34
3.1	Analyzed dwarf galaxies	48
3.2	Abundance statistics	56
3.3	Extremely low-metallicity dwarf galaxies	65
5.1	Fit parameters of properties versus distances	83

List of Figures

1.1	SDSS galaxy map	2
1.2	Dark matter simulation	3
1.3	Sky map highlighting voids and void galaxies	4
1.4	Absolute magnitude distribution of galaxies in SDSS DR7	5
1.5	Kirchoff's laws of spectroscopy	6
1.6	Sample (void) dwarf galaxy spectrum	7
2.1	[O III] and [S II] energy-level diagram	14
2.2	O ⁺ /O ⁺⁺ versus metallicity	17
2.3	Metallicity comparison to Yin et al. (2007)	21
2.4	Metallicity distribution of 135 dwarf galaxy sample	21
2.5	Metallicity distribution with no restriction on [O III] $\lambda 4363$	23
2.6	Metallicity comparison to Tremonti et al. (2004)	26
2.7	Stellar mass versus metallicity for 135 dwarf galaxy sample	27
2.8	(s)SFR versus metallicity for 135 dwarf galaxy sample	28
2.9	Distribution of (s)SFR for 135 dwarf galaxy sample compared to SDSS	29
2.10	Color versus metallicity for 135 dwarf galaxy sample	30
2.11	Color distribution of 135 dwarf galaxy sample compared to SDSS	30
3.1	[O III] and [N II] energy-level diagram	41
3.2	N/O versus N ⁺ /O ⁺	46
3.3	Nitrogen distribution of 135 dwarf galaxy sample	49
3.4	Metallicity distribution of star-forming galaxies with $-17 > M_r > -20$	50
3.5	Nitrogen distribution of star-forming galaxies with $-17 > M_r > -20$	51
3.6	N/O distribution of 135 dwarf galaxy sample	53
3.7	N/O distribution of star-forming galaxies with $-17 > M_r > -20$	54

3.8	N/O versus metallicity of 135 dwarf galaxy sample	57
3.9	N/H versus metallicity for 135 dwarf galaxy sample	58
3.10	Stellar mass versus N/O for 135 dwarf galaxy sample	59
3.11	Color versus N/O for 135 dwarf galaxy sample	60
3.12	Color versus sSFR for 135 dwarf galaxy sample	61
3.13	(s)SFR versus N/O for 135 dwarf galaxy sample	62
5.1	$u - r$ versus distance to nearest neighbor and group	76
5.2	sSFR versus distance to nearest neighbor and group	77
5.3	Metallicity versus distance to nearest neighbor and group	79
5.4	N/H versus distance to nearest neighbor and group	80
5.5	N/O versus distance to nearest neighbor and group	82
5.6	Sensitivity to peculiar velocity maximum	84
5.7	Color versus distance of full SDSS dwarf population	86
5.8	Distribution of absolute magnitudes of nearest neighbors	87
5.9	Color versus distance calculated with redshift	88
6.1	Optical color-magnitude diagram and histogram of $u - r$ in SDSS	94
6.2	NUV- r color-magnitude diagram of SDSS galaxies	97
6.3	Distribution of NUV- r of SDSS galaxies	97
6.4	Stellar mass distribution by morphological type	98
6.5	(s)SFR distribution by morphological type	99
6.6	Distribution of gas-phase chemical abundances in cross-matched SDSS DR7 – GALEX galaxies	100
6.7	Fraction of galaxies in CMD populations by morphological type	101
6.8	Gas-phase chemical abundance distributions for star-forming, composite, and AGN galaxies	104
A.1	[O III] ratio as a function of temperature	120
A.2	[S II] ratio as a function of density	121

Abstract

Observational evidence of the large-scale environmental influence on dwarf galaxy evolution

Kelly A. Douglass

Michael S. Vogeley, PhD

We investigate how the cosmic environment affects galaxy evolution in the Universe by studying gas-phase chemical abundances and other galaxy properties as a function of the large-scale environment and local density of galaxies. Using spectroscopic observations from the Sloan Digital Sky Survey Data Release 7, we estimate the oxygen and nitrogen abundances of 993 star-forming void dwarf galaxies and 759 star-forming dwarf galaxies in denser regions. We use the Direct T_e method for calculating the gas-phase chemical abundances in the dwarf galaxies because it is best suited for low metallicity, low mass galaxies. A substitute for the [O II] $\lambda 3727$ doublet is developed, permitting oxygen abundance estimates of SDSS dwarf galaxies at all redshifts with the Direct T_e method. We find that star-forming void dwarf galaxies have slightly higher oxygen abundances than star-forming dwarf galaxies in denser environments, but we find that void dwarf galaxies have slightly lower nitrogen abundances and lower N/O ratios than galaxies in denser regions. At smaller scales, we find that only the presence of a neighboring galaxy within $0.05 h^{-1}\text{Mpc}$ or $0.05r_{vir}$, or the presence of a group within $0.1 h^{-1}\text{Mpc}$, influences a dwarf galaxy's evolution. Dwarf galaxies within $0.05 h^{-1}\text{Mpc}$ or $0.05r_{vir}$ of another galaxy tend to be bluer, have higher sSFRs, and have higher oxygen and nitrogen abundances than average. In contrast, galaxies within $0.1 h^{-1}\text{Mpc}$ of the center of the closest group are redder, have lower oxygen abundances, and have higher N/O ratios than average. We also investigate how a galaxy transitions through the color-magnitude diagram, evolving from a blue, star-forming spiral or irregular galaxy in the blue sequence to a red elliptical galaxy in the red cloud through the green valley. We discover that combining a galaxy's color, color gradient, and inverse concentration index defines a galaxy's location on the color-magnitude diagram. The results indicate that there is a higher fraction of dwarf galaxies in denser regions than void dwarf galaxies in the green valley. From these analyses, we surmise that void dwarf galaxies experience delayed

star formation as predicted by the Λ CDM cosmology. We also conjecture that there is a dependence of the large-scale environment on cosmic downsizing. We present evidence that void dwarf galaxies may have a higher ratio of dark matter halo mass to stellar mass when compared to dwarf galaxies in denser environments.

Chapter 1: Introduction

Large galaxy surveys such as the Sloan Digital Sky Survey (SDSS; York et al., 2000) have revealed a non-uniform distribution of galaxies throughout the universe. Taking on a shape similar to that of a sponge-like topology (Gott et al., 1989) or a three-dimensional cosmic web (Bond et al., 1996), galaxies clump together in clusters and along filaments, leaving void regions between these large-scale structures. Evidence of this distribution can be seen in Fig. 1.1 for galaxies in the SDSS Data Release 7 (SDSS DR7; Abazajian et al., 2009). Based on these observations, dark matter simulations have been constructed which successfully reproduce the same large-scale structure. If we start with a mostly uniform distribution of dark matter at the Big Bang with quantum mechanical perturbations, Fig. 1.2 outlines the evolution of that dark matter up through the present. These snapshots from the Millenium Simulation project (Springel et al., 2005) show that small perturbations in the initial distribution of dark matter are amplified as the universe expands. Gravity causes the slightly overdense regions to collapse while simultaneously causing the underdense regions to expand. Due to dark matter's gravitational attraction, we believe that the baryonic mattter (matter which interacts electromagnetically) will trace the dark matter distribution, resulting in the galaxy distribution we observe today.

Existing in the cosmological voids, void galaxies are thought to demonstrate the fundamental characteristics of galactic evolution. Cosmic voids are an important environment for studying galaxy formation (see van de Weygaert & Platen, 2011, for a review). Gravitational clustering proceeds as if in a very low density universe, where the amassment of gravitationally bound dark matter halos ends relatively early and there is little subsequent interaction between the galaxies due to the lower density and the faster local Hubble expansion. Therefore, Λ CDM cosmology predicts that galaxies formed in voids should have lower mass and be retarded in their star formation when compared to those in denser regions (e.g., Gottlöber et al., 2003; Goldberg et al., 2005; Cen, 2011). Goldberg & Vogeley (2004) show that a void region that is only 10% of the mean density of the

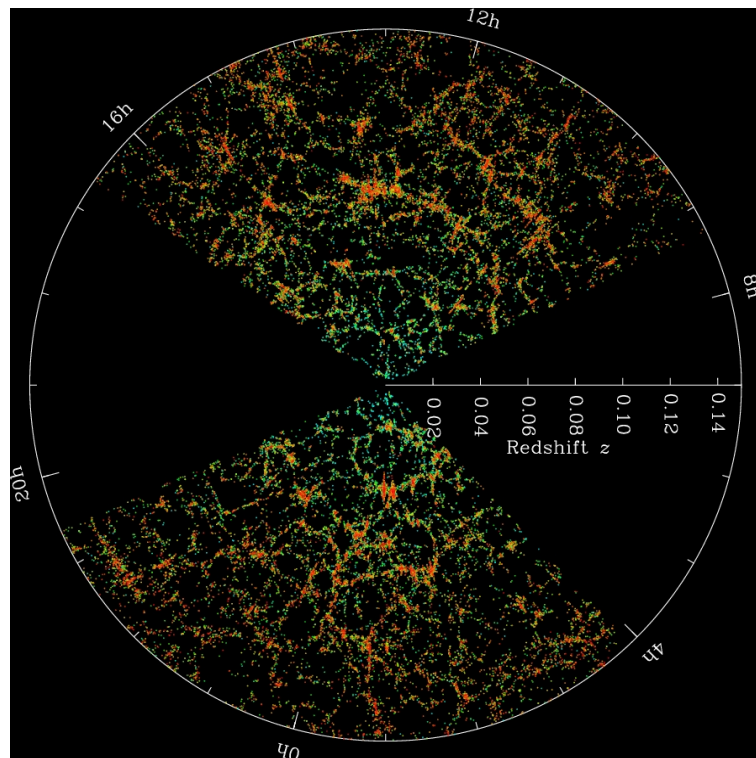


Figure 1.1: A slice through the SDSS galaxy distribution^a; each point on this plot is a galaxy. Large sky surveys such as SDSS have revealed a non-uniform distribution of galaxies throughout the universe. Dubbed the cosmic web, galaxies clump together in clusters and along filaments, leaving giant gaps between them (similar to a sponge).

^a<http://www.sdss.org/science/orangepie/>

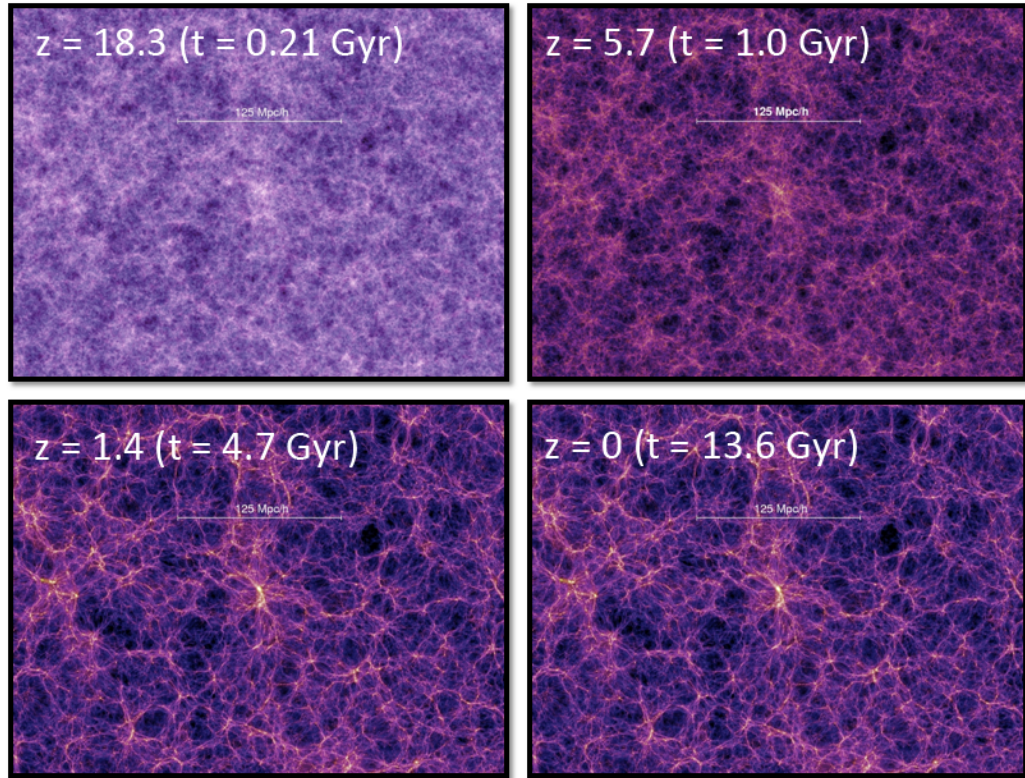


Figure 1.2: Snapshots of a portion of the Millenium Simulation^a showing the dark matter distribution at different points in time from 0.21 Gyr after the Big Bang to the present. Small perturbations in the initial distribution of dark matter are amplified as the universe expands. Gravity causes the slightly overdense regions to contract while simultaneously causing the underdense regions to expand.

^a<https://wwwmpa.mpa-garching.mpg.de/galform/virgo/millennium/>

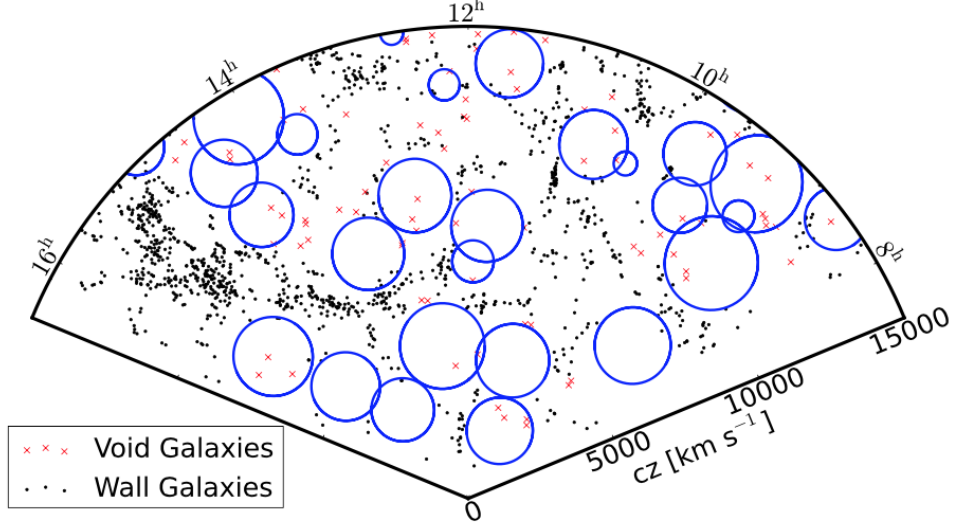


Figure 1.3: A $10 h^{-1}\text{Mpc}$ slice of SDSS DR7 (Moorman et al., 2014, Fig. 1) with void regions highlighted in blue circles. Void galaxies are shown as red points while wall galaxies are black. Existing in the cosmological voids (space between the galactic filaments), void galaxies are thought to demonstrate the fundamental characteristics of galactic evolution.

universe with $\Omega_{matter} = 0.3$, $h = 0.7$ dynamically evolves as if $\Omega_{matter} = 0.02$, $\Omega_\Lambda = 0.48$, and $h = 0.84$. Additionally, hydrodynamical cosmological simulations by Cen (2011) show that void galaxies may continue to form stars because the gas in voids remains below the critical entropy threshold (above which the cooling time exceeds the Hubble time). Void galaxies evolve in a relatively pristine environment where interactions are rare and star formation proceeds up to the present epoch because void galaxies are able to retain their gas. This contrasts with denser environments, where the chemical composition and evolution of galaxies are drastically altered due to mergers and tidal and/or ram-pressure stripping.

Observational studies of void galaxies have included investigation of photometric properties such as luminosity (Hoyle et al., 2005; Croton et al., 2005; Moorman et al., 2015), color and morphological type (Grogin & Geller, 2000; Rojas et al., 2004; Patiri et al., 2006; Park et al., 2007; von Benda-Beckmann & Müller, 2008; Hoyle et al., 2012), star formation rates estimated from optical spectroscopy and UV photometry (Rojas et al., 2005; Moorman et al., 2015; Beygu et al., 2016), and gas content (Kreckel et al., 2012; Moorman et al., 2016; Jones et al., 2016). When compared

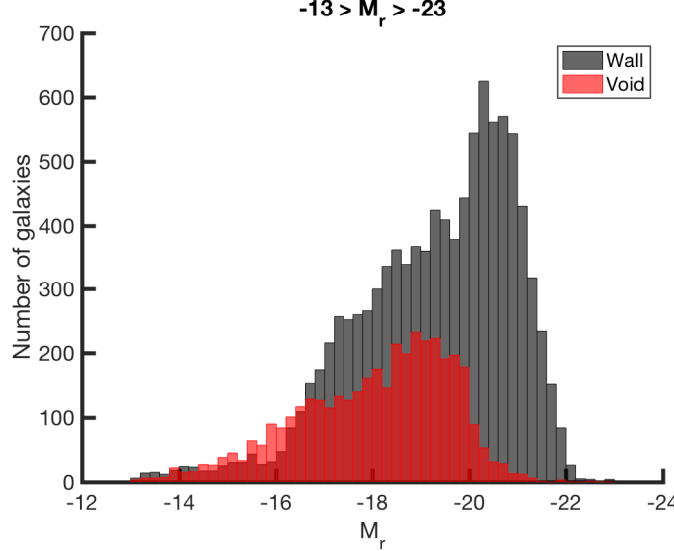


Figure 1.4: Absolute magnitude (M_r) distribution of galaxies in SDSS DR7, separated into void and wall environments. Dwarf galaxies are defined as galaxies with absolute magnitudes fainter than -17 ($M_r > -17$). For reference, the Milky Way has an absolute magnitude $M_r \approx -20$.

to galaxies in denser regions, void galaxies tend to be fainter, of late morphological types, bluer, forming stars at higher rates per unit stellar mass, and more gas rich.

In particular, we study the effects of the large-scale environment on the formation and evolution of dwarf galaxies. Fig. 1.4 shows the distribution of galaxies by their absolute magnitudes detected in SDSS DR7. Defined to be galaxies with absolute magnitudes fainter than -17 ($M_r > -17$), the low stellar masses of dwarf galaxies correspond to more shallow gravitational potential wells. This causes any environmental effects to have a more significant influence on dwarf galaxies than on galaxies with larger stellar masses. In addition, studying void dwarf galaxies will complement previous studies of dwarfs in groups and clusters because the assembly histories of low-mass galaxies are predicted to be very different (e.g., Gao & White, 2007; Lackner et al., 2012). Observations to date also show that the properties of dwarf galaxies vary dramatically with the environment (e.g., Ann et al., 2008; Geha et al., 2012).

The first stars that formed are thought to have been composed of hydrogen and helium (and trace amounts of other primordial elements). As stars burn, nucleosynthesis creates heavier elements at

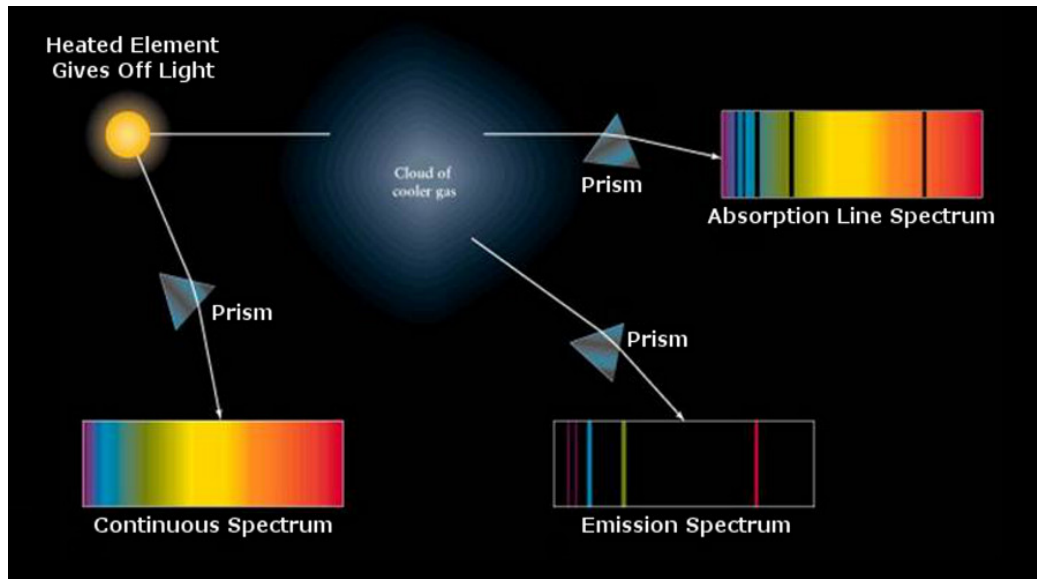


Figure 1.5: Three different viewpoints of the light emitted from a star and/or a cool cloud of gas, representing Kirchoff's laws of spectroscopy^a. A star emits light across all wavelengths, so the resulting spectrum is known as a continuous spectrum. Star's light that has passed through a cloud of cool gas before being observed is an absorption spectrum, where the elements in the cloud have absorbed some of the light at specific wavelengths (corresponding to the particular elements present in the gas). If observed off the line-of-sight of the star, the light emitted from the cloud of cooler gas results in an emission spectrum, where the gas is re-radiating the light it absorbed from the star.

^a<http://courses.atlas.illinois.edu/spring2011/astr/astr210/LECTURES/Lect12.html>

the core. When the stars expel their contents in supernovae and stellar winds, the heavier elements are distributed between the surrounding interstellar gas and circumgalactic medium. By measuring the ratio of elements heavier than helium (“metals”) relative to the hydrogen content, we measure the integrated star formation history of the galaxy. This “metallicity” is commonly expressed as $12 + \log(\text{O/H})$, although it is sometimes given in units of the solar metallicity, Z/Z_{\odot} .

We use a galaxy’s spectrum to measure various properties of the stellar population and interstellar medium. A galaxy’s spectrum is a superposition of light from the stars and emission lines from the interstellar gas. The observer’s viewpoint determines the type of spectrum measured. As shown in Fig. 1.5, if we separate a star’s light by its wavelength, we will observe a continuous spectrum, since its photosphere is close to a blackbody. If instead we observe the starlight after it has passed through a cloud of cooler gas (relative to the temperature of the star), we will measure an absorption line spectrum; the elements in the gas cloud have absorbed some of the star’s light at specific wavelengths

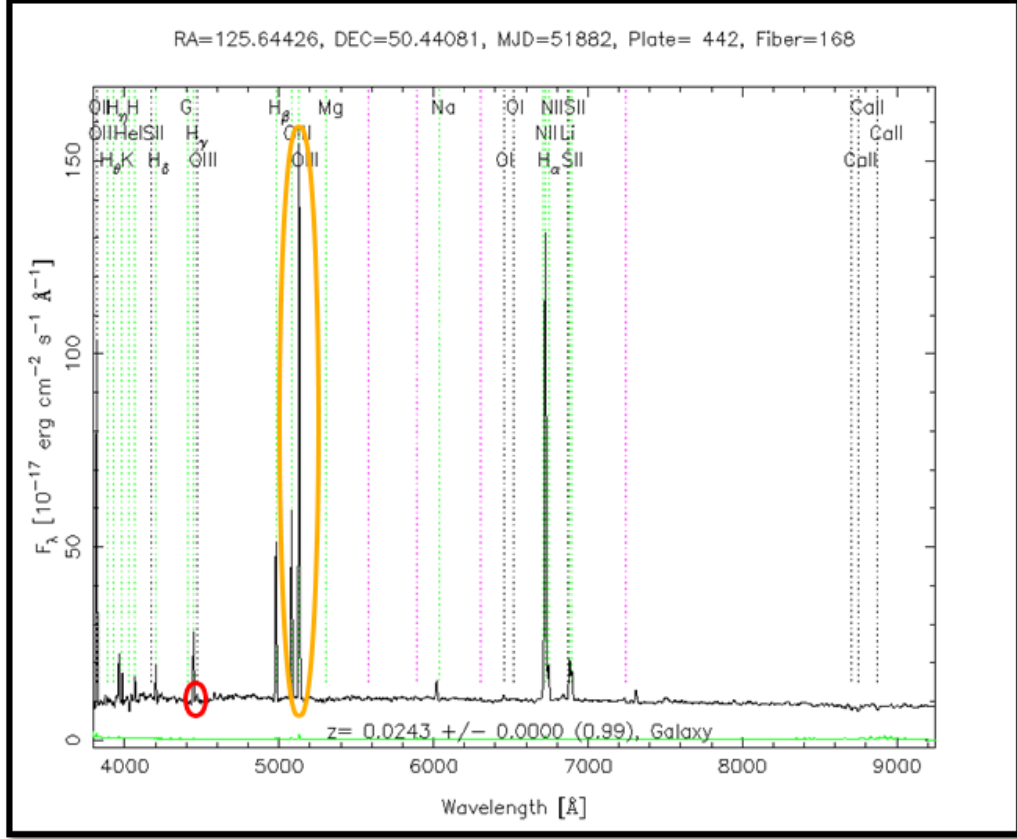


Figure 1.6: Example SDSS DR7 spectrum^a — this is a void dwarf galaxy whose gas-phase chemical abundances are slightly above average. The [O III] $\lambda 4363$ auroral line is circled in red, while the [O III] $\lambda\lambda 4959, 5007$ doublet is circled in yellow.

^a<http://cas.sdss.org/dr7/en/get/specById.asp?ID=124634771904004096>

corresponding to the particular ions present. Finally, if we only observe the light emitted from the cool gas cloud, we will measure an emission line spectrum. The method we employ to estimate the metallicity of a galaxy requires the detection of particular emission lines. We study the gas-phase chemical abundances of H II regions in a galaxy, where the light is coming from low-density gas partially ionized by UV photons emitted from young, hot stars. Therefore, we are measuring the abundances of the elements produced in previous generations of stars.

The ion transitions observed in the optical part of the spectrum (where SDSS DR7 operates) consist of forbidden transitions. As explained in detail in Section A, forbidden transitions have much longer lifetimes than the allowed electric dipole electron transitions. These transitions strongly depend on the temperature and density of the electron gas, because the long lifetimes allow the

atoms to easily collisionally de-excite. By taking the ratio of the [O III] $\lambda 4363$ auroral line to the [O III] $\lambda\lambda 4959, 5007$ doublet, we can get an estimate of the temperature of the gas. These lines are highlighted on the example SDSS DR7 spectrum shown in Fig. 1.6.

Oxygen is used as a proxy to measure the metallicity of an H II region, because oxygen is the most abundant element in the universe after hydrogen and helium (Emsley, 2011). It also has strong emission lines in the visible wavelength range, so it is relatively easy to observe. Oxygen emission is the most effective cooling source in an H II region, so lower metallicities correspond to higher temperatures. There are three main factors which determine the strength of an emission line: the gas temperature, the electron density, and the relative number of ions in the gas. It is possible to calculate the number ratios for any of the heavy elements with respect to hydrogen once the electron temperature and density of the interstellar gas are estimated.

We want to understand how the cosmic environment affects the evolution of a galaxy and what influence it has on a galaxy’s star formation. To do this, we compare the properties of galaxies living in voids with galaxies in denser regions in an effort to understand how the properties of the gas and the history of star formation in a galaxy depend on the environment. We then try to infer what these results tell us about the dark matter structure and history of the galaxy. In Chapter 2, we calculate and compare the metallicity of 135 star-forming dwarf galaxies as a function of their large-scale environment. We continue studying this galaxy sample in Chapter 3 by estimating their ratios of nitrogen to oxygen and looking at how that depends on the large-scale environment. To expand our dwarf galaxy sample, we derive an approximation for the amount of singly-ionized oxygen and repeat our analysis of the large-scale environmental influence on the gas-phase chemical abundances of 1920 star-forming dwarf galaxies in Chapter 4. In Chapter 5, we investigate how the dwarf galaxies’ properties depend on the galaxies’ distances to the nearest neighbors and groups. Finally, in an effort to better understand how galaxies evolve from blue, star-forming systems to “red and dead,” we discover a way to classify galaxies into their location on the color-magnitude diagram in Chapter 6. We present our conclusions and suggestions for future research in Chapter 7.

Chapter 2: Determining the large-scale environmental dependence of gas-phase metallicity in dwarf galaxies

This chapter is published in the *Astrophysical Journal*, 2017 (Vol. 834, pages 186–198) by Kelly A. Douglass & Michael S. Vogeley; it will be referenced as Douglass & Vogeley (2017a).

Abstract

We study how the cosmic environment affects galaxy evolution in the Universe by comparing the metallicities of dwarf galaxies in voids with dwarf galaxies in more dense regions. Ratios of the fluxes of emission lines, particularly those of the forbidden [O III] and [S II] transitions, provide estimates of a region’s electron temperature and number density. From these two quantities and the emission line fluxes [O II] $\lambda 3727$, [O III] $\lambda 4363$, and [O III] $\lambda\lambda 4959, 5007$, we estimate the abundance of oxygen with the Direct T_e method. We estimate the metallicity of 42 blue, star-forming void dwarf galaxies and 89 blue, star-forming dwarf galaxies in more dense regions using spectroscopic observations from the Sloan Digital Sky Survey Data Release 7, as re-processed in the MPA-JHU value-added catalog. We find very little difference between the two sets of galaxies, indicating little influence from the large-scale environment on their chemical evolution. Of particular interest are a number of extremely metal-poor dwarf galaxies that are less prevalent in voids than in the denser regions.

2.1 Introduction

Galaxy redshift surveys have shown that the large-scale structure of the galaxy distribution is similar to that of a three-dimensional cosmic web (Bond et al., 1996) in which the voids (large, underdense regions that fill upwards of 60% of space) separate galaxy clusters connected by thin filaments of galaxies. The voids found in early surveys (e.g., Gregory & Thompson, 1978; Kirshner et al., 1981; de Lapparent et al., 1986) proved to be an ubiquitous feature of large-scale structure. Analyses of the Sloan Digital Sky Survey (Abazajian et al., 2009; Ahn et al., 2012) have yielded catalogs of 10^3

voids (Pan et al., 2012; Sutter et al., 2014).

These cosmic voids are an important environment for studying galaxy formation (see van de Weygaert & Platen (2011) for a review). Gravitational clustering within a void proceeds as if in a very low density universe, in which aggregation of gravitationally bound dark matter halos ends relatively early and there is relatively little subsequent interaction between galaxies, both because of the lower density and the faster local Hubble expansion. Thus, the Λ CDM cosmology predicts that galaxies formed in voids should have lower mass and may be retarded in their star formation when compared to those in more dense environments (e.g., Gottlöber et al., 2003; Goldberg et al., 2005; Cen, 2011). Goldberg & Vogeley (2004) show that the interior of a spherical void with 10% of the mean density in a $\Omega_{matter} = 0.3$, $h = 0.7$ universe evolves dynamically like an $\Omega_{matter} = 0.02$, $\Omega_\Lambda = 0.48$, $h = 0.84$ universe. Hydrodynamical cosmological simulations by Cen (2011) show that the gas in voids remains below the critical entropy threshold, allowing the void galaxies to continue forming stars. While the more dense environment of cluster galaxies drastically alters their chemical composition and future evolution through the relatively frequent occurrences of mergers, tidal stripping, and/or ram-pressure stripping, void galaxies evolve in a relatively pristine environment where interactions are far less frequent and star formation may proceed up to the present epoch because void galaxies are able to retain their gas.

The effects of the void environment should be most obvious in the dwarf galaxies. Dwarf galaxies are sensitive to many astrophysical effects, including cosmological reionization, internal feedback from supernova and photoheating from star formation, external effects from tidal interactions and ram pressure stripping, small-scale details of dark matter halo assembly, and properties of dark matter. Many of these effects have been invoked to attempt to resolve the discrepancy between the mass function of galaxy halos predicted by Λ CDM and the observed, much smaller density of dwarf galaxies observed in voids (see, e.g., Kravtsov (2009) for a review). It is critical to explore dwarfs in voids to complement studies of dwarfs in groups and clusters because the assembly histories of low-mass galaxies are predicted to be very different (e.g., Gao & White, 2007; Lackner et al., 2012) and observations to date show that the properties of dwarfs vary dramatically with environment

(e.g., Ann et al., 2008; Geha et al., 2012). Diffuse cold-mode accretion, rather than mergers, has been suggested to be the dominant mechanism for growing dark matter halos in voids (e.g., Kereš et al., 2005; Fakhouri & Ma, 2009). Late-time gas accretion may be possible in voids if void galaxies retain a baryonic reservoir up to the present epoch. Thus, these few, lonely, faint galaxies test important features of the structure formation model and our understanding of galaxy formation “gastrophysics.”

Observational studies of void galaxies have included examination of photometric properties such as luminosity (Hoyle et al., 2005; Croton et al., 2005; Moorman et al., 2015), color and morphological type (Grogin & Geller, 2000; Rojas et al., 2004; Patiri et al., 2006; Park et al., 2007; von Benda-Beckmann & Müller, 2008; Hoyle et al., 2012), star formation rates estimated from optical spectroscopy and UV photometry (Rojas et al., 2005; Moorman et al., 2015; Beygu et al., 2016), and gas content (Kreckel et al., 2012; Moorman et al., 2016; Jones et al., 2016). Void galaxies tend to be of lower luminosity, of late morphological type, blue, have relatively high rates of star formation per stellar mass, and gas rich.

Another important diagnostic of galaxy formation is metallicity, which is a measure of the integrated star formation history and is frequently characterized by the ratio of the oxygen to hydrogen atomic density (often $Z = 12 + \log(\text{O}/\text{H})$, though sometimes given in units of the solar metallicity, Z/Z_{\odot}). The metallicity should depend on the galaxy’s star formation history, specifically the percentage of the galaxy’s gas that has been processed in stars (Guseva et al., 2009). If void galaxies have only recently started forming stars or have recently accreted unprocessed gas, we would expect these galaxies to have a lower metallicity than those in more dense regions (whose star formation started earlier due to e.g., tidally-triggered star formation). Furthermore, gas-phase metallicity is affected by the evolution of a galaxy’s stellar population and the composition of its interstellar medium (ISM). It reveals a galaxy’s history of releasing metals into the ISM via supernovae and stellar winds, ejecting gas via galactic outflows, and accreting gas from the surrounding environment (see, e.g., Cooper et al., 2008; Cybulski et al., 2014; Hirschmann et al., 2014, and references therein). Understanding the evolution of metallicity in galaxies is therefore crucial in uncovering the details

of galactic evolution.

Observations by Cooper et al. (2008); Deng (2011); Filho et al. (2015); Pustilnik et al. (2006, 2011b,a, 2013); Pustilnik (2014) appear to support the hypothesis of lower metallicity in void galaxies, while Kreckel et al. (2015) find no effect of the void environment on their sample of eight void dwarf galaxies. Most of the conclusions of previous work are based on samples containing only a handful of galaxies. Because large sky surveys like SDSS contain a substantial collection of dwarf galaxies, we can now analyze the dwarf galaxy population in the relatively nearby universe to test this hypothesis with more statistical significance. In particular, the main galaxy sample of SDSS DR7 covers a large enough volume to identify over 1000 voids (Pan et al., 2012) and provides spectroscopy to permit metallicity estimates of void dwarf galaxies. We make use of the reprocessed spectroscopic data from the MPA-JHU catalog¹ to study the metallicity of the large collection of dwarf galaxies in SDSS DR7. As explained by Tremonti et al. (2004), the spectra in the MPA-JHU catalog are analyzed with a more detailed stellar continuum, permitting the weaker emission lines to become more apparent. With the dependence of our analysis on weak emission lines (especially [OIII] $\lambda 4363$), this detailed treatment of the weak emission lines should produce more accurate results. We study the metallicity of these galaxies as a function of large-scale environment, testing the hypothesis that void dwarf galaxies have lower gas-phase metallicities than dwarf galaxies in more dense regions.

Our paper is organized as follows. Section 2 describes the theory and method for using various emission lines to estimate the metallicity of galaxies. We review the source of our data and errors in Section 3. Section 4 includes the results of our metallicity calculations, and we discuss the likelihood of any large-scale environmental influence on these results in Section 5. Finally, Section 6 summarizes our conclusions and discusses future work.

¹ Available at <http://www.mpa-garching.mpg.de/SDSS/DR7/>

2.2 Estimation of galaxy metallicity from optical spectroscopy

2.2.1 Overview of Methods

We characterize the galaxy metallicity using oxygen because it is relatively abundant, it emits strong lines for several ionization states in the optical regime, and a ratio of its lines provides a good estimate of the electron temperature (Kewley & Dopita, 2002). Here, we describe the theory and method we employ to estimate oxygen abundances in dwarf galaxies.

UV photons from young stars in an HII region keep the interstellar gas partially ionized. Optical photons are either absorbed and re-emitted throughout the region at resonant frequencies (resulting in classically permitted electron transitions), or the electrons are collisionally excited (resulting in classically forbidden electron transitions). Collisional excitation of the lower energy levels of metal ions is possible because these levels are only a few eV above the ground state (De Robertis et al., 1987). Consequently, the UV-optical spectrum contains some of the most useful diagnostic emission lines. Due to observational constraints of SDSS DR7 (the spectrometer’s wavelength range and the signal-to-noise of the resulting spectra; see Section 2.3), not all these emission lines are easily measured.

Three classes of methods have been developed to estimate the gas-phase metallicity of a galaxy, which we label as direct, theoretical, and empirical. Direct- T_e methods are based on a measurement of the [OIII] $\lambda 4363$ auroral line, from which a “direct” estimate of the electron temperature can be made (e.g., Izotov et al., 2006; Kniazev et al., 2008; Pilyugin & Thuan, 2007; Yin et al., 2007). Theoretical methods are based on photoionization models (e.g., Kewley & Dopita, 2002). Empirical methods make an indirect estimate of the electron temperature based on calibrated relationships between direct metallicity estimates and other strong-line ratios in HII regions (see, for example, Pettini & Pagel, 2004; Pilyugin & Mattsson, 2011; Dopita et al., 2013; Lara-Lopez et al., 2013; Marino et al., 2013). While each of these methods provides an estimate for the metallicity, they are all developed for use on sets of galaxies with different characteristics (stellar mass or gas-phase metallicity, for example). Previously, most theoretical and empirical methods have been calibrated with galaxies of larger stellar mass and higher luminosity. Because the properties of dwarf galaxies

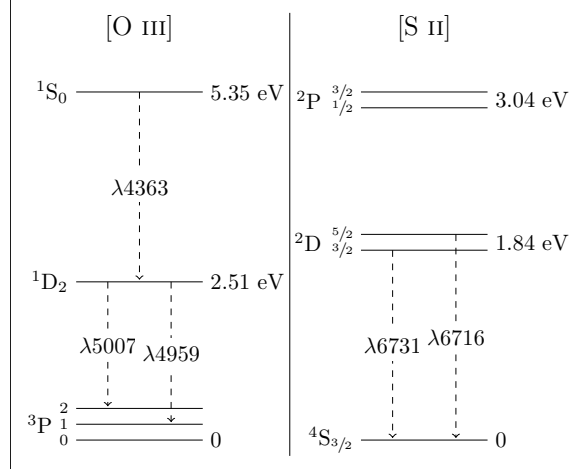


Figure 2.1: Energy-level diagram for [OIII] ($2p^2$) and [SII] ($3p^3$) ions. The most important transitions are shown; all are in the visible spectrum. These forbidden transitions in oxygen provide an estimate of the electron temperature in the interstellar gas, while the forbidden sulfur transitions provide an estimate of the electron number density. With estimates of the electron temperature and number density, we can convert emission line flux ratios into chemical abundance ratios.

differ from those of higher luminosity (and larger stellar mass), most of these methods drastically over- or under-estimate the gas-phase metallicity for dwarf galaxies. Consequently, we must exercise caution when applying these various calculation methods for estimating the metallicity of dwarf galaxies. We attempt to avoid any calibration issues by estimating gas-phase metallicity using the direct- T_e method. This method relies on the weak [OIII] $\lambda 4363$ emission line, which limits the number of dwarf galaxies we can analyze. However, because this method provides more reliable metallicity estimates than any of the others for dwarf galaxies, we chose quality over quantity in our results.

2.2.2 [O III]

There are three significant emission lines for doubly-ionized oxygen. The relative excitation rates to the ${}^1\text{S}$ and ${}^1\text{D}$ energy levels depend very strongly on the electron temperature, T_e ; therefore, the relative strengths of these emitted lines can be used to measure the electron temperature (Osterbrock, 1989). In the low-density limit ($n_e < 10^5 \text{ cm}^{-3}$), most excitations to the ${}^1\text{D}$ level result in an emission of a photon with a wavelength of either 5007Å or 4959Å, as shown in Fig. 2.1. Most excitations up to ${}^1\text{S}$ produce a photon of wavelength 4363Å, followed by a photon of either of the two previous

wavelengths (since the electron is now in the ${}^1\text{D}$ level).

At higher densities, collisional de-excitation begins to influence these emission rates (Osterbrock, 1989). Because the ${}^1\text{D}$ level has a longer lifetime than the ${}^1\text{S}$ state, it is collisionally de-excited at lower electron densities. This weakens the $\lambda 4959$ and $\lambda 5007$ emission lines. At the same time, the additional collisional excitations of the ${}^1\text{D}$ state permitted by the higher electron densities strengthen the $\lambda 4363$ emission line.

[OIII] $\lambda 4363$ is a temperature-sensitive forbidden transition line of doubly-ionized oxygen that is the preferred line to use when measuring the metallicity of galaxies. Since the most effective cooling channel in these HII regions is oxygen line emission, lower metallicity regions have higher temperatures (Saintonge, 2007). Collisional excitations up to this energy level are more common at higher temperatures, since there are more electrons with the kinetic energy required to excite the O^{++} ion to this energy level. As a result, the line strength of [OIII] $\lambda 4363$ correlates with the region's temperature and is therefore anticorrelated with the metallicity of the galaxy. [OIII] $\lambda 4363$ is already one to two orders of magnitude weaker than the [OIII] $\lambda\lambda 4959, 5007$ doublet, so it is very difficult to obtain an accurate ratio with this line. It is for these reasons that other “empirical” relations were developed for metallicity calculations, eliminating the need for an electron temperature estimate from this emission line.

Given an electron temperature and density, the flux ratio of the [OIII] $\lambda\lambda 4959, 5007$ doublet to $\text{H}\beta$ provides an abundance estimate for doubly-ionized oxygen.

2.2.3 [O II]

A less temperature-sensitive line than [OIII] $\lambda 4363$, the [OII] $\lambda 3727$ forbidden transition doublet of singly-ionized oxygen is often used in metallicity calculations. With an electron temperature and density, its flux provides an estimate of the abundance of singly-ionized oxygen. In SDSS spectra, this line can be observed for objects with a redshift greater than 0.02. However, because dwarf galaxies are inherently faint objects ($M_r > -17$), they are targeted for spectroscopy in SDSS only out to redshift $z \sim 0.03$, thus we can only estimate the metallicity of dwarf galaxies in the redshift range $0.02 < z < 0.03$.

2.2.4 [S II]

Just as we are able to measure the electron temperature from [OIII] transitions, we can estimate the electron number density from [SII] transitions. Below a density of about 100 cm^{-3} , the [SII] $\lambda 6716/\lambda 6731$ ratio has a weak dependence on the density. All our galaxies fall within this low-density regime, so we assume a low-density limit of $n_e = 100 \text{ cm}^{-3}$.

2.2.5 Direct T_e method

We use the method published by Izotov et al. (2006), which is based on the astrophysics in Osterbrock (1989). It makes use of the [OIII] $\lambda 4363$, $\lambda\lambda 4959, 5007$ lines and the [OII] $\lambda 3727$ doublet. While often regarded as the most accurate estimate of the metallicity, it is difficult to employ due to the restrictions on [OIII] $\lambda 4363$. Consequently, this method is best suited for low-redshift, low-metallicity galaxies. The electron temperature is derived by solving the following system of equations:

$$t_3 = \frac{1.432}{\log[(\lambda 4959 + \lambda 5007)/\lambda 4363] - \log C_T} \quad (2.1)$$

where $t_3 = 10^{-4}T_e(\text{O}^{++})$ and

$$C_T = (8.44 - 1.09t_3 + 0.5t_3^2 - 0.08t_3^3) \frac{1 + 0.0004x_3}{1 + 0.044x_3} \quad (2.2)$$

where $x_3 = 10^{-4}n_e t_3^{-0.5}$. The ionic abundances are then found with the equations

$$12 + \log \left(\frac{\text{O}^+}{\text{H}^+} \right) = \log \frac{\lambda 3727}{\text{H}\beta} + 5.961 + \frac{1.676}{t_2} - 0.40 \log t_2 - 0.034t_2 + \log(1 + 1.35x_2) \quad (2.3)$$

$$12 + \log \left(\frac{\text{O}^{++}}{\text{H}^+} \right) = \log \frac{\lambda 4959 + \lambda 5007}{\text{H}\beta} + 6.200 + \frac{1.251}{t_3} - 0.55 \log t_3 - 0.014t_3 \quad (2.4)$$

where $t_2 = 10^{-4}T_e(\text{O}^+)$, $t_2 = 0.7t_3 + 0.3$ (Garnett, 1992), and $x_2 = 10^{-4}n_e t_2^{-0.5}$. Andrews & Martini (2013) show that this relation between $T_e(\text{O}^+)$ and $T_e(\text{O}^{++})$ may overestimate the temperature in the low ionization zone, causing the calculated metallicities to be underestimated. Because we care only about the relative metallicity values of the galaxies, this effect will only affect our results in

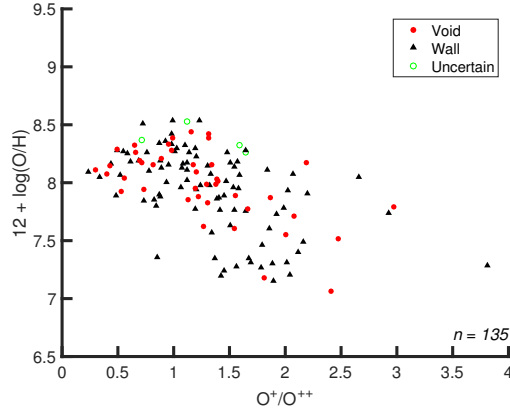


Figure 2.2: Metallicity of our 135 dwarf galaxies as a function of O^+/O^{++} . While either O^+ or O^{++} can dominate our galaxies’ oxygen abundances, only those with low metallicities (high temperatures) and with O^+ dominating the abundance will be affected by the temperature overestimate of the low-ionization zone as found by Andrews & Martini (2013). The small number of galaxies (15/135) that may suffer from this possible temperature overestimate do not affect our results.

galaxies where O^+ dominates the oxygen abundance (where $O^+/O^{++} > 1$) in higher temperature regions (or low metallicities). As shown in Fig. 2.2, this affects perhaps fifteen galaxies and does not change our conclusions.

The total gas-phase oxygen abundance is equal to the sum of the abundances of each of the ionized populations:

$$\frac{O}{H} = \frac{O^{++}}{H^+} + \frac{O^+}{H^+} \quad (2.5)$$

2.3 SDSS data and galaxy selection

The SDSS Data Release 7 (DR7) (Abazajian et al., 2009) is a wide-field multi-band imaging and spectroscopic survey, using drift scanning to map approximately one-quarter of the northern sky. Photometric data in the five band SDSS system — u , g , r , i , and z — are taken with a dedicated 2.5-meter telescope at the Apache Point Observatory in New Mexico (Fukugita et al., 1996; Gunn et al., 1998). Galaxies with a Petrosian r -band magnitude $m_r < 17.77$ are selected for spectroscopic analysis (Lupton et al., 2001; Strauss et al., 2002). The spectra have an observed wavelength range of 3800Å to 9200Å with a resolution $\lambda/\Delta\lambda \sim 1800$, and are taken using two double fiber-fed spectrographs and fiber plug plates with a minimum fiber separation of 55 arcseconds (Blanton

et al., 2003). The emission line flux data used in this study are from the MPA-JHU value-added catalog, which is based on the SDSS DR7 sample of galaxies. Absolute magnitudes, colors, and all other additional data are from the KIAS value-added galaxy catalog (Choi et al., 2010).

2.3.1 Spectroscopic selection

To satisfy the needs of our analysis, we make the following cuts to our sample. All analyzed galaxies must have relatively recent star formation, since UV photons are needed to excite the interstellar gas to produce the required emission lines. As a result, each galaxy must have a star-forming BPT classification by Brinchmann et al. (2004). In addition, because we analyze only dwarf galaxies ($M_r > -17$), there is a natural redshift upper limit of 0.03 on the samples; dwarf galaxies at higher redshifts are not bright enough to be included in the spectroscopic data of SDSS. For a galaxy to be analyzed, we require a minimum 5σ detection of the H β emission line and at least a 1σ detection of the [OIII] $\lambda 4363$ forbidden transition. The restriction on both these lines eliminate those galaxies with a low S/N spectrum. This is particularly important for [OIII] $\lambda 4363$, as it is inherently a weak emission line. We are aware that implementing this restriction on [OIII] $\lambda 4363$ eliminates those galaxies with higher metallicities, since the strength of this line is inversely proportional to the metallicity of the galaxy (see Sec. 2.2.2 for details). However, we show that this restriction does not affect our conclusions on the large-scale environmental dependence on the gas-phase metallicity.

In addition, we also eliminate galaxies with temperature estimates $T_e(\text{OIII}) > 3 \times 10^4$ K. Gas temperatures above this threshold are not physical for an HII region (inferred from Osterbrock, 1989; Izotov et al., 2006; Luridiana et al., 2015).

For the dwarf galaxies in our sample, the [OII] $\lambda 3727$ spectral line is very close to the edge of the spectrometer due to their maximum redshift $z < 0.03$. Consequently, its flux measurement is not always reliable. Therefore, the flux values labeled `oii_flux` in the MPA-JHU catalog are used instead of the combined flux values measured for the [OII] $\lambda\lambda 3726, 3729$ doublet. Because the velocity dispersion is not fixed when measuring the flux found in `oii_flux`, the resulting measurements tend to be more realistic than those measured with the fixed dispersion (C. Tremonti, private communication). In addition, those galaxies with remaining erroneous measurements for the [OII]

$\lambda 3727$ doublet were removed by hand, after comparing the listed flux values to the spectra by eye. All spectral lines used in the analysis must have a flux greater than 0, to ensure that they are emission lines.

2.3.2 Void classification

Void galaxies are identified using the void catalog compiled by Pan et al. (2012), which was built based on the galaxies in SDSS DR7 catalog. Starting with galaxies with absolute magnitudes $M_r < -20$, the VoidFinder algorithm of Hoyle & Vogeley (2002) removes all isolated galaxies (defined as having the third nearest neighbor more than $7 h^{-1}$ Mpc away). After applying a grid to the remaining galaxies, spheres are grown from all empty grid cells (cells containing no galaxies). A sphere reaches its maximum size when it encounters four galaxies on its surface. To be classified as a void (or part of one), a sphere must have a minimum 10 Mpc radius. If two spheres overlap by more than 10%, they are considered part of the same void. See Hoyle & Vogeley (2002) for a more detailed description of the VoidFinder algorithm. Those galaxies that fall within these void spheres are classified as void galaxies. Those galaxies that lie outside the spheres are classified as wall galaxies. Because we cannot identify any voids within 10 Mpc of the edge of the survey, we do not include the galaxies that fall within this region in either the void or wall sample (throughout this paper, these galaxies are labeled as “Uncertain”).

Of the $\sim 800,000$ galaxies with spectra available in SDSS DR7, 9519 are dwarf galaxies. Applying the spectroscopic cuts, 42 void dwarf galaxies, 89 wall dwarf galaxies, and 4 dwarf galaxies with uncertain large-scale environments are left to analyze (for a total of 135 dwarf galaxies, 131 of which are used in the environmental tests).

2.4 Metallicity analysis and results

Our primary objective is to perform a relative measurement of metallicity of dwarf galaxies to discern how the large-scale environment affects their chemical evolution. As discussed in Section 2.2, the strength of and ability to observe different spectral lines between various surveys and observations require multiple methods to be developed for metallicity calculations. In this paper, we use only the

Direct T_e method, because no other method has yet been calibrated using dwarf galaxies. The results from the various methods are not directly comparable; while they all return metallicities within the same range, the same galaxy can have very different metallicity values depending on which method is used. Conversions between methods have been developed (see Kewley & Ellison, 2008), but it is not clear that these conversions would be accurate for dwarf galaxies. Unfortunately, there are not enough galaxies available in our sample to calibrate these other methods for dwarf galaxies.

All line ratios listed are ratios of the emission line fluxes. Galaxies with low metallicities have $Z = 12 + \log(\text{O/H}) < 7.6$ (Pustilnik et al., 2006); galaxies with high metallicities have $Z > 8.2$ (Pilyugin et al., 2006). The solar metallicity is $Z_\odot = 8.69 \pm 0.05$ (Asplund et al., 2009).

2.4.1 Estimation of uncertainties and confirmation of our method

We estimate uncertainties in the computed metallicity using a Monte-Carlo method. Using the measured line fluxes and scaled uncertainty estimates² from the MPA-JHU catalog, 100,000 different metallicities are calculated for a given galaxy. For each estimate, the flux of a line is drawn from a normal distribution, with the expectation value being the original measured flux and the standard deviation being the given error in the flux measurement. We require all simulated line fluxes to be positive, as negative flux values would result in erroneous metallicity values. The standard deviation in the set of these 100,000 calculated values is used as the error in the metallicity estimate for the galaxy. As a result, these uncertainties tend to be larger than those quoted in other sources, as they include more information than just the quality of the fit used to derive the metallicity.

We compare results of our analysis of the same set of SDSS galaxies that Yin et al. (2007) analyze to confirm that our code was working properly, since Yin et al. (2007) also uses the metallicity method outlined in Izotov et al. (2006). The results of this comparison can be seen in Fig. 2.3. Yin et al. (2007) also uses the MPA-JHU catalog as the source for their data, so our results should be identical.

2.4.2 Results

Metallicities calculated using the Direct T_e method for our dwarf galaxy sample are listed in Table 2.1, along with other key identification for the galaxies (including whether they are a void or wall

²As described at http://wwwmpa.mpa-garching.mpg.de/SDSS/DR7/raw_data.html

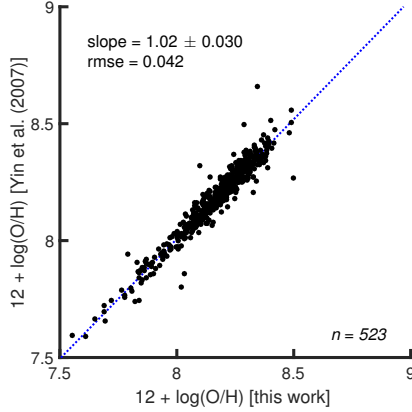


Figure 2.3: Metallicity ($12 + \log(\text{O/H})$) comparison between our calculated estimates and those made by Yin et al. (2007). Error bars have been omitted for clarity. These are not the dwarf galaxies analyzed in this paper, but rather the sample of galaxies analyzed by Yin et al. (2007) to confirm that our version of the calculation is correct. Both Yin et al. (2007) and we have used the metallicity method outlined by Izotov et al. (2006).

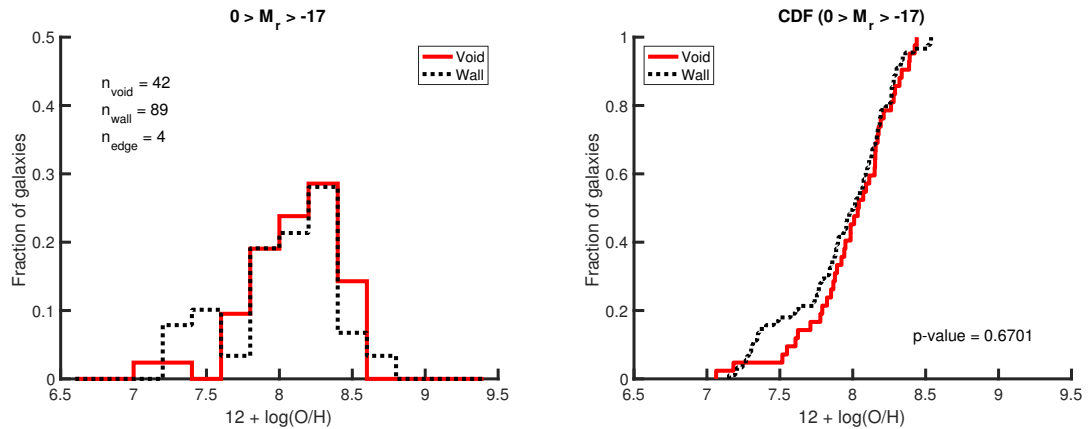


Figure 2.4: Histogram and associated cumulative distribution function of the gas-phase metallicity of void dwarf (red solid line) and wall dwarf (black dashed line) galaxies. A two-sample KS test of the two data sets results in an asymptotic p -value of 0.67, indicating a 67% probability that a test statistic greater than the observed value of 0.13 will be seen. This is reflected visually, as there appears to be very little difference in the two populations, indicating that there is little large-scale environmental influence on the metallicity of dwarf galaxies.

Table 2.1: Five of the 135 dwarf galaxies analyzed from SDSS DR7. The flux values for all required emission lines can be found in the MPA-JHU value-added catalog. Metallicity values are calculated using the direct T_e method, with error estimates via a Monte Carlo method. The void catalog of Pan et al. (2012) is used to classify the galaxies as either Void or Wall. If a galaxy is located too close to the boundary of the SDSS survey to identify whether or not it is inside a void, it is labeled as Uncertain. Table 2.1 is published in its entirety online in a machine-readable format. A portion is shown here for guidance regarding its form and content.

Index ^a	R.A.	Decl.	Redshift	M_r	$12 + \log(\frac{O}{H})$	Void/Wall
63713	09 ^h 20 ^m 04 ^s .27	-00°30'08".97	0.0257	-16.73	7.80 ±0.41	Wall
73537	09 ^h 25 ^m 24 ^s .23	+00°12'40".39	0.0250	-16.94	7.94 ±0.34	Wall
75442	13 ^h 13 ^m 24 ^s .25	+00°15'02".95	0.0264	-16.81	7.55 ±0.35	Void
168874	11 ^h 45 ^m 13 ^s .16	-01°48'17".68	0.0273	-16.99	8.16 ±0.31	Wall
184308	09 ^h 39 ^m 09 ^s .38	+00°59'04".15	0.0244	-16.73	7.36 ±0.43	Wall

galaxy). A histogram of the resulting metallicities is shown in Fig. 2.4. As can be seen in Fig. 2.4, there is very little difference in the spread of metallicity values in dwarf galaxies between voids and walls. A two-sample Kolmogorov-Smirnov (KS) test quantifies this observation — it produced a test statistic of 0.13, corresponding to a probability of 67% that a test statistic greater than or equal to that observed will be measured if the void sample were drawn from the wall sample; the cumulative distribution function (CDF) of these samples can be seen on the right in Fig. 2.4.

The requirement of a minimum 1σ detection of [OIII] $\lambda 4363$ eliminates galaxies with a low-quality spectrum and those with a weak [OIII] $\lambda 4363$ line. Since this line is inversely proportional to the oxygen abundance in the interstellar gas, this biases the sample towards more low-metallicity galaxies. To see how much this cut affects the results, we perform the same analysis with no minimum detection limit of [OIII] $\lambda 4363$. As can be seen in Fig. 2.5, this adds a substantial number of galaxies to the sample (there are now 126 void galaxies and 270 wall galaxies analyzed), predominately in the high-metallicity regime. As Table 2.2 makes apparent, there is now a higher percentage of void dwarf galaxies with high metallicities than wall dwarf galaxies. However, the uncertainties in the metallicity estimates for $12 + \log(O/H) > 8.2$ are almost 0.5 dex, due to the extremely weak [OIII] $\lambda 4363$ auroral line. Because of these uncertainties, the difference in the distributions may not be statistically significant.

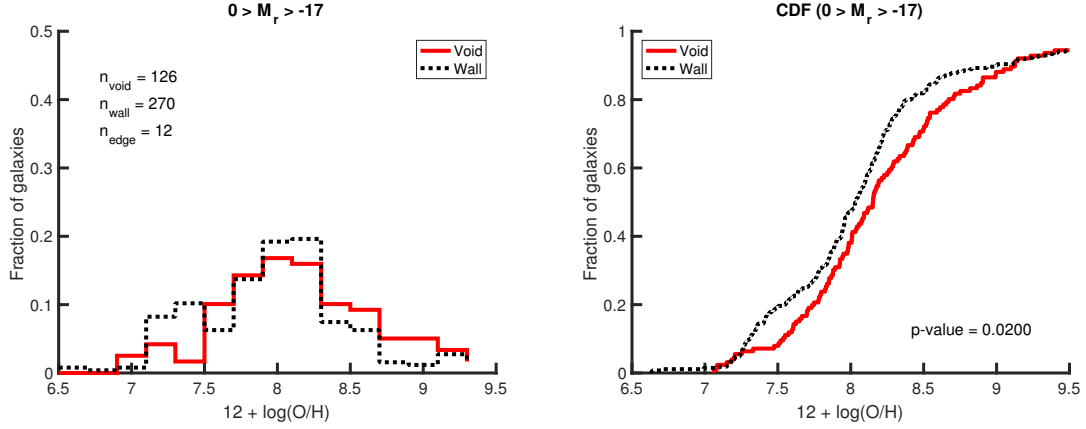


Figure 2.5: Histogram and associated cumulative distribution function comparing the gas-phase metallicity of void dwarf (red solid line) and wall dwarf (black dashed line) galaxies, testing the effect of the S/N restriction on the auroral [OIII] $\lambda 4363$ line. The galaxies here have no minimum detection of [OIII] $\lambda 4363$ line. As expected, eliminating the restriction on this line includes more high metallicity galaxies to the sample, shifting the void dwarf galaxy distribution to have higher metallicities than the wall dwarf galaxies. However, due to the significant uncertainties in the metallicity estimates for $12 + \log(\text{O/H}) > 8.2$ due to the weak [OIII] $\lambda 4363$ auroral line, this difference in the distributions may not be statistically significant.

Table 2.2: Percentages of galaxies with calculated metallicities within the labeled metallicity ranges, with the number of galaxies in each category in parentheses. Removing the S/N restriction on [OIII] $\lambda 4363$ especially increases the number of dwarf galaxies with high metallicities, changing the distribution so that void dwarf galaxies have higher metallicities than wall dwarf galaxies. However, due to the large uncertainties in the metallicity estimates for $12 + \log(\text{O/H}) > 8.2$, this difference in the distributions may not be statistically significant.

	$Z < 7.6$	$7.6 \leq Z < 8.2$	$Z \geq 8.2$
1 σ restriction on [OIII] $\lambda 4363$			
Void	9.52% (4)	66.67% (28)	23.81% (10)
Wall	19.10% (17)	59.55% (53)	21.35% (19)
No restriction on [OIII] $\lambda 4363$			
Void	13.33% (16)	45.83% (55)	40.83% (49)
Wall	23.26% (60)	46.12% (119)	30.62% (79)

2.4.3 Sources of systematic error

It is well-known that many physical properties of galaxies vary with the distance from the center of the galaxy (Bell & de Jong, 2000). Therefore, a metallicity measurement is dependent on the location of the spectroscopic fiber on the galaxy. If not all the light of the galaxy is contained within the fiber of the spectrograph, the estimated metallicity will not necessarily be representative of a global metallicity value. Indeed, it has been shown that different parts of a galaxy have different metallicity values (Bell & de Jong, 2000). In SDSS, the fiber size is 3 arcseconds – this corresponds to a physical diameter between 1.29 kpc and 1.93 kpc at redshifts $0.02 < z < 0.03$. For many of the dwarf galaxies, this covers more than 50% of the galaxy’s luminous surface. The fiber is almost always centered on the brightest spot of the galaxy. For spiral and elliptical galaxies, this is often the center of the galaxy. Since the metallicity of the center of a galaxy is often higher than at its edge, these metallicity values may be overestimates of the global metallicity. Many dwarf galaxies are irregular galaxies, where the fiber is instead focused on a bright HII region.

Due to the requirements we place on the emission lines for the galaxies, we are inherently limiting our sample to only blue, star-forming galaxies. This is not a representative sample of the dwarf galaxy population. Rather, in this study we are only able to comment on the large-scale environmental influence on blue, star-forming dwarf galaxies in a narrow redshift range. Unfortunately, we cannot measure the metallicity of red dwarf galaxies with the Direct T_e method, since we need the UV photons from young stars to excite the interstellar gas.

2.4.4 Comparison to previously published metallicity measurements

To place our metallicity measurements in the context of previous work, we compare our results to the metallicity values measured by Tremonti et al. (2004). While we both use data from the MPA-JHU value-added catalog, Tremonti et al. (2004) employs an empirical method for estimating the metallicity, which is based on calibrated relationships between direct metallicity values and strong-line ratios. The results of this comparison are shown in Figure 2.6. Unfortunately, the range of metallicity values found by Tremonti et al. (2004) is limited to those galaxies with high metallicities ($12 + \log(\text{O}/\text{H}) > 8.5$), due to the characteristics of their sample and their method; they found less

than 2% of their total sample to have metallicities less than 8.5. Kennicutt et al. (2003) shows that methods which make extensive use of the strong emission lines (so-called “strong-line” methods) can overestimate the metallicity abundances by as much as 0.3 dex. A similar comparison is made in Yin et al. (2007), where they too find that the metallicity estimates of Tremonti et al. (2004) are overestimated by 0.34 dex on average. This can be seen quite clearly in Figure 2.6, as there is no correlation between galaxies with our estimates of $12 + \log(\text{O/H}) < 8$ and the metallicities measured by Tremonti et al. (2004), since their metallicities are much higher than ours. The formal correlation coefficient between these two data sets is 0.00 ± 0.087 ; the correlation coefficient for those galaxies we measure to have metallicities greater than 7.6 (so excluding the low-metallicity galaxies) is 0.12 ± 0.093 . While this shows a slightly stronger correlation, we realize that these galaxies cover a limited range of metallicity values. As a result, any scatter due to the errors in the calculations will result in a low correlation coefficient, which is what we see. Therefore, by Fig. 2.6, we can see that there is a reasonable agreement between our metallicity values and those of Tremonti et al. (2004), excluding those galaxies we found to have extremely low metallicity values.

While it is known that there are systematic offsets between different metallicity calculation methods (Kewley & Ellison, 2008), that does not seem to be the case in the relation between our metallicities (measured with the Direct T_e method) and those of Tremonti et al. (2004) (measured with a combination of “strong-line” methods). While the metallicity estimates by Tremonti et al. (2004) do not appear to be significantly biased at $8 < 12 + \log(\text{O/H}) < 8.5$, they overestimate the metallicities for low-metallicity galaxies.

2.4.5 Mass-metallicity relation

A strong correlation between the stellar mass and metallicity of galaxies reflects the fundamental connection between galactic mass and the chemical evolution of galaxies. We use stellar mass estimates from the MPA-JHU catalog to examine the mass-metallicity relation in our sample of 135 dwarf galaxies. We have also included those galaxies from the MPA-JHU catalog with metallicity estimates from Tremonti et al. (2004) to place our sample in context. Due to the narrow range of masses in our sample, it is difficult to derive an accurate fit to the data. However, we make

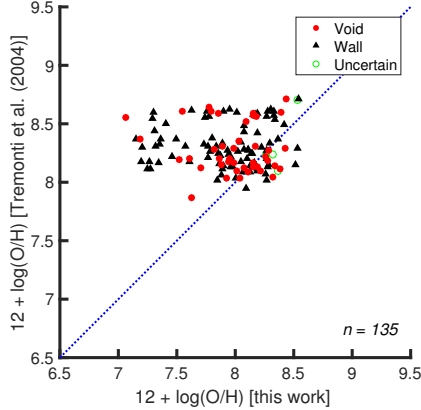


Figure 2.6: Metallicity ($12 + \log(\text{O/H})$) comparison between our calculated estimates and those made by Tremonti et al. (2004). Error bars have been omitted for clarity. Excepting the extreme low-metallicity galaxies we found, most galaxies agree reasonably well with the values already published. It is important to note that the strong-line methods (like those used by Tremonti et al., 2004) are not calibrated for low-metallicity values and are known to overestimate the metallicity by as much as 0.3 dex (Kennicutt et al., 2003). Thus, it is not surprising that oxygen abundances measured using the direct method find lower metallicity, particularly at very low metallicities.

comparisons to three published mass-metallicity relations (Tremonti et al., 2004; Mannucci et al., 2010; Andrews & Martini, 2013). As can be seen in Fig. 2.7, the fit by Mannucci et al. (2010) diverges at the low-mass limit, and the relations of Tremonti et al. (2004) and Andrews & Martini (2013) predict metallicities that are higher than measured for most galaxies in this sample. It is important to note that two of these relations are only calibrated down to a stellar mass of $10^{8.5} M_{\odot}$. In Fig. 2.7, these relations have been extended to $10^{7.5} M_{\odot}$, in order to continue past our galaxy sample.

In addition to looking at the overall mass-metallicity relation for dwarf galaxies, we can also investigate the difference in the relation between galaxies in voids and those in more dense regions. There appear to be no significant differences in the two populations, indicating minimal influence from the large-scale environment on the mass-metallicity relation of these dwarf galaxies. Hughes et al. (2013) also find that the stellar mass-metallicity relation is independent of large-scale environment. This prompts the conclusion that the internal evolutionary processes of a galaxy have a greater influence on its chemical evolution than its large-scale environment. We expect this depen-

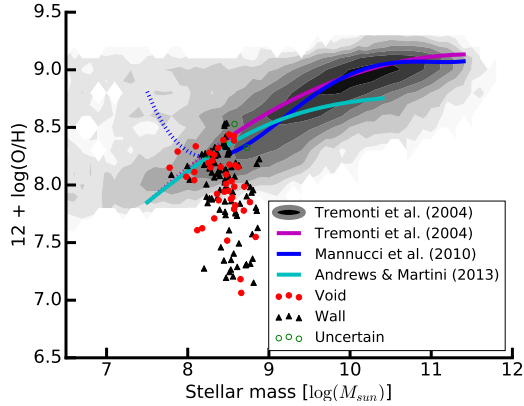


Figure 2.7: Stellar mass versus metallicity of the 135 analyzed dwarf galaxies. Error bars have been omitted for clarity. Due to the limited range of mass (all our galaxies are within a small range of masses, since we are looking only at dwarf galaxies), we cannot derive our own relation between the mass and metallicity. Some previously published relations are plotted over our data for comparison. To place our sample in context, we have also included (grey contours) those galaxies from the MPA-JHU catalog with metallicity estimates by Tremonti et al. (2004). It was from these galaxies that the published relation of Tremonti et al. (2004) was derived.

dence of the chemical content of a galaxy on its stellar mass, since the accumulated metals reflect the integrated history of star formation. However, we would expect an environmental dependence to appear as well, if void galaxies are in an earlier stage of evolution and/or are continuing to accrete fresh gas.

2.4.6 SFR-metallicity relation

A fundamental diagnostic of the star formation history of galaxies is the relation between stellar mass, metallicity, and star formation rate. Therefore, we also look at the relationship between the (specific) star formation rate and metallicity of these 135 dwarf galaxies. The total (specific) star formation rate estimates for these galaxies are from the MPA-JHU value-added catalog, based on the technique discussed in Brinchmann et al. (2004). For low-mass galaxies, Henry et al. (2013) show that the metallicity is inversely proportional to the star formation rate of a galaxy. However, this is not what is observed in our data, as seen in Fig. 2.8. The correlation coefficient between the total (specific) star formation rate and the metallicity $r_{sSFR} = 0.49 \pm 0.066$ and $r_{SFR} = 0.52 \pm 0.063$, showing a positive correlation between the two properties. Indeed, those galaxies with the lowest metallicities have some of the lowest (specific) star formation rates among the dwarf galaxies in

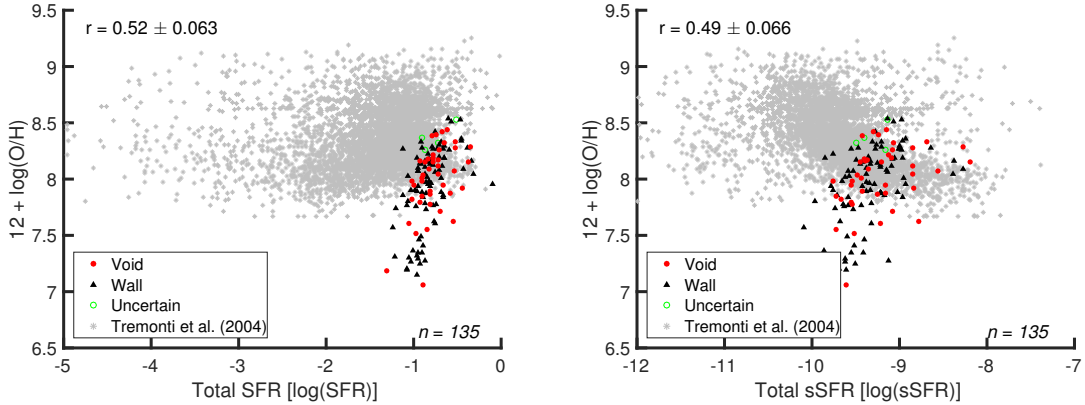


Figure 2.8: Total star formation rate (SFR) and specific star formation rate (sSFR) versus metallicity of the 135 analyzed dwarf galaxies. Error bars have been omitted for clarity. We also plot (grey stars) dwarf galaxies ($M_r > -17$) with metallicity estimates by Tremonti et al. (2004), to place our results in context. It is significant to note that the majority of our galaxies are on the upper end of the SFR and sSFR for dwarf galaxies, as shown in Fig. 2.9. Note that those galaxies with metallicities $12 + \log(\text{O/H}) < 7.6$ are on the lower end of the range of sSFR of the dwarf galaxies in our sample.

our sample. Since we are limiting our sample to only star-forming galaxies, the (s)SFR must be relatively high to emit the UV photons needed to ionize the gas. As a result, all low (s)SFR galaxies will be eliminated from our sample, as seen in Fig. 2.9. In addition, due to the behavior of the [OIII] $\lambda 4363$ auroral line, all galaxies with metallicities $12 + \log(\text{O/H}) \gtrsim 8.5$ are also eliminated from the sample. As a result, we are only calculating the metallicity of galaxies in the lower right corners of the (s)SFR plots in Fig. 2.8, which is why we see the unexpected correlation. There does not seem to be a difference between the void and wall galaxies in this relation, indicating no large-scale environmental influence on the (s)SFR-Z relation.

2.4.7 Color-metallicity relation

Metallicity is expected to have a positive correlation with color, as older galaxies are expected to have higher metallicities, since they have had more time to convert their gas into heavier elements through star formation. Therefore, we also look at the color–metallicity relation of our sample of 135 galaxies – these relations can be seen in Fig. 2.10. To place our galaxies in the context of other dwarf galaxies, we have included the sample of dwarf galaxies for which Tremonti et al. (2004) has estimated metallicities (grey stars in the figures).

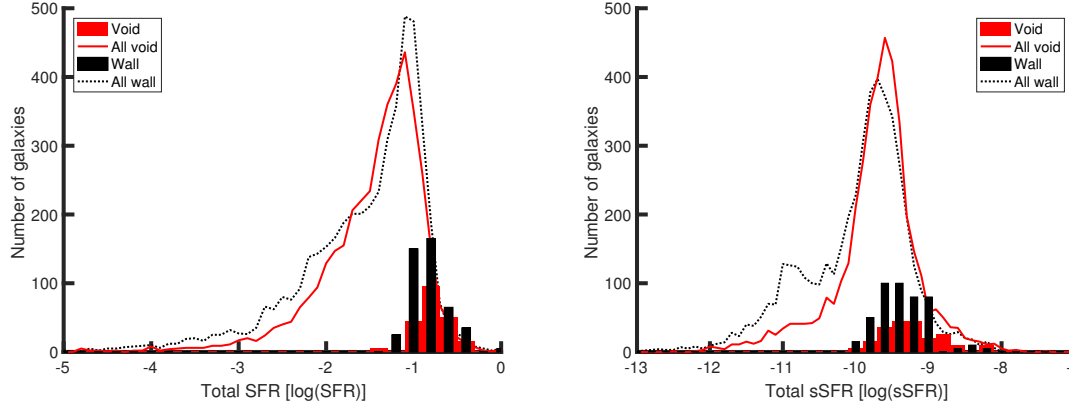


Figure 2.9: Distribution of the total star formation rate (SFR) and specific star formation rate (sSFR) for void and wall dwarf galaxies in SDSS are shown in the red solid and black dashed lines. Our sample of dwarf galaxies (with metallicity values) is shown in the red and black bars (scaled by a factor of 5 for greater visibility). We are looking only at the highest SFR found in dwarf galaxies; the sSFR for our sample of dwarf galaxies follows the distribution of all dwarf galaxies. There is clearly a selection bias against lower SFR.

As we can see in Fig. 2.11, by overlaying our distribution of dwarf galaxies on Fig. 4 of Hoyle et al. (2012), all of our dwarf galaxies are members of the blue dwarf galaxy population. (The Gaussian parameters for the curves are taken from Table 3 in Hoyle et al. (2012).) This is as expected, since the Direct T_e method requires measurements of the emission lines of the galaxies; these emission lines are caused by the UV photons of newly formed stars, indicating a star-forming galaxy and giving the galaxy a blue color.

While the majority of our galaxies follow the positive correlation between color and metallicity, the group of extremely low-metallicity galaxies is less blue than their metallicities would indicate. However, when compared to the red/blue curves in Fig. 2.11, these galaxies occupy the typical range of blue dwarf galaxies, so their colors are not unique. There is no clear separation between the void and wall dwarf galaxies in Fig. 2.10, indicating that there is little or no large-scale environmental influence on the color-metallicity relation of these galaxies.

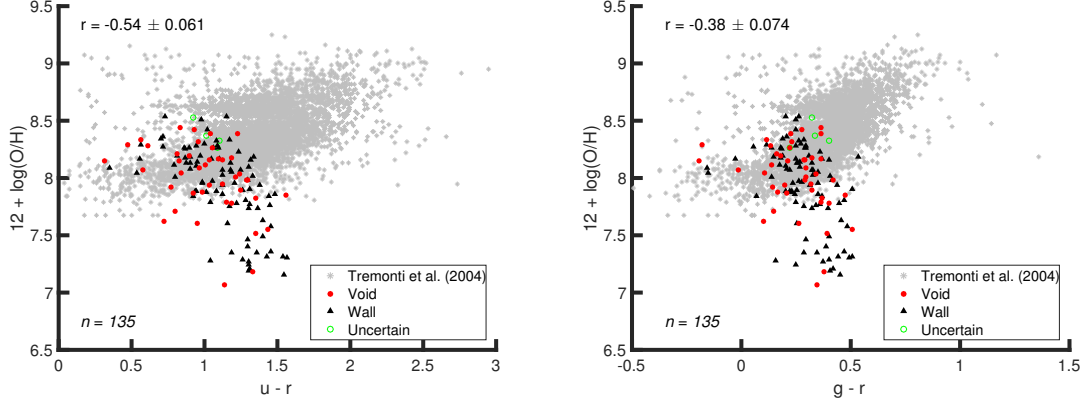


Figure 2.10: Color ($u-r$ and $g-r$) versus metallicity of the 135 analyzed dwarf galaxies. Error bars have been omitted for clarity. Metallicity is expected to have a positive correlation with color, as older galaxies are expected to have higher metallicities. To place our galaxies in the context of the dwarf galaxy population, we also plot (grey stars) dwarf galaxies ($M_r > -17$) with metallicity estimates by Tremonti et al. (2004). We find no significant difference between the void and wall dwarf galaxies, indicating little to no large-scale environmental influence on the color-metallicity relation.

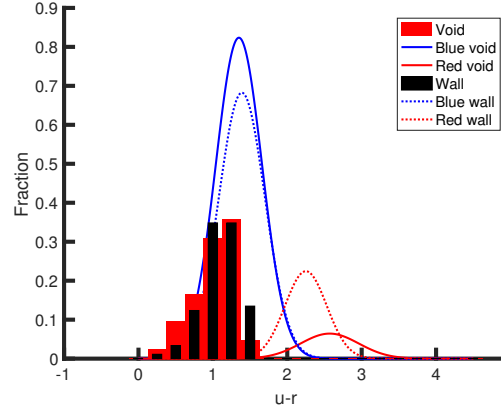


Figure 2.11: The $u - r$ color distribution of our 135 dwarf galaxies (red/black histograms) as compared to the color distribution of all SDSS dwarf galaxies as found in Fig. 4 of Hoyle et al. (2012) (red/blue curves). It is clear that our galaxies are among the bluest dwarf galaxies in SDSS.

2.5 Discussion

2.5.1 Comparison to literature results

We find no clear distinction between the metallicities of dwarf galaxies in voids and dwarf galaxies in more dense regions. This result agrees with the results of Mouhcine et al. (2007); Cooper et al. (2008); Nicholls et al. (2014b); Kreckel et al. (2015) but disproves our initial hypothesis and contradicts the published results of Pustilnik et al. (2006, 2011b); Pustilnik (2014); Sánchez Almeida et al. (2016). Cooper et al. (2008) concludes that metal-rich galaxies preferentially reside in high-density regions. Due to our requirement on the [OIII] $\lambda 4363$ auroral line, we have very few dwarf galaxies with high metallicities. As a result, we are not able to confirm their conclusions. Deng (2011) also reports a relationship between environment and metallicity. However, he highlights a large difference in metallicity as a function of redshift which correlates with his two samples. It is possible that the dependence he found is actually the result of a systematic dependence on redshift in their metallicity calculation.

Many studies suggest that the metallicity of void galaxies should, on average, be lower than that of galaxies in more dense regions. Mouhcine et al. (2007) and Cooper et al. (2008) both perform statistical studies of this relationship on SDSS DR4, and Deng (2011) repeats this with the DR7 data (only looking at galaxies with a redshift $z > 0.02$). Mouhcine et al. (2007) conclude that the relation between stellar mass and metallicity is much stronger than that between a galaxy's environment and its metallicity. Cooper et al. (2008) find a more substantial correlation between a galaxy's environment and its metallicity, but point out that the noise of the different methods used to calculate metallicity is larger than any environment-metallicity relation. Our analysis shows that there is very little difference between void and wall dwarf galaxies, suggesting that the large-scale environment does not strongly influence a dwarf galaxy's chemical evolution.

2.5.2 Large-scale environmental influence

Consideration of interactions between the interstellar medium (ISM), circumgalactic medium (CGM), and intergalactic medium (IGM) suggests that void galaxies should have relatively lower metallicity than galaxies in denser environments. We find no such trend, perhaps because the IGM around

star-forming “wall galaxies” in our sample is similar to that of void galaxies.

Simulations by Cen (2011) show that the entropy of gas in the IGM in voids remains below the critical entropy (defined to be when the cooling time of the gas is equal to the Hubble time), so the gas from the IGM can cool and fall into a void galaxy’s CGM. In a galaxy’s ISM, supernovae expel gas (primarily metal-rich) into the CGM. This gas has a higher metallicity than the average metallicity of the ISM (shown by Muratov et al., 2017). While some of this gas reaches the outer edge of the CGM, most of it cools and falls back onto the galaxy’s ISM, after having mixed with the hydrogen that has entered the CGM from the IGM. Therefore, the gas falling back into the galaxy’s ISM has a lower metallicity than the galaxy’s ISM.

In contrast to the void galaxies, the IGM around most wall galaxies is not cool enough to fall back onto the CGM. Cen (2011) shows that, in general, the IGM of a wall galaxy has an entropy higher than the threshold for cooling. As a result, most of the gas that falls back onto a wall galaxy’s ISM is not as diluted as what falls onto a void galaxy’s ISM. This is where our hypothesis originated: because wall galaxies no longer have a source of cool hydrogen in the IGM, their metallicities will be higher than that of the void galaxies (for a fixed stellar mass).

However, Fig. 2.4 does not reveal a lower metallicity in void galaxies. Instead, our results indicate that there is no difference in the distribution of metallicities in wall and void galaxies. In detail, Fig. 10 of Cen (2011) shows that not all wall galaxies rise above the entropy threshold. This is also coincident with the sSFR of the galaxies — those galaxies with higher sSFRs are below the entropy threshold, while those with low sSFRs are above (independent of their large-scale environment). Since all our galaxies have relatively high sSFRs (as required by the analysis — star formation is required to detect the emission lines necessary for the metallicity calculations), it is possible that our population of wall dwarf galaxies is still surrounded by a cool IGM, similar to that of the void galaxies. As a result, the wall galaxies still have a source of cool hydrogen, so the resulting distribution of the metallicities in the wall and void dwarf galaxies is the same. Brisbin & Harwit (2012) show that most star-forming galaxies with $M_* < 2.0 \times 10^{10} M_\odot$ appear to be fed by the infall of pristine or low-metallicity gas. Moran et al. (2012) also find that the lowest-mass galaxies

($\log(M_*) < 10.2 M_\odot$) have a sharp decline in their metallicity at large radii; coupled with a strong correlation to the galaxies' HI masses, they concluded that this indicates newly accreted pristine gas in the galaxies. It appears that the large-scale ($10 h^{-1}$ Mpc) has little effect on the chemical evolution of galaxies; a galaxy's medium-scale ($2 h^{-1}$ Mpc) environment might have much more influence on its chemical evolution.

2.5.3 Extreme low-metallicity galaxies

Based on observations of six extremely low-metallicity galaxies found in voids, Pustilnik et al. (2006, 2011b, 2013) infer that there is a fractionally larger population of metal-poor galaxies located in voids than in more dense regions. Filho et al. (2015) study the environment of 140 extremely metal-poor galaxies and find that they preferentially reside in low-density environments in the local universe. Of the 135 galaxies we analyze, twenty-one have extremely low gas-phase metallicity values ($12 + \log(\text{O/H}) < 7.6$); they are highlighted in Table 2.3. Of these twenty-one galaxies, only four are found in voids (roughly 10% of the dwarf void population measured) and seventeen are located in more dense regions (about 19% of the dwarf wall population measured). These population fractions do not support the existence of a special population of extreme metal-poor galaxies in voids, although the statistics are very small. None of these galaxies share the same local environment (none are neighbors to each other). In addition, Fig. 2.4 shows no evidence to support a special population of extremely metal-poor galaxies in the voids, as extremely metal-poor galaxies are more prevalent in the more dense regions.

We find that these twenty-one extremely metal-poor galaxies are redder and have a lower (s)SFR than the others when looking at the color (Fig. 2.10) and (specific) star formation rate (Fig. 2.8) of the 135 analyzed galaxies. The [OIII] $\lambda 4363$ auroral line is within the noise of the spectra in thirteen of these extremely metal-poor dwarf galaxies. While normally such a weak detection of this line corresponds to a high metallicity (see Sec. 2.2.2 for details), most of the spectra of these twenty-one galaxies have very low S/N overall. As a result, it is not surprising that [OIII] $\lambda 4363$ is within the noise here. Further study of these twenty-one galaxies is recommended, to confirm these low metallicity values.

Table 2.3: Details of the 21 extreme low gas-phase metallicity ($12 + \log(\text{O}/\text{H}) < 7.6$) galaxies found. Four of these galaxies are located in voids (about 10% of the void dwarf population measured) and seventeen are in more dense regions (about 19% of the wall dwarf population measured); thus, there does not seem to be a special population of extreme low-metallicity galaxies in voids. Further study of these galaxies is recommended to confirm metallicity values and identify any shared characteristics.

Index ^a	R.A.	Decl.	Redshift	$12 + \log (\frac{\text{O}}{\text{H}})$	Void/Wall
268470	13 ^h 18 ^m 17 ^s .82	+02°12'59".83	0.0252	7.06 ± 0.37	Void
1422637	14 ^h 18 ^m 12 ^s .14	+13°59'33".98	0.0261	7.15 ± 0.41	Wall
839665	08 ^h 09 ^m 53 ^s .53	+29°17'04".82	0.0281	7.18 ± 0.44	Void
1168448	11 ^h 06 ^m 41 ^s .00	+45°19'09".28	0.0220	7.19 ± 0.46	Wall
1299291	12 ^h 17 ^m 14 ^s .02	+43°18'53".36	0.0233	7.21 ± 0.42	Wall
1170573	11 ^h 05 ^m 39 ^s .42	+46°03'28".37	0.0250	7.24 ± 0.34	Wall
2288717	10 ^h 46 ^m 12 ^s .18	+21°31'37".37	0.0248	7.27 ± 0.48	Wall
955643	11 ^h 42 ^m 03 ^s .02	+49°21'25".18	0.0244	7.28 ± 0.44	Wall
1344311	12 ^h 33 ^m 13 ^s .64	+11°10'28".46	0.0245	7.29 ± 0.50	Wall
1254352	13 ^h 29 ^m 02 ^s .45	+10°54'55".80	0.0237	7.30 ± 0.44	Wall
1857820	08 ^h 45 ^m 00 ^s .34	+27°16'47".04	0.0257	7.31 ± 0.48	Wall
866876	09 ^h 04 ^m 57 ^s .96	+41°29'36".42	0.0240	7.32 ± 0.40	Wall
833588	08 ^h 43 ^m 10 ^s .71	+43°08'53".58	0.0245	7.34 ± 0.41	Wall
283263	14 ^h 14 ^m 12 ^s .88	+01°50'12".88	0.0255	7.35 ± 0.43	Wall
184308	09 ^h 39 ^m 09 ^s .38	+00°59'04".15	0.0244	7.36 ± 0.43	Wall
1389829	14 ^h 31 ^m 01 ^s .38	+38°04'21".50	0.0269	7.41 ± 0.46	Wall
858951	09 ^h 31 ^m 39 ^s .60	+49°49'56".85	0.0251	7.46 ± 0.46	Wall
1270221	13 ^h 27 ^m 39 ^s .85	+50°54'09".69	0.0295	7.49 ± 0.43	Wall
431383	08 ^h 58 ^m 44 ^s .96	+50°29'58".98	0.0230	7.52 ± 0.60	Void
75442	13 ^h 13 ^m 24 ^s .25	+00°15'02".95	0.0264	7.55 ± 0.35	Void
1322765	14 ^h 15 ^m 05 ^s .58	+36°22'57".77	0.0273	7.57 ± 0.40	Wall

2.6 Conclusions

Using spectroscopic line flux measurements of galaxies in the SDSS DR7 sample available through the MPA-JHU catalog, we estimate the metallicity of dwarf galaxies based on the Direct T_e method. From the 135 galaxies analyzed, there appears to be no large-scale environmental dependence of the metallicity of these galaxies, as the distributions of metallicity values are very similar for those residing in voids and those in more dense regions. Thus, the large-scale (~ 10 Mpc) environment does not appear to strongly influence the chemical evolution of dwarf galaxies.

We examine the relationship between metallicity and other physical characteristics of our dwarf galaxies. In the mass-metallicity relation, our galaxies are at the low-mass extreme; the extreme low metallicity galaxies we found are scattered below this relation. All our dwarf galaxies are at the upper limit in total (s)SFR, and they are on the blue end of the color spectrum. There is no large-scale environmental dependence of the metallicity in any of these categories.

No special population of extremely metal-poor galaxies is found in the voids, as extremely metal-deficient galaxies are found in both voids and walls. A more detailed study of these twenty-one galaxies is recommended, to confirm their metallicity values and discover characteristics shared by the population.

Although over 800,000 galaxies in SDSS DR7 have spectroscopic observations, only 135 are dwarf galaxies with metal line fluxes necessary to estimate gas-phase oxygen abundances using the Direct T_e method. Unfortunately, this was not enough to re-calibrate any of the more common methods used to calculate metallicity for use on dwarf galaxies. Better data are required to discern the metallicity of a larger selection of dwarf galaxies, from which accurate calibrations can be developed. These estimated ionic abundances can then be compared with predictions of the environmental dependence of star formation and metallicity from high-resolution hydrodynamic simulations.

Chapter 3: Large-scale environmental dependence of the abundance ratio of nitrogen to oxygen in blue, star-forming galaxies fainter than L_*

This chapter is published in the *Astrophysical Journal*, 2017 (Vol. 837, pages 42–55) by Kelly A. Douglass & Michael S. Vogeley; it will be referenced as Douglass & Vogeley (2017b).

Abstract

We examine how the cosmic environment affects the chemical evolution of galaxies in the universe by comparing the N/O ratio of dwarf galaxies in voids with dwarf galaxies in denser regions. Ratios of the forbidden [O III] and [S II] transitions provide estimates of a region’s electron temperature and number density. We estimate the abundances of oxygen and nitrogen using these temperature and density estimates and the emission-line fluxes [O II] $\lambda 3727$, [O III] $\lambda\lambda 4959, 5007$, and [N II] $\lambda\lambda 6548, 6584$ with the direct T_e method. Using spectroscopic observations from the Sloan Digital Sky Survey Data Release 7, we are able to estimate the N/O ratio in 42 void dwarf galaxies and 89 dwarf galaxies in denser regions. The N/O ratio for void dwarfs ($M_r > -17$) is slightly lower ($\sim 12\%$) than for dwarf galaxies in denser regions. We also estimate the nitrogen and oxygen abundances of 2050 void galaxies and 3883 galaxies in denser regions with $M_r > -20$. These somewhat brighter galaxies (but still fainter than L_*) also display similar minor shifts in the N/O ratio. The shifts in the average and median element abundance values in all absolute magnitude bins studied are in the same direction, suggesting that the large-scale environment may influence the chemical evolution of galaxies. We discuss possible causes of such a large-scale environmental dependence of the chemical evolution of galaxies, including retarded star formation and a higher ratio of dark matter halo mass to stellar mass in void galaxies.

3.1 Introduction

The measurement of the abundance of heavier elements relative to hydrogen in a galaxy can indicate the galaxy’s evolutionary stage. As stars evolve, they slowly convert hydrogen into heavier elements,

increasing the ratio of the heavier elements (oxygen, nitrogen, etc.) to hydrogen. The ratio of oxygen to hydrogen is often used to determine the chemical evolution of a galaxy because oxygen is the most abundant element in the universe (after hydrogen and helium) and because oxygen has very strong emission lines in the optical regime that cover a range of ionization states (Kewley & Dopita, 2002).

It is instructive to also study the relative abundances of the heavy elements in a galaxy. Rather than indicating the amount of hydrogen converted to heavier elements, the ratio of two heavy elements can reveal important details about the nucleosynthesis process and the chemical conditions of the galaxy when the last star formation episode occurred (Izotov & Thuan, 1999). One of the easiest and most informative ratios to study is nitrogen to oxygen.

From what we currently understand of stellar nucleosynthesis, we can group its products into two classes: primary and secondary elements. The yields of primary elements (carbon and oxygen, for example) are independent of the initial metallicity of the star, while the yields of secondary elements depend on the initial abundance of heavy elements in the star. Nitrogen is unique — it can behave as both a primary and secondary element (Matteucci, 1986). Nitrogen is produced during the CNO cycle, which is one of the two main processes of hydrogen burning in a star. The CNO cycle fuses four protons into a helium atom with two positrons and two electron neutrinos as by-products. It tends to occur in more massive stars than our Sun, due to the higher temperature required for the fusion processes involved. Carbon is a catalyst of the CNO cycle, not a product. As a result, if carbon is not initially present within the star, then nitrogen is produced in the same relative abundance as carbon and oxygen — nitrogen behaves as a primary element. However, if the interstellar medium (ISM) has a relatively high abundance of heavier elements from previous star formation episodes, then nitrogen behaves as a secondary element, since its production is based on carbon and oxygen produced prior to the star's creation.

The majority of the production of oxygen and nitrogen is thought to occur in different mass stars — nitrogen is produced in the CNO cycle of intermediate-mass stars ($4M_{\odot} < M_* < 8M_{\odot}$), while oxygen is primarily produced in the helium-, carbon-, and neon-burning stages of higher-mass stars ($M_* > 4M_{\odot}$) (Henry et al., 2000, 2006). The CNO cycle can occur in lower-mass stars (the

minimum temperature is only 1.5×10^7 K), but it requires carbon as a catalyst. If there is already carbon present in a star at its birth, the CNO cycle can commence much earlier in the star's lifetime than if it is composed primarily of hydrogen at its birth.

A measurement of the N/O ratio indicates where a galaxy is in its chemical evolution. The relative amounts of these two elements can be influenced by nucleosynthesis, a galaxy's star formation history, and/or a varying initial mass function (IMF), for example. The star formation history of a galaxy can be strongly influenced by the galaxy's environment. Galactic interactions can cause bursts of star formation in addition to secular star formation. Due to the time delay in the release of nitrogen and oxygen from the stellar population, galaxies that have more recently experienced star formation will result in lower N/O ratios (since oxygen is released sooner than nitrogen, due to higher-mass stars being responsible for the production of oxygen). In addition to this time delay, if a galaxy has enough heavy elements present in its gas at the time of the stars' births, secondary nitrogen will be produced in addition to primary. This would result in higher N/O ratios, and there would be a correlation between the metallicity and the N/O ratio in the galaxies.

Large galaxy redshift surveys have shown that the large-scale structure of galaxies is similar to that of a three-dimensional cosmic web (Bond et al., 1996), where voids (large, underdense regions that occupy approximately 60% of space) separate galaxy clusters that are connected by thin filaments of galaxies. These cosmic voids are an important environment for studying galaxy formation (see van de Weygaert & Platen, 2011, for a review), as the Λ CDM cosmology predicts void galaxies to have lower mass and be retarded in their star formation when compared to those in denser environments (e.g., Gottlöber et al., 2003; Goldberg et al., 2005; Cen, 2011). Because dwarf galaxies are sensitive to many astrophysical effects, including cosmological reionization, internal feedback from supernovae and photoheating from star formation, external effects from tidal interactions and ram pressure stripping, small-scale details of dark matter halo assembly, and properties of dark matter, they should be the most sensitive to the effects of the void environment.

Previous work by Douglass & Vogeley (2017a) (hereafter Paper I) shows that there is no large-scale environmental dependence of the amount of oxygen in dwarf galaxies, in contrast to earlier

studies by Pustilnik et al. (2006), Cooper et al. (2008), Deng (2011), and Filho et al. (2015), for example. One of the main arguments for the existence of an environmental dependence of the metallicity of galaxies centers around the idea that void galaxies are surrounded by pristine hydrogen that is unavailable to galaxies in denser regions. By looking at just N/O, we remove the hydrogen dependence of the relative abundances. Detecting a difference in the N/O ratio due to the large-scale environment would indicate that the cosmic environment has some influence on the nucleosynthesis of secondary elements. In addition, if the environment does have some very minor effect on the metallicity of a galaxy, removing the hydrogen dependence could amplify this effect above the noise of the data. Combined with the metallicity results in Paper I, we might be able to discern a large-scale environmental effect on the chemical evolution of galaxies.

Large-scale sky surveys like the Sloan Digital Sky Survey (SDSS; Abazajian et al., 2009) contain a large sample of dwarf galaxies, allowing us to analyze the dwarf galaxy population in the nearby universe with more statistical significance. Over 1000 voids have been identified in SDSS DR7 (Pan et al., 2012), and SDSS provides spectroscopy to permit abundance estimates of those dwarf galaxies found in these voids. Thus, we are able to estimate the N/O ratio as a function of large-scale environment for the largest sample of dwarf galaxies to date.

We make use of the MPA-JHU catalog’s reprocessed spectroscopic data¹ to study the N/O abundance ratio of a large collection of dwarf galaxies in SDSS DR7. Because our analysis depends on the weak [OIII] $\lambda 4363$ auroral line, the MPA-JHU catalog’s more detailed treatment of the stellar continuum permits the weaker emission lines to become more apparent. As a result, using this catalog’s flux measurements should improve the accuracy of our results. We study the N/O abundance ratio of these dwarf galaxies as a function of large-scale environment to discern whether the large-scale environment has an effect on the relative abundance of heavier elements in dwarf galaxies.

Our paper is organized as follows. Section 2 describes the method used to estimate the chemical abundances in galaxies. We remind the reader of the source of our data in Section 3. Section 4

¹Available at <http://www.mpa-garching.mpg.de/SDSS/DR7/>

includes the results of our analysis, and Section 5 is a discussion of the implications of our results on the large-scale environmental effects on galaxy evolution. Finally, Section 6 summarizes our conclusions and discusses future work.

3.2 Estimation of gas-phase chemical abundances from optical spectroscopy

We study a galaxy's oxygen and nitrogen abundances because they are relatively abundant elements, they emit strong lines in the optical regime (including for several ionization states in oxygen), and a ratio of some of the oxygen lines provides a good estimate of the electron temperature (Kewley & Dopita, 2002). What follows is a description of the theory and methods we employ to estimate the oxygen and nitrogen abundances in dwarf galaxies.

3.2.1 [N II]

The energy-level diagram for the various transitions of [N II] is very similar to that of [O III], since they have the same electron ground-state configuration $((1s)^2(2s)^2(2p)^2)$. The similarities can be seen in Fig. 3.1. Therefore, an estimate of the electron temperature can be made from the [N II] $\lambda 5755$ emission line. However, this line is weaker than the [O III] $\lambda 4363$ auroral line (since there is less N than O in galaxies), so we use the [O III] auroral line for our temperature estimates, as in Paper I. After obtaining a temperature and density estimate, we use the [N II] $\lambda\lambda 6548, 6584$ doublet to estimate the abundance of singly ionized nitrogen in a galaxy.

3.2.2 Direct T_e method

We use the same method to calculate the nitrogen abundance as in Paper I to estimate the oxygen abundance. However, here we use the [N II] $\lambda\lambda 6548, 6584$ doublet instead of the [O II] $\lambda 3727$ and [O III] $\lambda\lambda 4959, 5007$ doublets. Because the temperature estimate depends on the auroral line [O III] $\lambda 4363$, this method is often difficult to employ. As a result, it works best with low-redshift, low-metallicity galaxies. The electron temperature is derived by solving the following system of equations:

$$t_3 = \frac{1.432}{\log[(\lambda 4959 + \lambda 5007)/\lambda 4363] - \log C_T} \quad (3.1)$$

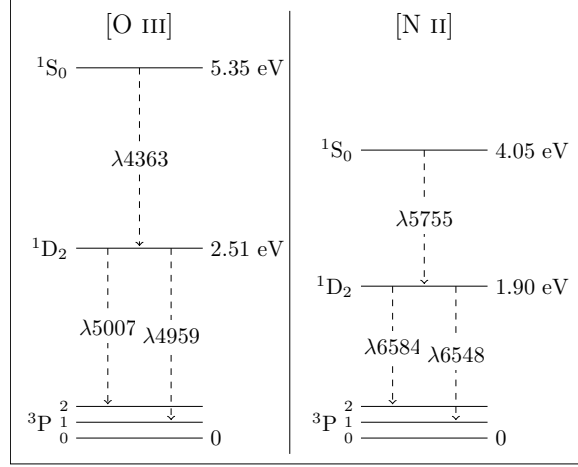


Figure 3.1: Energy-level diagram for [O III] and [N II] ($2p^2$) ions. The most important transitions are shown; all are in the visible spectrum. These forbidden transitions in both oxygen and nitrogen provide an estimate of the electron temperature in the interstellar gas. Because oxygen is more abundant, we use the oxygen lines to estimate the temperature of the gas.

where $t_3 = 10^{-4}T_e(O^{++})$ and

$$C_T = (8.44 - 1.09t_3 + 0.5t_3^2 - 0.08t_3^3) \frac{1 + 0.0004x_3}{1 + 0.044x_3} \quad (3.2)$$

where $x_3 = 10^{-4}n_e t_3^{-0.5}$. The ionic abundances are then found with the equations

$$12 + \log \left(\frac{O^{++}}{H^+} \right) = \log \frac{\lambda 4959 + \lambda 5007}{H\beta} + 6.200 + \frac{1.251}{t_3} - 0.55 \log t_3 - 0.014t_3 \quad (3.3)$$

$$12 + \log \left(\frac{O^+}{H^+} \right) = \log \frac{\lambda 3727}{H\beta} + 5.961 + \frac{1.676}{t_2} - 0.40 \log t_2 - 0.034t_2 + \log(1 + 1.35x_2) \quad (3.4)$$

$$12 + \log \left(\frac{N^+}{H^+} \right) = \log \frac{\lambda 6548 + \lambda 6584}{H\beta} + 6.234 + \frac{0.950}{t_2} - 0.42 \log t_2 - 0.027t_2 + \log(1 + 0.116x_2) \quad (3.5)$$

where $t_2 = 10^{-4}T_e(O^+)$ and $x_2 = 10^{-4}n_e t_2^{-0.5}$. We assume that $T_e(N^+) = T_e(O^+)$.

The signal-to-noise ratio of the SDSS spectra is too low to directly estimate the temperature of the gas in the low-ionization zone. As a result, we use the relation $t_2 = 0.7t_3 + 0.3$ by Garnett (1992). This relation has been shown to overestimate this temperature (Andrews & Martini, 2013). Since the metal emission lines are the primary method of cooling for the gas, a high temperature corresponds

to a low metallicity. Therefore, an overestimate of the temperature results in an underestimated abundance. As shown in Paper I, this only affects perhaps 15 of the dwarf galaxies in our sample and does not influence our conclusions.

The sum of the abundances of each of the element's ionization states is equal to the total abundance of any element, whether or not all ionization states are observed. Most of oxygen exists as either singly or doubly ionized, so the total oxygen abundance is

$$\frac{O}{H} = \frac{O^{++}}{H^+} + \frac{O^+}{H^+} \quad (3.6)$$

Since we can only observe the nitrogen abundance in one of the main ionization states, we use an ionization correction factor (ICF) to account for the missing states. For any element X, the total abundance is

$$\frac{X}{H} = \sum_i ICF_i \frac{X^i}{H} \quad (3.7)$$

For nitrogen, we employ the ICFs as defined in Izotov et al. (2006):

$$ICF(N^+) = \begin{cases} -0.825v + 0.718 + \frac{0.853}{v} & \text{low } Z \\ -0.809v + 0.712 + \frac{0.852}{v} & \text{intermed } Z \\ 1.467v + 1.752 + \frac{0.688}{v} & \text{high } Z \end{cases} \quad (3.8)$$

where $v = O^+/(O^+ + O^{++})$. The range for low Z covers galaxies with $12 + \log(O/H) \leq 7.2$, while high Z includes galaxies with $12 + \log(O/H) \geq 8.2$. For galaxies with $7.2 < 12 + \log(O/H) < 7.6$, the values for the ICFs are a linear interpolation between the low- Z and intermediate- Z values, while the ICFs for galaxies with $7.6 < 12 + \log(O/H) < 8.2$ are a linear interpolation between the intermediate- Z and high- Z values.

The N/O ratio can be found from the O/H and N/H ratios:

$$\log\left(\frac{N}{O}\right) = \left[12 + \log\left(\frac{N}{H}\right)\right] - \left[12 + \log\left(\frac{O}{H}\right)\right] \quad (3.9)$$

3.3 SDSS data and galaxy selection

The SDSS Data Release 7 (DR7; Abazajian et al., 2009) uses drift scanning to map approximately one-quarter of the northern sky; it is a wide-field multiband imaging and spectroscopic survey. A dedicated 2.5 m telescope at the Apache Point Observatory in New Mexico (Fukugita et al., 1996; Gunn et al., 1998) takes the photometric data in the five-band SDSS system — u , g , r , i , and z . Galaxies selected for spectroscopic analysis must have a Petrosian r -band magnitude $m_r < 17.77$ (Lupton et al., 2001; Strauss et al., 2002). Two double fiber-fed spectrographs and fiber plug plates take the spectra in an observed wavelength range of 3800–9200 Å with a resolution $\lambda/\Delta\lambda \sim 1800$ and a minimum fiber separation of 55" (Blanton et al., 2003). As in Paper I, we use the emission-line flux data from the MPA-JHU value-added catalog, which is based on the SDSS DR7 sample of galaxies. Total star formation rates and total specific star formation rates are also from the MPA-JHU value-added catalog, following the technique discussed in Brinchmann et al. (2004). The MPA-JHU catalog is also the source of the stellar mass estimates used, as calculated in Tremonti et al. (2004), following the method outlined in Kauffmann et al. (2003). The KIAS value-added galaxy catalog (Choi et al., 2010) is our source of the absolute magnitudes and colors of the galaxies.

3.3.1 Spectroscopic selection

The following requirements are implemented on the SDSS DR7 main spectroscopic galaxy sample described above. We use the same requirements for our sample as in Paper I; all galaxies must have

1. $M_r > -17$ (dwarf galaxies);
2. a minimum 5σ detection of $H\beta$;
3. a minimum 1σ detection of [O III] $\lambda 4363$;
4. a flux > 0 for all other required lines;
5. $T_e(\text{O III}) < 3 \times 10^4$ K;
6. a star-forming BPT classification by Brinchmann et al. (2004).

We also use the `oii_flux` value from the MPA-JHU catalog in place of their [O II] $\lambda\lambda 3726, 3729$ flux measurement since we are working at such low redshifts ($0.02 < z < 0.03$). Detailed descriptions of these criteria can be found in Section 3.1 of Paper I.

3.3.2 Void classification

The large-scale environment of the galaxies was determined using the void catalog constructed by Pan et al. (2012), which is based on the galaxies in the SDSS DR7 catalog. The VoidFinder algorithm of Hoyle & Vogeley (2002) removes all isolated galaxies with absolute magnitudes $M_r < -20$ (a galaxy is defined to be isolated if its third nearest neighbor is more than $7 h^{-1}$ Mpc away). Placing a grid over the remaining galaxies, VoidFinder grows spheres in the centers of all grid cells that contain no galaxies. The spheres expand until they encounter four galaxies on the surface. To be considered part of a void, a sphere must have a minimum radius of 10 Mpc; two spheres that overlap by more than 10% are considered part of the same void. We refer the reader to Hoyle & Vogeley (2002) for a more detailed description of the VoidFinder algorithm. Using these voids, galaxies that live within any void sphere are classified as a void galaxy; those that are outside the spheres are considered wall galaxies. Due to the construction of the void spheres, we cannot identify any voids within 10 Mpc of the edge of the survey. As a result, the large-scale environment of any galaxy within this boundary is uncertain.

9519 of the $\sim 800,000$ galaxies with spectra available in SDSS DR7 are dwarf galaxies ($M_r > -17$). 42 void dwarf galaxies, 89 wall dwarf galaxies, and 4 dwarf galaxies with uncertain large-scale environments are left to analyze after applying the spectroscopic cuts (or 135 dwarf galaxies in total, 131 of which are used in the environmental study).

3.4 Abundance analysis and results

Our primary objective is to perform a relative measurement of the N/O ratio of dwarf galaxies to discern how the large-scale environment affects their chemical evolution. As discussed in Paper I, multiple methods have been developed for metallicity calculations based on the quality of the spectra. We use only the direct T_e method for our abundance calculations, due to the limited galaxy

types used in the calibration or theoretical development of other methods.

For reference, the solar metallicity $Z_{\odot} = 8.69 \pm 0.05$ (Asplund et al., 2009).

3.4.1 Estimation of uncertainties and comparison of N/O and N⁺/O⁺

We estimate uncertainties in the computed abundances using a Monte Carlo method. We calculate 100,000 abundance estimates using the measured line fluxes and scaled uncertainty estimates. A new positive “fake” line flux is drawn from a normal distribution for each abundance estimate. The standard deviation in the sets of 100,000 calculated abundance values is used for the error in the abundance calculation. A more in-depth description of this process can be found in Paper I.

It has been common practice to assume that $\text{N}/\text{O} \cong \text{N}^{+}/\text{O}^{+}$, thus eliminating the need for the ICF in Eqn. 3.7. We find that this is a reasonable but slightly biased approximation, agreeing with the results of Nava et al. (2006). A comparison of the N/O ratio and the N⁺/O⁺ ratio for our set of dwarf galaxies can be seen in Fig. 3.2; galaxies with absolute magnitudes $M_r > -20$ are shown in gray for context. A linear fit to all star-forming galaxies with magnitudes $M_r > -20$ has a slope of only 0.927 ± 0.0018 , with an rms error of 0.032 for the fit. This comparison indicates that lower values of the N⁺/O⁺ ratio underestimate the N/O ratio, while higher values of N⁺/O⁺ overestimate the N/O ratio. Throughout this paper, we study the N/O ratio using ICF-corrected estimates of N/O (Eqns. 3.8 and 3.9).

3.4.2 Sources of systematic error

There is a radial dependence of many physical properties of galaxies (Bell & de Jong, 2000). Consequently, abundance estimates may depend on the locations of the spectroscopic fiber on the galaxy. If all of the galaxy’s light is not contained within the fiber of the spectrograph, the estimated abundances will not necessarily be representative of global abundance values. For example, Bell & de Jong (2000) show that the metallicity is not constant throughout a galaxy. Due to the spatially resolved spectra produced by MaNGA of SDSS-IV (SDSS Collaboration et al., 2016), a statistically significant measure of the radial dependence of a galaxy’s metallicity should soon be possible (Wilkinson et al., 2015). In SDSS DR7, the fiber diameter is 3”, corresponding to a physical diam-

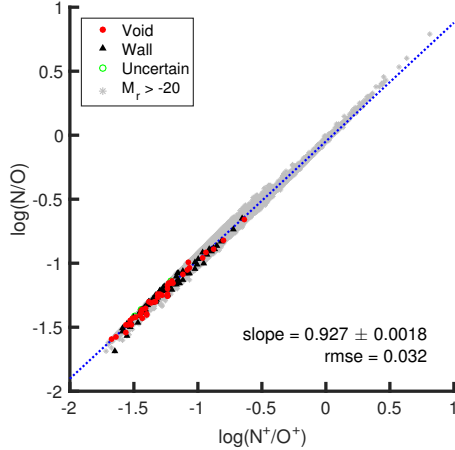


Figure 3.2: Comparison of the N/O and N⁺/O⁺ abundance ratios for our dwarf galaxies. Brighter galaxies ($M_r > -20$) are shown in gray for context. All our star-forming galaxies with $M_r > -20$ roughly follow the approximation that N/O \cong N⁺/O⁺, which is often assumed in other studies of the abundance ratio of nitrogen to oxygen. In this paper, we will be using the abundance ratio N/O for our analysis.

eter between 1.29 and 1.93 kpc at redshifts $0.02 < z < 0.03$. This covers a majority of most dwarf galaxies' luminous surfaces. The fiber is almost always placed on the brightest spot of the galaxy, which is often the center of the galaxy for spiral and ellipticals. Since the metallicity has been shown to decrease at large radius, these abundance values may be overestimates of the global abundances. Since many dwarf galaxies are irregular galaxies, the fiber is instead focused on a bright H II region. As a result, we are estimating the abundances of the gas from which stars recently formed.

We are implicitly limiting our sample of galaxies to only blue, star-forming dwarf galaxies as a result of our selection criteria outlined in Section 3.3.1. Consequently, this is not a representative sample of the full dwarf galaxy population. In this study we are only able to discuss the large-scale environmental influence on blue, star-forming dwarf galaxies within a narrow redshift range. It is impossible to use the direct T_e method to measure the chemical abundances of red dwarf galaxies because the UV photons from young stars are needed to excite the interstellar gas.

3.4.3 Galaxy abundances

Abundances estimated using the direct T_e method for our dwarf galaxy sample are listed in Table 3.1, along with other important characteristics and identification for the galaxies (including their

large-scale environment classification).

Oxygen and nitrogen abundances

Histograms of the resulting oxygen and nitrogen abundances are shown in Figs. 2.4 and 3.3, respectively. Both figures show very little difference in the distribution of abundance values in dwarf galaxies between voids and walls. A two-sample Kolmogorov-Smirnov (K-S) test quantifies this observation — it produced a test statistic of 0.13 for oxygen and 0.11 for nitrogen, corresponding to a probability of 67.1% and 83.8%, respectively, that a test statistic greater than or equal to this calculated test statistic will be measured if the void sample were drawn from the wall sample. The cumulative distribution function (CDF) of these samples can be seen in the right panel of Figures 2.4 and 3.3. The K-S test quantifies the visual impression in these figures that the distributions of oxygen and nitrogen abundances are similar for dwarf galaxies in voids and walls.

The average and median values of the dwarf galaxy abundances indicate very little large-scale environmental influence on the oxygen and nitrogen abundances. The average oxygen abundance for void dwarf galaxies is 7.99 ± 0.049 and the median is 8.04, while the average for wall dwarf galaxies is 7.93 ± 0.036 with a median value of 8.01. This implies that the wall dwarf galaxies have lower oxygen abundances by an average of 0.07 ± 0.060 relative to the void dwarf galaxies; the shift in the median values is 0.03 for the dwarf galaxies, with wall dwarf galaxies having lower oxygen abundances than void dwarf galaxies. There is also a shift in the nitrogen abundances for the dwarf galaxies: void dwarf galaxies have an average nitrogen abundance of 6.74 ± 0.035 and a median of 6.77, while the wall dwarf galaxies have an average nitrogen abundance of 6.72 ± 0.025 and a median of 6.75. Again, wall dwarf galaxies have, on average, 0.02 ± 0.043 lower nitrogen abundances than the void dwarf galaxies (the median shift for the nitrogen abundance of dwarf galaxies is 0.01, with wall galaxies lower than void dwarf galaxies). These shifts are within the uncertainty, so they are not statistically significant — if there is a large-scale environmental influence on the abundances of oxygen and nitrogen relative to hydrogen in dwarf galaxies, it is small.

To see how our results of the environmental dependence of dwarf galaxies compare with somewhat brighter galaxies, we perform the same analysis on galaxies with absolute magnitudes $-17 > M_r >$

Table 3.1: Five of the 135 dwarf galaxies analyzed from SDSS DR7. The flux values for all required emission lines can be found in the MPA-JHU value-added catalog. Metallicity values are calculated using the direct T_e method, with error estimates via a Monte Carlo method. The void catalog of Pan et al. (2012) is used to classify the galaxies as either Void or Wall. If a galaxy is located too close to the boundary of the SDSS to identify whether or not it is inside a void, it is labeled as Uncertain. (This table is available in its entirety in machine-readable form.)

Index ^a	R.A.	Decl.	Redshift	M_r	$12 + \log \left(\frac{O}{H} \right)$	$12 + \log \left(\frac{N}{H} \right)$	$\log \left(\frac{N}{O} \right)$	Void/Wall			
63713	09 ^h 20 ^m 04 ^s .27	-00°30'08".97	0.0257	-16.73	7.80	±0.41	6.83	±0.28	-0.97	±0.49	Wall
73537	09 ^h 25 ^m 24 ^s .23	+00°12'40".39	0.0250	-16.94	7.94	±0.34	6.76	±0.24	-1.18	±0.41	Wall
75442	13 ^h 13 ^m 24 ^s .25	+00°15'02".95	0.0264	-16.81	7.55	±0.35	6.73	±0.24	-0.82	±0.42	Void
168874	11 ^h 45 ^m 13 ^s .16	-01°48'17".68	0.0273	-16.99	8.16	±0.31	6.94	±0.21	-1.21	±0.37	Wall
184308	09 ^h 39 ^m 09 ^s .38	+00°59'04".15	0.0244	-16.73	7.36	±0.43	6.71	±0.31	-0.65	±0.53	Wall

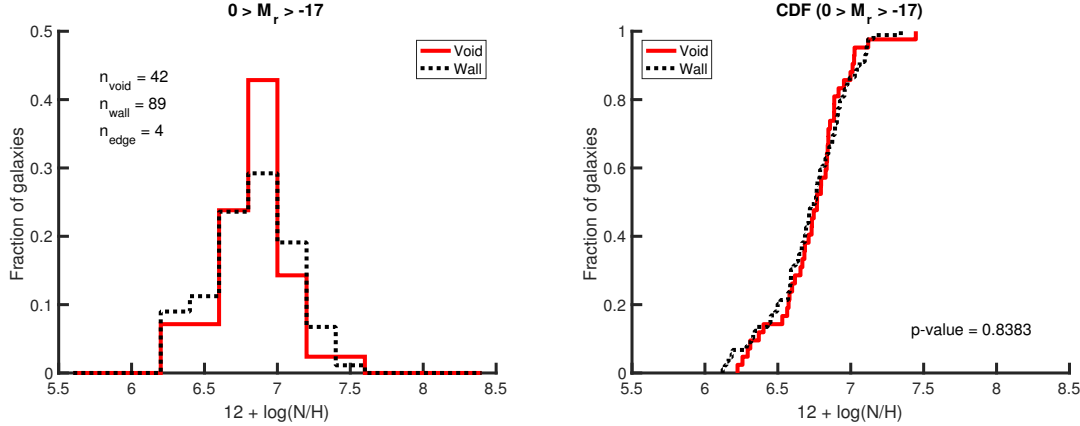


Figure 3.3: Abundance of nitrogen relative to hydrogen of void dwarf (red solid line) and wall dwarf (black dashed line) galaxies. A two-sample K-S test of the two data sets results in an asymptotic p -value of 0.84, indicating an 84% probability that a test statistic greater than the observed value of 0.11 will be seen if the void sample is drawn from the wall sample. This is reflected visually, as there appears to be very little difference between the two populations, indicating that there is little large-scale environmental influence on the nitrogen abundance of dwarf galaxies.

–20. The results of this analysis can be seen in Figs. 3.4 and 3.5. As the dwarf galaxies have already shown, there is no obvious large-scale environmental dependence of the oxygen and nitrogen abundances of these brighter galaxies. The results of a two-sample K-S test (listed in Table 3.2) mostly support this conclusion. In the brightest magnitude bin (galaxies with $-19 > M_r > -20$), the K-S test returns a p -value of only 0.00062 for the oxygen abundances, indicating only a 0.062% chance that there will be a test statistic greater than 0.07 if the void sample is drawn from the wall sample. The oxygen abundances for void galaxies are higher than the wall galaxies by an average of 0.04 ± 0.017 in this absolute magnitude bin, reinforcing the results of the K-S test that there is a large-scale environmental influence on the oxygen abundance in galaxies with magnitudes $-19 > M_r > -20$. While the results of the K-S test are not as convincing for this magnitude range in the nitrogen abundances, there is still an average shift of 0.02 ± 0.011 toward higher nitrogen abundances for void galaxies. While only one magnitude bin shows a statistically significant shift between the two environments, all magnitude bins are shifted in the same direction. This trend suggests that there may be a mild influence on the chemical evolution of galaxies due to their large-scale environment.

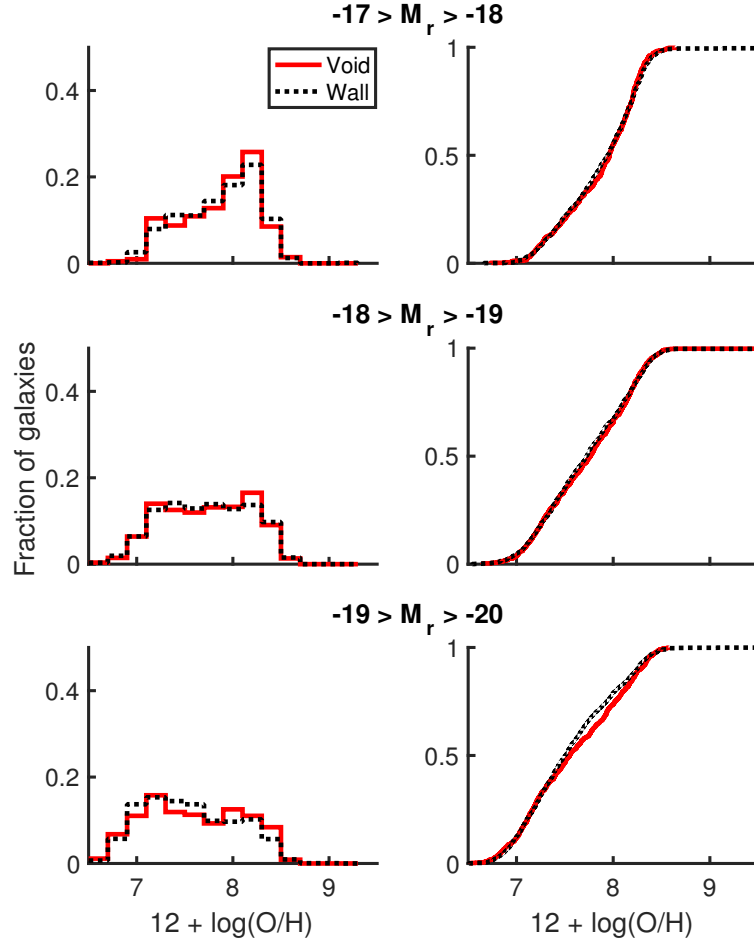


Figure 3.4: Gas-phase oxygen abundances relative to hydrogen of void (red solid line) and wall (black dashed line) star-forming galaxies with $-17 > M_r > -18$ (top), $-18 > M_r > -19$ (middle), and $-19 > M_r > -20$ (bottom). The results of a two-sample K-S test of the two data sets in each absolute magnitude range can be found in Table 3.2. These results are reflected visually, as there appears to be very little difference between the two populations (regardless of absolute magnitude), indicating that there is little large-scale environmental influence on the oxygen abundance of star-forming galaxies with absolute magnitudes $-17 > M_r > -20$.

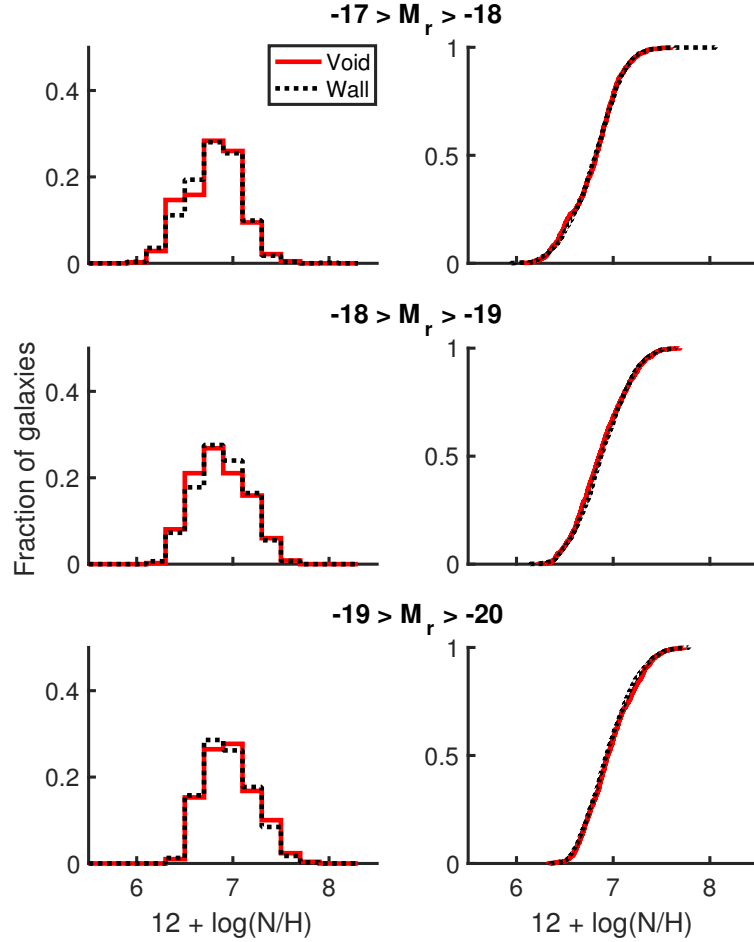


Figure 3.5: Abundance of nitrogen relative to hydrogen of void (red solid line) and wall (black dashed line) star-forming galaxies with $-17 > M_r > -18$ (top), $-18 > M_r > -19$ (middle), and $-19 > M_r > -20$ (bottom). The results of a two-sample K-S test of the two data sets in each absolute magnitude range can be found in Table 3.2. These results are reflected visually, as there appears to be very little difference between the two populations (regardless of absolute magnitude), indicating that there is little large-scale environmental influence on the nitrogen abundance of star-forming galaxies with absolute magnitudes $-17 > M_r > -20$.

We note that there appears to be a shift in the oxygen and nitrogen abundances between the absolute magnitude bins in Figs. 3.4 and 3.5 that is opposite to what is predicted by the mass-metallicity relation (Tremonti et al., 2004). This shift toward lower oxygen abundances as the galaxies increase in brightness is possibly due to the fact that the metallicity estimates are so dependent on the temperature-sensitive [O III] $\lambda 4363$ auroral line. As galaxies increase in metallicity, this line becomes weaker (as its strength is inversely proportional to the temperature). If the flux of this line is being underestimated, then the temperature is being overestimated, and therefore the oxygen and nitrogen abundances are being underestimated. If we are seeing an underestimate of flux of the [O III] $\lambda 4363$ emission line (and therefore an overestimate of the temperature in the region), then we should see a shift toward lower N/H values as the absolute magnitude is increased as well. This pattern can be seen in Fig. 3.5.

Ratio of nitrogen to oxygen

In addition to studying the oxygen and nitrogen abundances relative to hydrogen, we also look at the ratio of nitrogen to oxygen. The N/O abundance ratio suggests a slightly stronger environmental influence on the chemical evolution of dwarf galaxies than the oxygen and nitrogen abundances individually. As can be seen in Fig. 3.6, there is a shift in the N/O ratio to lower values in the void dwarf galaxies than in the wall dwarf galaxies. This difference is quantified in the K-S test — the test returned a probability of 11.1% that a test statistic greater than or equal to 0.22 will be measured if the void sample was drawn from the wall sample. The void dwarf galaxies have lower N/O ratios by an average of 0.05 ± 0.074 than the wall dwarf galaxies; the difference in the median values of the N/O ratio in the void and wall dwarf galaxy samples is 0.07. However, like the shifts seen in the oxygen and nitrogen abundances, the shift in the N/O ratio for dwarf galaxies is not statistically significant.

We perform the same analysis with the N/O ratio on somewhat brighter galaxies, up through $M_r > -20$; the results of this analysis can be seen in Fig. 3.7 and in Table 3.2. The shift toward lower N/O ratios for the void galaxies is small for all magnitude bins. The direction of the shift between environments for the N/O ratio is consistent for all absolute magnitude bins: void galaxies

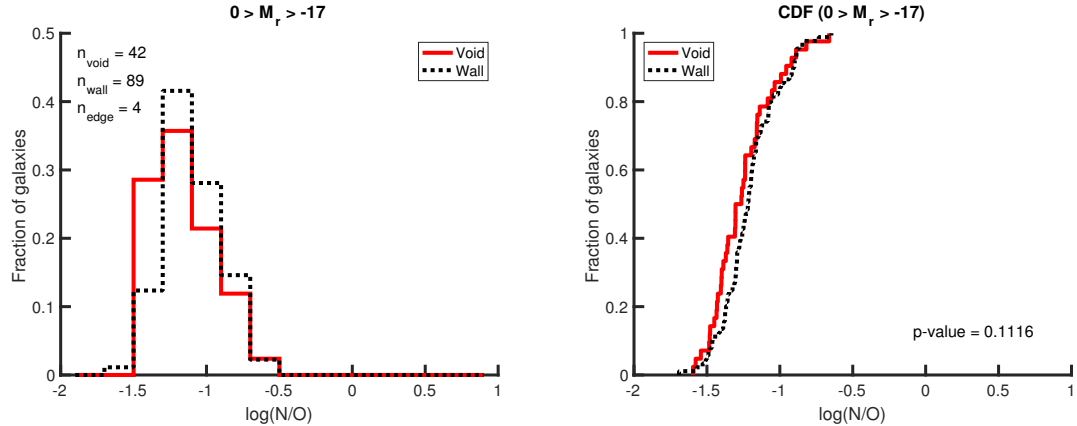


Figure 3.6: Ratio of nitrogen to oxygen of void dwarf (red solid line) and wall dwarf (black dashed line) galaxies. A two-sample K-S test of the two data sets results in an asymptotic p -value of 0.11, indicating an 11% probability that a test statistic greater than the observed value of 0.22 will be seen if the void sample was drawn from the wall sample. This is reflected visually, as the void galaxies appear to have a lower value of N/O than the wall galaxies. This is suggestive of a large-scale environmental influence on the relative chemical abundances in dwarf galaxies.

have slightly lower N/O ratios than wall galaxies. This is only very weak evidence of a large-scale environmental influence on the relative abundances of elements in galaxies, but it is worth testing for in larger samples.

Figure 3.7 indicates a shift toward higher values in the peak of the N/O distribution as the absolute magnitude of the galaxies increases. There is a known positive correlation between the N/O ratio and the stellar mass of a galaxy, as discussed in Sec. 3.4.5 below. To test whether this relation is causing the shift seen in Figs. 3.6 and 3.7, we downsampled the wall galaxies in each magnitude bin to match the void sample. The original shifts in the N/O ratio seen were still present after the downsampling; the observed shift in the N/O ratio is not due to any variations in the distribution of the stellar masses between the two environments. In addition, if we are overestimating the temperatures in these galaxies as a result of an incorrect measurement of [O III] $\lambda 4363$ (discussed above in Section 3.4.3), that effect should cancel when we look at the ratio of nitrogen to oxygen. This shift toward higher N/O values as a function of absolute magnitude indicates that brighter galaxies produce more nitrogen than fainter galaxies (relative to their oxygen abundance). This result is consistent with the theory that nitrogen behaves as a secondary element in

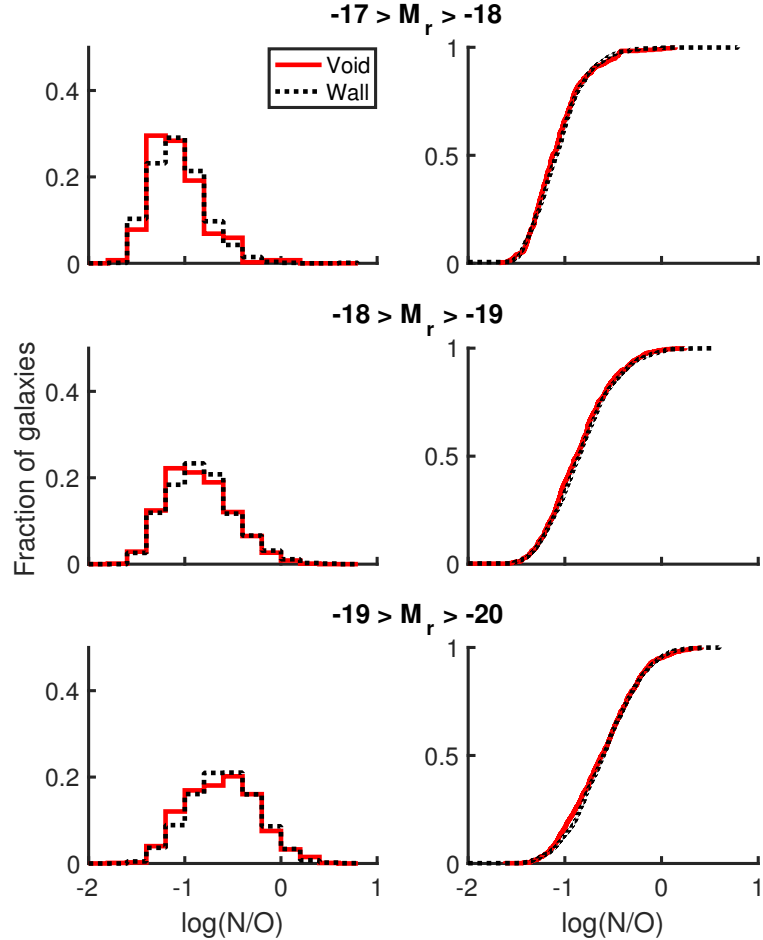


Figure 3.7: Ratio of nitrogen to oxygen of void (red solid line) and wall (black dashed line) star-forming galaxies with $-17 > M_r > -18$ (top), $-18 > M_r > -19$ (middle), and $-19 > M_r > -20$ (bottom). The results of a two-sample K-S test of the two data sets in each absolute magnitude range can be found in Table 3.2, in addition to other statistics of the samples. Both the histograms, CDFs, and statistics suggest a very slight difference between the two populations, indicating a mild large-scale environmental influence on the relative chemical abundances of star-forming galaxies with absolute magnitudes $-17 > M_r > -20$.

galaxies with high enough metallicity, if we assume a positive correlation between absolute magnitude and metallicity.

3.4.4 N/O versus O/H

Comparing the N/O ratio with the gas-phase oxygen abundance in a galaxy can help us understand the nucleosynthesis of nitrogen in galaxies. When the metallicity of a galaxy is low, stars created from this gas do not have enough carbon to efficiently produce helium via the CNO cycle. As a result, any nitrogen produced in these stars will behave as a primary element — it will be produced in the same relative quantity as oxygen. However, when the metallicity of a galaxy is high enough, stars are created with enough seed carbon to initiate the CNO cycle at an earlier stage in the star’s life. As a result, nitrogen will behave as a secondary element and will be produced in a larger quantity relative to the primary elements (like oxygen and carbon). By studying the relation between N/O and the metallicity of a galaxy, we should be able to discern the critical metallicity at which nitrogen switches from a primary to a secondary element.

Our results for N/O versus metallicity can be seen in Fig. 3.8. Unlike many previous comparisons of N/O and metallicity (for example, Vila Costas & Edmunds, 1993; Thuan et al., 1995; Henry et al., 2000; Pilyugin et al., 2002; Lee et al., 2004; Pilyugin et al., 2004; Nava et al., 2006; van Zee & Haynes, 2006; Pérez-Montero & Contini, 2009; Amorín et al., 2010; Berg et al., 2012), we do not find a constant value for N/O as a function of O/H for dwarf galaxies (nor for any of the somewhat brighter galaxies). Shields et al. (1991), Contini et al. (2002), and Nicholls et al. (2014a) also find little or no evidence of a plateau in their study. Instead of a constant value for N/O as a function of O/H at low metallicities, we find a slight decrease in the N/O ratio as the metallicity increases; a linear fit to the dwarf galaxies reveals a slope of -0.38 ± 0.078 . This is close to the footnoted results of Andrews & Martini (2013), who find a slope of -0.21 for their stellar-mass-binned galaxies with metallicities $12 + \log(\text{O}/\text{H}) < 8.5$. The average value of $\log(\text{N}/\text{O})$ for the void dwarf galaxies is -1.25 ± 0.060 with a median value of -1.28 , while the average value for the wall dwarf galaxies is -1.21 ± 0.044 with a median of -1.22 . As shown in Fig. 3.6, the void dwarf galaxies have slightly less nitrogen relative to oxygen than do dwarf galaxies in denser regions. Both these median values

Table 3.2: Statistics of the gas-phase oxygen, nitrogen, and nitrogen relative to oxygen abundances in void and wall galaxies in each of the absolute magnitude ranges listed. Most of these results are not statistically significant, as shown in Figs. 2.4–3.7. However, the shifts in chemical abundances between the two environments are predominately in the same direction for each of the magnitude bins, suggesting that there is some influence on the chemical evolution of galaxies by the large-scale environment. Void galaxies have slightly higher oxygen and nitrogen abundances than wall galaxies, but void galaxies have slightly lower N/O ratios than wall galaxies.

Abs. Mag. Range	Environment	# of Galaxies	Average	Median	Average Shift ^a	Median Shift ^a	K-S Test Statistic	p-value
$12 + \log(\text{O/H})$								
Dwarf galaxies	Void	42	7.99 ± 0.049	8.04	-0.07 ± 0.060	-0.03	0.1322	0.6701
	Wall	89	7.93 ± 0.036	8.01				
	Void	423	7.87 ± 0.016	7.96	0.01 ± 0.020	-0.02	0.0455	0.5799
	Wall	895	7.88 ± 0.012	7.94				
-17 > M_r > -18	Void	829	7.74 ± 0.013	7.76	-0.01 ± 0.016	-0.04	0.0385	0.4000
	Wall	1498	7.73 ± 0.009	7.73				
-18 > M_r > -19	Void	798	7.59 ± 0.013	7.55	-0.04 ± 0.017	-0.05	0.0741	0.0062
	Wall	1490	7.55 ± 0.010	7.50				
$12 + \log(\text{N/H})$								
Dwarf galaxies	Void	42	6.74 ± 0.035	6.77	-0.02 ± 0.043	-0.01	0.1129	0.8383
	Wall	89	6.72 ± 0.025	6.75				
	Void	423	6.80 ± 0.011	6.82	0.00 ± 0.014	-0.01	0.0401	0.7364
	Wall	895	6.80 ± 0.008	6.81				
-17 > M_r > -18	Void	829	6.87 ± 0.009	6.85	0.01 ± 0.011	0.02	0.0538	0.0873
	Wall	1498	6.89 ± 0.007	6.87				
-18 > M_r > -19	Void	798	6.97 ± 0.009	6.94	-0.02 ± 0.011	-0.02	0.0455	0.2272
	Wall	1490	6.95 ± 0.007	6.93				
$\log(\text{N/O})$								
Dwarf galaxies	Void	42	-1.25 ± 0.060	-1.28	0.05 ± 0.074	0.07	0.2191	0.1116
	Wall	89	-1.21 ± 0.044	-1.22				
	Void	423	-1.08 ± 0.020	-1.13	-0.00 ± 0.024	0.04	0.0588	0.2657
	Wall	895	-1.08 ± 0.014	-1.09				
-17 > M_r > -18	Void	829	-0.86 ± 0.015	-0.88	0.02 ± 0.019	0.03	0.0550	0.0763
	Wall	1498	-0.84 ± 0.012	-0.85				
-18 > M_r > -19	Void	798	-0.62 ± 0.016	-0.62	0.02 ± 0.020	0.02	0.0564	0.0715
	Wall	1490	-0.60 ± 0.012	-0.60				

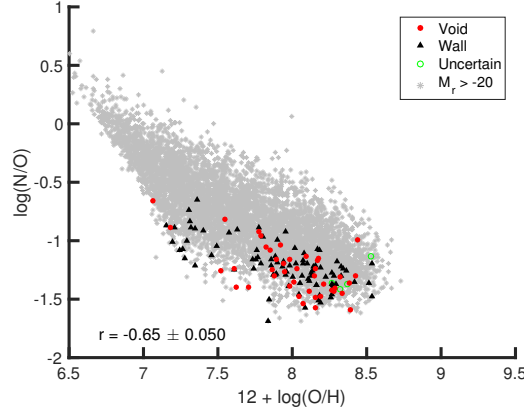


Figure 3.8: N/O as a function of O/H for star-forming void (red circles) and wall (black triangles) dwarf galaxies. Error bars have been omitted for clarity. N/O is expected to be constant for $12 + \log(O/H) \lesssim 8.5$, as the metallicity of a galaxy’s ISM is too low for stars to be created with enough of the heavy elements to undergo the CNO cycle early enough in their lifetimes. As a result, nitrogen behaves as a primary element at galactic metallicities less than approximately 8.5. To place the dwarf galaxies in the context of the general galaxy population, we also plot (gray stars) all star-forming galaxies fainter than $M_r > -20$.

are higher than that of Andrews & Martini (2013), and these average values are higher than that of Izotov & Thuan (1999) and Nava et al. (2006).

If a plateau in the O/H–N/O relation exists, then we should see a slope of 1 in the O/H–N/H relation. When looking at N/H as a function of O/H in Fig. 3.9, we see that there is a correlation between the nitrogen and oxygen abundances. However, a best fit to the dwarf galaxies reveals a slope of only 0.62 ± 0.078 — the nitrogen abundance increases at a slower rate than the oxygen abundance. This result matches the negative relationship between the metallicity and the N/O ratio seen in Fig. 3.8. If we examine only the low-metallicity ($12 + \log(O/H) < 7.6$) star-forming galaxies with $M_r > -20$, a linear fit produces a slope of 0.05 ± 0.019 in Fig. 3.9 and a slope of -0.94 ± 0.019 in Fig. 3.8. This is in sharp contrast to the star-forming galaxies with $M_r > -20$ that have metallicities $12 + \log(O/H) > 7.6$, where their slope in Fig. 3.9 is 0.60 ± 0.022 and -0.39 ± 0.023 in Fig. 3.8. It appears that the nitrogen production is independent of the amount of oxygen produced in low-metallicity systems. At normal metallicities ($7.6 < 12 + \log(O/H) < 8.5$), there exists a positive relationship between the production of nitrogen and oxygen, although the ratio of N/O produced depends on the galaxy’s metallicity.

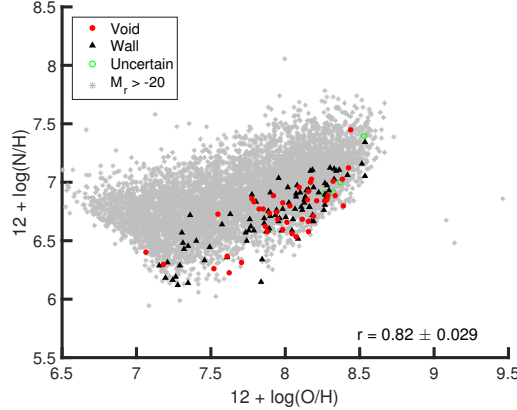


Figure 3.9: N/H as a function of O/H for star-forming void (red circles) and wall (black triangles) dwarf galaxies. Error bars have been omitted for clarity. There is a positive correlation between the two abundances. With a best-fit slope less than 1, we see that the synthesis of nitrogen in these galaxies is primary.

There is no difference between void and wall galaxies in the relationship of oxygen and nitrogen production in the low-metallicity sample. There is a slight difference in slopes between the void and wall galaxies with normal metallicities, where the void galaxies have a larger slope in the relationship between O/H and N/H and a smaller slope in the relationship between O/H and N/O. While statistically significant, the difference in the slopes between the two environments is not large enough to be physically relevant. The significant scatter in both Figs. 3.9 and 3.8 indicates that the described relationships between the production of nitrogen and oxygen are only global trends in the nucleosynthesis of the galaxies.

3.4.5 Mass–N/O relation

Just as there is a well-known mass–metallicity relation for galaxies (where the metallicity increases with stellar mass; see, e.g., Tremonti et al., 2004), there is also a mass–N/O relation. We expect to see a primary N/O plateau in the mass–N/O relation, since galaxies with lower stellar masses have not yet produced enough heavy elements to synthesize more nitrogen than oxygen. Beyond the low-mass limit, there should be a steady increase in the N/O ratio as a function of stellar mass, due to secondary nitrogen enrichment. Our dwarf galaxies in Fig. 3.10 show a steady increase in N/O as a function of stellar mass; there is a hint of the beginnings of a plateau for $\log(M_*/M_\odot) \lesssim 8$. The

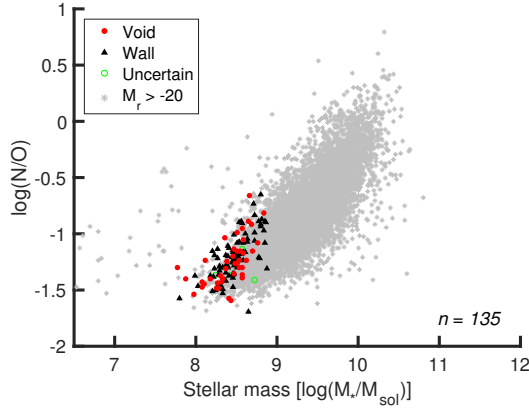


Figure 3.10: Mass–N/O relation for star-forming void (red circles) and wall (black triangles) dwarf galaxies. Error bars have been omitted for clarity. N/O is expected to remain constant for low stellar masses and increase steadily for larger masses, due to the mass-metallicity relation and the primary vs. secondary synthesis of nitrogen. To place the dwarf galaxies in the context of the general galaxy population, we also plot (gray stars) the star-forming galaxies with $M_r > -20$.

lack of a plateau here could be a result of our limited stellar mass range for the dwarf galaxies. A linear fit to our dwarf galaxies reveals a slope of 0.6 ± 0.12 , which is much stronger than the slope of 0.30 found by Andrews & Martini (2013).

From Fig. 3.10, we conclude that the N/O plateau, if one exists, starts around $\log(M_*/M_{\odot}) \approx 8$. This is at a much lower mass than that found by Andrews & Martini (2013) — they claim the N/O plateau exists for galaxies with $\log(M_*/M_{\odot}) < 8.9$. However, our relationship between stellar mass and N/O matches Fig. 3 of Amorín et al. (2010), as well as the results of Pérez-Montero & Contini (2009) and Pérez-Montero et al. (2013). None of our data samples display an obvious N/O plateau above a stellar mass $\log(M_*/M_{\odot}) > 8$, indicative of primary nitrogen versus secondary nitrogen production in galaxies. This could indicate that the switch from primary to secondary nitrogen production occurs at a much lower stellar mass than found by Andrews & Martini (2013). More low-mass galaxies are needed to extend this relation below $\log(M_*/M_{\odot}) < 8$.

3.4.6 Color–N/O relation

As van Zee & Haynes (2006) and Berg et al. (2012) discuss, a time delay between the release of nitrogen and oxygen will result in a positive relationship between the N/O ratio and the color of

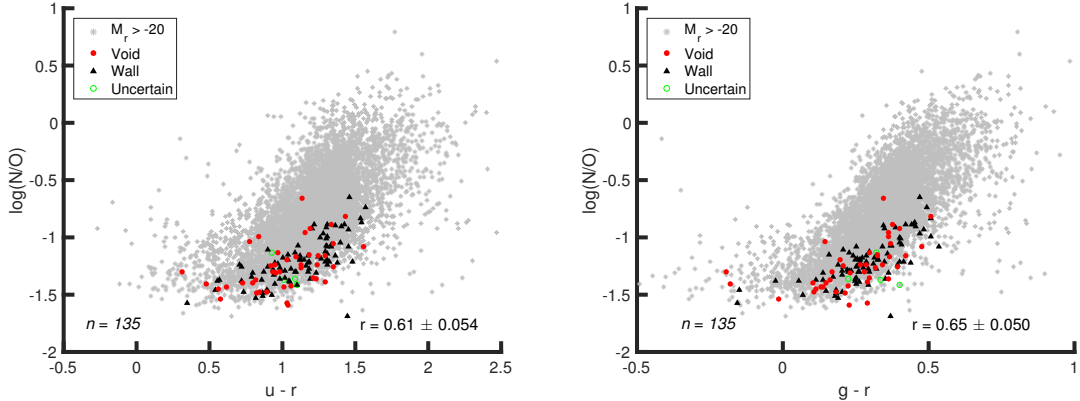


Figure 3.11: Color ($u - r$ and $g - r$) vs. N/O ratio for star-forming void (red circles) and wall (black triangles) dwarf galaxies. Error bars have been omitted for clarity. N/O is expected to increase as galaxies become redder if there is a time delay between the release of oxygen and nitrogen. To place the dwarf galaxies in context, we also plot the star-forming galaxies with $M_r > -20$ (gray stars).

a galaxy. If oxygen is primarily produced in higher-mass stars (and since these stars die earlier than the intermediate-mass stars responsible for the synthesis of nitrogen), then, for a given star formation episode, the oxygen produced will be released on a shorter time scale than the nitrogen. As a result, the amount of nitrogen relative to oxygen should increase as the hotter, more massive stars die and the galaxy becomes redder. This is exactly what we see in Fig. 3.11. We use rest-frame colors K -corrected to a redshift of 0.1; they are corrected for galactic extinction and calculated with model magnitudes (Choi et al., 2010). van Zee & Haynes (2006) and Berg et al. (2012) also found an increase in the N/O ratio as a function of color.

3.4.7 (s)SFR–N/O relation

We expect there to be a correlation between SFR or sSFR (per unit stellar mass) and the N/O ratio in galaxies as a result of the positive correlations between the SFR and stellar mass of a galaxy (Brinchmann et al., 2004) and the sSFR and the color of a galaxy (Fig. 3.12). As shown in Fig. 3.10, the N/O ratio increases with increasing stellar mass. As a result, we expect there to be a positive correlation between the SFR and N/O ratio in our galaxies. This can be seen in the sample of star-forming galaxies with $M_r > -20$ in the left panel of Fig. 3.13. Due to the large scatter in this relation, the blue star-forming dwarf galaxies exhibit a negative correlation between their N/O

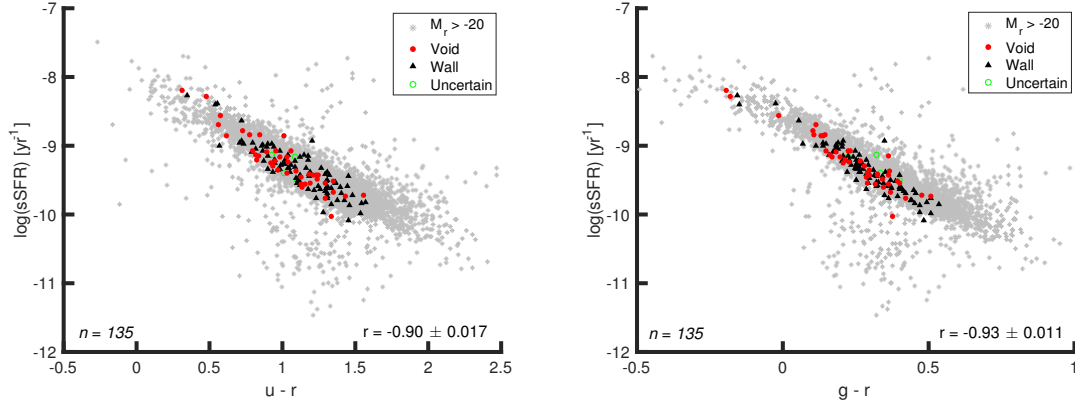


Figure 3.12: Color ($u - r$ and $g - r$) vs. sSFR for star-forming void (red circles) and wall (black triangles) dwarf galaxies. It is obvious that there is a negative correlation between the $\log(sSFR)$ and the color of a galaxy. To place the dwarf galaxies in context, we also show the star-forming galaxies with $M_r > -20$ (gray stars).

ratios and their SFRs. These SFR are aperture corrected to estimate the total SFR in the galaxy (not just within the SDSS fiber).

The N/O ratio is expected to decrease as sSFR increases in galaxies, as is shown in the right panel of Fig. 3.13. Bluer galaxies have higher sSFR. Fig. 3.11 shows that there is a positive correlation between the color and the N/O ratio, such that bluer galaxies have lower N/O ratios. As a result, we are not surprised to see that the N/O ratio decreases as the sSFR increases.

3.5 Large-scale environmental influence

The majority of the shifts in the gas-phase abundances of oxygen, nitrogen, and the N/O ratio seen in galaxies fainter than L_* are small and statistically insignificant. However, they occur in almost the same direction across all magnitude bins. This trend suggests that the gas-phase abundances may be influenced by the galaxies' large-scale environments. Shields et al. (1991) find no offset in the N/O ratio between cluster and field galaxies, despite the difference in O/H they observe. Similar to us, Contini et al. (2002) and Pilyugin et al. (2002) also find a statistically insignificant shift in the N/O ratio of cluster galaxies, although they find that these galaxies have lower N/O ratios than field spiral galaxies. Based on Fig. 3.6 and the statistics in Table 3.2, we find weak evidence that void dwarf galaxies have a smaller N/O ratio than dwarf galaxies in denser regions. This means that void

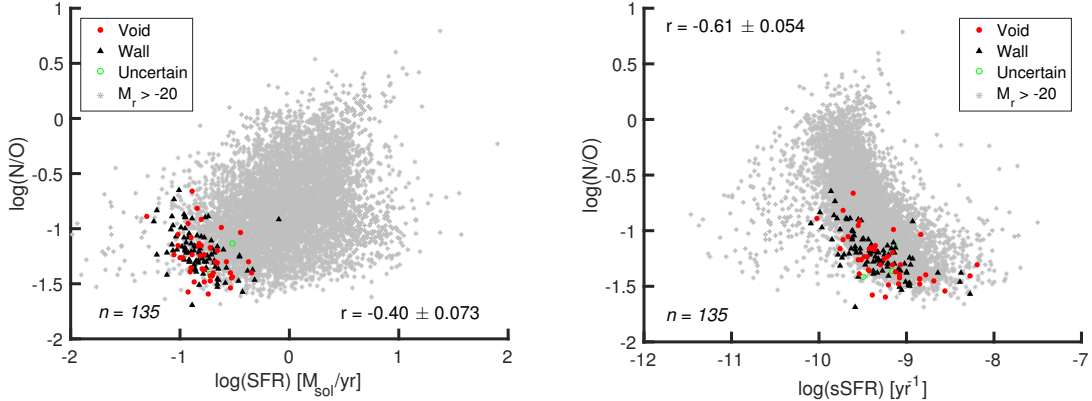


Figure 3.13: SFR–N/O and sSFR–N/O relations for star-forming void (red circles) and wall (black triangles) dwarf galaxies. Error bars have been omitted for clarity. Based on the correlations between SFR and stellar mass and sSFR and color, we expect the N/O ratio to increase with increasing SFR and decrease with sSFR. To place the dwarf galaxies in context, we also show the star-forming galaxies with $M_r > -20$ (gray stars).

dwarf galaxies may have more oxygen than wall dwarf galaxies, and/or void dwarf galaxies could have less nitrogen than wall dwarf galaxies. Here we discuss these possibilities and explore their implications for the large-scale environmental impact on the formation and evolution of galaxies.

Table 3.2 suggests a slight large-scale environmental dependence of the oxygen and nitrogen abundances (relative to hydrogen), where void galaxies have slightly more O/H and N/H than wall galaxies. This small difference is not apparent when looking at Figs. 2.4 and 3.3. However, the N/O ratio amplifies this large-scale environmental effect so that a shift in the mean (or median) of the two populations can be seen in Fig. 3.6. We hesitate to combine the results across all magnitude bins in an effort to improve their significance. Instead, we look toward the future to analyze a larger sample of galaxies to increase the statistical significance of these results.

3.5.1 Higher metallicities in void dwarf galaxies

A slightly higher metallicity in void dwarf galaxies than wall dwarf galaxies may be evidence of a difference in the ratio of dark matter halo mass to stellar mass between the two environments. Simulations by Jung et al. (2014) and Tonnesen & Cen (2015) show that the dark matter halo masses of void central galaxies are larger than those of wall central galaxies for a given stellar mass. Due to their environment, void dwarf galaxies are more likely to be in the center of their own dark matter

halo. Wall dwarf galaxies, on the other hand, are much more likely to be a satellite galaxy within a much larger dark matter halo; the simulation results mentioned above would not apply to these wall dwarf galaxies. However, because the wall dwarf galaxies studied here have sufficiently high sSFRs, they most likely live in a small-scale environment very similar to that of the void dwarf galaxies, as discussed in Paper I. As a result, it is likely that (and should be tested to see whether) the wall dwarf galaxies in this study are actually central galaxies.

Applying the results of these simulations to our dwarf galaxy sample, if the ratio of dark matter halo mass to stellar mass is larger in void galaxies, the metals ejected from a void galaxy's ISM into its circumgalactic medium are more likely to fall back onto the ISM than in a wall galaxy with the same stellar mass, since the void galaxy's virial radius and potential well are larger. As a result, two dwarf galaxies with the same stellar mass in these two different large-scale environments can have different metallicities — void dwarf galaxies would have higher metallicities than wall dwarf galaxies, matching what we see in Table 3.2.

3.5.2 Lower N/O ratios in void dwarf galaxies

A difference in the N/O ratio between void dwarf galaxies and wall dwarf galaxies could be a result of the difference in the synthesis of nitrogen in galaxies within these two large-scale environments. If void galaxies are retarded in their star formation (as simulations of the Λ CDM cosmology suggest), then cosmic downsizing would reduce the SFR at late times much more in wall galaxies than in void galaxies. As a result, the minimum gas-phase metallicity required for the production of secondary nitrogen in walls would be achieved at an earlier time in the galaxy's lifetime than in a void galaxy. This would cause the N/O ratio in wall galaxies to be larger than that in voids. van Zee & Haynes (2006) suggest that a galaxy with a declining SFR (wall galaxies) will have a higher nitrogen-to-oxygen yield than a galaxy with a constant SFR (void galaxies). This is due to more oxygen being released into the ISM as a result of the ongoing star formation in the void galaxies. This explanation is supported by the color–N/O diagram in Fig. 3.11, which reveals that redder galaxies have higher N/O ratios. The correlation between color and the N/O ratio found in van Zee & Haynes (2006), Berg et al. (2012), and Fig. 3.11 is a result of declining SFRs (van Zee & Haynes, 2006). Therefore,

the shift in the N/O ratio we see between void and wall galaxies may be observational evidence of retarded star formation in void galaxies as a result of cosmic downsizing.

Another explanation that would lead to a shift in the N/O ratio between environments is a difference in the ratio of intermediate- and high-mass stars produced in void and wall dwarf galaxies. For there to be more oxygen relative to nitrogen in void dwarf galaxies, the percent of higher-mass stars produced in a star formation episode would be higher than that in wall dwarf galaxies. This would indicate a varying IMF as a function of large-scale environment. Previous studies have been inconclusive when testing for a varying IMF (see Kroupa, 2001, 2002; Hoversten & Glazebrook, 2008; Meurer et al., 2009, for example). It is beyond the scope of this paper to elaborate on this explanation.

3.5.3 N/O ratio for extremely low metallicity galaxies

While Paper I shows that there is not a special population of extremely low metallicity dwarf galaxies residing in voids, we want to look in particular at the N/O ratio of extremely low metallicity galaxies. For the 21 dwarf galaxies with $12 + \log(\text{O}/\text{H}) < 7.6$ identified in Paper I, we see from Fig. 3.9 that their N/H ratios are also some of the lowest in the dwarf galaxy sample. However, as shown in Fig. 3.8, their N/O ratios cover the range of N/O ratio values of all the dwarf galaxies studied. This is consistent with the expectation that nitrogen behaves as a primary element for galaxies with low and moderate metallicities. Details of these 21 dwarf galaxies with extremely low metallicities are listed in Table 3.3, including their gas-phase chemical abundances.

3.6 Conclusions

The nucleosynthesis of nitrogen is a vital component of the chemical evolution of galaxies in our universe. We estimate the nitrogen abundance and N/O ratio of dwarf galaxies using the direct T_e method and spectroscopic line flux measurements from the SDSS DR7 sample as reprocessed in the MPA-JHU catalog. The 135 galaxies analyzed suggest a slight large-scale environmental dependence of the N/O ratio, where void dwarf galaxies could have a lower N/O ratio than dwarf galaxies in denser environments. Thus, the large-scale (~ 10 Mpc) environment might influence the chemical

Table 3.3: Details of 21 extremely low gas-phase metallicity ($12 + \log(\text{O}/\text{H}) < 7.6$) galaxies identified in Paper I. While the N/H values for all these galaxies are also extremely low, the N/O ratios span the range covered by the remainder of the dwarf galaxy sample studied. Further study of these galaxies is recommended to confirm the abundance values and identify any shared characteristics.

Index ^a	R.A.	Decl.	Redshift	$12 + \log(\frac{\text{O}}{\text{H}})$	$12 + \log(\frac{\text{N}}{\text{H}})$	$\log(\frac{\text{N}}{\text{O}})$	Void/Wall			
268470	13 ^h 18 ^m 17 ^s .82	+02°12'59".83	0.0252	7.06	±0.37	6.40	±0.25	-0.66	±0.45	Void
1422637	14 ^h 18 ^m 12 ^s .14	+13°59'33".98	0.0261	7.15	±0.41	6.29	±0.28	-0.87	±0.50	Wall
839665	08 ^h 09 ^m 53 ^s .53	+29°17'04".82	0.0281	7.18	±0.44	6.29	±0.31	-0.89	±0.54	Void
1168448	11 ^h 06 ^m 41 ^s .00	+45°19'09".28	0.0220	7.19	±0.46	6.18	±0.32	-1.01	±0.57	Wall
1299291	12 ^h 17 ^m 14 ^s .02	+43°18'53".36	0.0233	7.21	±0.42	6.32	±0.29	-0.89	±0.51	Wall
1170573	11 ^h 05 ^m 39 ^s .42	+46°03'28".37	0.0250	7.24	±0.34	6.16	±0.23	-1.08	±0.41	Wall
2288717	10 ^h 46 ^m 12 ^s .18	+21°31'37".37	0.0248	7.27	±0.48	6.19	±0.33	-1.08	±0.58	Wall
955643	11 ^h 42 ^m 03 ^s .02	+49°21'25".18	0.0244	7.28	±0.44	6.12	±0.30	-1.15	±0.53	Wall
1344311	12 ^h 33 ^m 13 ^s .64	+11°10'28".46	0.0245	7.29	±0.50	6.29	±0.34	-1.00	±0.61	Wall
1254352	13 ^h 29 ^m 02 ^s .45	+10°54'55".80	0.0237	7.30	±0.44	6.57	±0.30	-0.73	±0.54	Wall
1857820	08 ^h 45 ^m 00 ^s .34	+27°16'47".04	0.0257	7.31	±0.48	6.48	±0.33	-0.83	±0.59	Wall
866876	09 ^h 04 ^m 57 ^s .96	+41°29'36".42	0.0240	7.32	±0.40	6.43	±0.28	-0.89	±0.49	Wall
833588	08 ^h 43 ^m 10 ^s .71	+43°08'53".58	0.0245	7.34	±0.41	6.14	±0.29	-1.21	±0.50	Wall
283263	14 ^h 14 ^m 12 ^s .88	+01°50'12".88	0.0255	7.35	±0.43	6.45	±0.29	-0.90	±0.52	Wall
184308	09 ^h 39 ^m 09 ^s .38	+00°59'04".15	0.0244	7.36	±0.43	6.71	±0.31	-0.65	±0.53	Wall
1389829	14 ^h 31 ^m 01 ^s .38	+38°04'21".50	0.0269	7.41	±0.46	6.50	±0.32	-0.91	±0.56	Wall
858951	09 ^h 31 ^m 39 ^s .60	+49°49'56".85	0.0251	7.46	±0.46	6.33	±0.32	-1.13	±0.57	Wall
1270221	13 ^h 27 ^m 39 ^s .85	+50°54'09".69	0.0295	7.49	±0.43	6.45	±0.30	-1.04	±0.52	Wall
431383	08 ^h 58 ^m 44 ^s .96	+50°29'58".98	0.0230	7.52	±0.60	6.26	±0.31	-1.26	±0.68	Void
75442	12 ^h 13 ^m 24 ^s .25	+00°15'02".95	0.0264	7.55	±0.35	6.73	±0.24	-0.82	±0.42	Void
1322765	14 ^h 15 ^m 05 ^s .58	+36°22'57".77	0.0273	7.57	±0.40	6.64	±0.28	-0.93	±0.48	Wall

evolution of dwarf galaxies.

We find small, statistically insignificant shifts in the mean (or median) N/O ratio for galaxies between the void and denser regions across all blue, star-forming galaxies with $M_r > -20$. These shifts are somewhat more significant, however, when we look at the entire sample of galaxies. Each magnitude bin is shifted in the same direction, and are potentially very interesting, as they might indicate delayed star formation histories, more constant SFRs, and larger ratios of dark-matter-halo-mass to stellar mass in void galaxies, as discussed in Section 3.5. A larger sample would help test these results. We look to increase the sample and probe a larger magnitude (and mass) range of dwarf galaxies in Douglass & Vogeley (2017, in preparation).

In addition, we look at the relationship between the N/O ratio and other physical characteristics of our dwarf galaxies. In the relation between N/O and O/H, our galaxies all reside on the so-called “nitrogen plateau,” where the N/O ratio is predicted to be constant for low and intermediate metallicities. However, instead of a constant value for these galaxies, we find a negative correlation between the N/O and O/H ratios. Our dwarf galaxies show a positive correlation between stellar mass and the N/O ratio. These dwarf galaxies have some of the lowest N/O ratios for both their color and (s)SFR. Beyond the suggestive large-scale environmental dependence of the N/O ratio, there is no clear large-scale environmental dependence in any of these relationships.

The N/O ratios of the extremely metal-poor dwarf galaxies are no different than those of the remaining dwarf galaxy sample, though their N/H abundance is also extremely low. A more detailed study of these 21 extremely metal-poor dwarf galaxies is recommended to confirm their abundance values and discover any characteristics shared by the population.

Although SDSS provides spectroscopic observations for over 800,000 galaxies, only 135 are dwarf galaxies with emission-line fluxes necessary to estimate the gas-phase chemical abundances using the direct T_e method. The greatest limiting factor in this sample is the requirement of the [O II] $\lambda 3727$ doublet in the abundance calculations. We seek to develop a work-around for this emission line in Douglass & Vogeley (2017, in preparation) to greatly increase our sample of dwarf galaxies with abundance estimates. These estimated ionic abundances can then be compared with environ-

mental dependence of star formation and abundance predictions from high-resolution hydrodynamic simulations.

Further tests may refine our understanding of the environmental scale that is important for determining the chemical evolution of dwarf galaxies. In particular, it will be important to examine whether the influence of relatively small-scale (~ 2 Mpc) environments is more significant to a dwarf galaxy's chemical evolution than the larger-scale environment investigated here. In previous work, both Kreckel et al. (2015) and Beygu et al. (2017) find little evidence to support a significant large-scale environmental influence on the gas content, chemical content, or SFR of void galaxies. Future work will expand on these studies with a larger sample and the possible influence they might have on the dwarf galaxies' chemical contents and SFRs. Beygu et al. (2017) also investigate any connection between a galaxy's physical properties and its location within a void. We also look to study this possible connection with the increased sample size of dwarf galaxies in Douglass & Vogeley (2017, in preparation).

Chapter 4: Large-scale environmental dependence of chemical abundances in dwarf galaxies and implications for connecting star formation and halo mass

This chapter has been submitted to the *Astrophysical Journal* by Kelly A. Douglass, Michael S. Vogeley, and Renyue Cen; it will be referenced as Douglass et. al (2017).

Chapter 5: The influence of the small-scale environment on dwarf galaxy evolution

This work was done in collaboration with Daniele Schneider for her senior thesis “The effects of small-scale environment on dwarf galaxies.”

5.1 Introduction

Large galaxy redshift surveys have shown that the large-scale structure of the distribution of galaxies in the universe is similar to that of a three-dimensional cosmic web (Bond et al., 1996), where galaxy clusters are connected by thin filaments of galaxies and are separated by voids (large, underdense regions that occupy close to 60% of space). Over the last few decades, the Sloan Digital Sky Survey (Abazajian et al., 2009; Ahn et al., 2012) has accelerated the research into the influence of the large-scale environment on the formation and evolution of galaxies.

Because gravitational clustering within a void proceeds as if in a very low-density universe, cosmic voids are an important environment for studying galaxy formation (see van de Weygaert & Platen, 2011, for a review). The Λ CDM cosmology predicts that galaxies formed in voids have lower masses and are retarded in their star formation when compared to those in more dense environments (Gottlöber et al., 2003; Goldberg et al., 2005; Cen, 2011). The effects of the void environment should be most obvious in dwarf galaxies due to their minimal gravitational potential. As a result, they are more sensitive to astrophysical effects such as cosmological reionization, internal feedback from supernovae and photoheating from star formation, small-scale details of dark matter halo assembly, and the properties of dark matter.

Observations have shown that the properties of dwarf galaxies vary dramatically with the environment (e.g., Ann et al., 2008; Geha et al., 2012). Void galaxies have been found to have lower stellar mass (Hoyle et al., 2005; Croton et al., 2005; Moorman et al., 2015), be bluer and of a later type (Grogin & Geller, 2000; Rojas et al., 2004; Patiri et al., 2006; Park et al., 2007; von Benda-Beckmann & Müller, 2008; Hoyle et al., 2012), have higher star formation rates (Rojas et al., 2005;

Moorman et al., 2015; Beygu et al., 2016), and be more gas rich (Kreckel et al., 2012; Moorman et al., 2016; Jones et al., 2016) than galaxies in denser regions.

In conjunction with the large-scale environment, the small-scale environment ($\sim 1 h^{-1}\text{Mpc}$) has also been found to influence a galaxy's evolution. A well-established morphology-density relation exists (Dressler, 1980), where the fraction of late-type galaxies is inversely proportional to the local density. Ellison et al. (2009) determined that a galaxy's local environment influences a galaxy's evolution more than its large-scale environment. Likewise, Rupke et al. (2008) concluded that interacting galaxies have suppressed metallicities, because interactions induce flows of hydrogen. Park & Choi (2009) found that, for galaxies with $M_r < -19$, galaxy interactions out to the virial radius of the nearest neighbor influence the evolution of the target galaxy. They determine that the large-scale environment has a minimal effect on the evolution of a galaxy once the luminosity and morphology are taken into account.

We want to understand if the small-scale environment is more influential in a galaxy's evolution than its large-scale environment. One important question within the small-scale environment asks if tidal influences due to the nearest neighbor galaxy or gravitational potentials from the nearest galaxy group are more influential in a galaxy's evolution. A group consists of multiple galaxies that share the same dark matter halo. A group member will interact gravitationally with all other group members, not just its nearest neighbor. And a galaxy near a group, but not within it, may also experience strong tidal effects from the group similar to and stronger than those from a neighboring galaxy.

5.2 Calculating distances

We employ two different spatial metrics to determine the best way to locate a galaxy's nearest neighbor. Within a relative velocity $v_{rel} < 300 \text{ km/s}$, we use either the physically closest galaxy in units of $h^{-1}\text{Mpc}$ or the galaxy within the smallest fraction of its virial radius; both these methods are described below in further detail. The two methods result in different neighboring galaxies for about 40% of our dwarf galaxy sample.

5.2.1 Peculiar velocity

A galaxy's redshift is composed of both the expansion of the universe and the galaxy's peculiar velocity (its motion relative to its surrounding galaxies and environment). Known as the “Finger of God” effect, the peculiar velocity causes galaxy groups and clusters to appear extended along the line of sight when using redshift as a distance measurement. When we calculate distances on large scales, the peculiar velocity is negligible. However, when we study the distance between two objects in the universe on a small scale (within a few $h^{-1}\text{Mpc}$), the peculiar velocity dominates. The relative velocity v_{rel} between galaxies a and b is defined as

$$v_{rel} = |z_a - z_b|c \quad (5.1)$$

where z is the redshift. We require all neighbors to have a maximum relative velocity $v_{rel} < 300 \text{ km/s}$. We show in Sec. 5.4.3 that our results are insensitive to this value.

5.2.2 Sky separation in $h^{-1}\text{Mpc}$

The projected distance between two galaxies is found by projecting the two galaxies onto a sphere of radius \bar{r} , where \bar{r} is the average distance from Earth of the two galaxies. This assumes that two galaxies which are gravitationally bound are in a system where the relative velocity between us and it is 0 and that \bar{r} is the distance to the center of the system. The distance to the system is calculated as

$$\bar{r} = \frac{\bar{z}c}{H_0} \quad (5.2)$$

where \bar{z} is the average redshift of the two galaxies, c is the speed of light, and H_0 is the Hubble constant. Each galaxy's right ascension (RA) and declination (dec.) are converted to Cartesian coordinates to find their sky separation.

5.2.3 Fractional virial radii

From Hwang & Park (2010), we calculate the virial radius of a galaxy to be

$$r_{vir} = (3L\gamma/4\pi/200\rho_c)^{1/3} \quad (5.3)$$

where L is the galaxy's luminosity, γ is the mass-to-light ratio, and ρ_c is the critical density of the universe. The critical density is the density at which evenly distributed gas would collapse to form a galaxy. The mass-to-light ratio depends on the galaxy's morphology type, where $\gamma_{early} = 2\gamma_{late}$. Hwang & Park (2010) defines $200\rho_c = 740\bar{\rho}$, where $\bar{\rho} = (0.0223 \pm 0.0005)(\gamma_{late}L_{-20})(h^{-1}\text{Mpc})^3$. We can then rewrite Eqn. 5.3 as

$$r_{vir} = \left(\frac{3}{4 \times 740 \times 0.0223\pi} \frac{\gamma}{\gamma_{late}} \frac{L}{L_{-20}} \right)^{1/3} \quad (5.4)$$

where L_{-20} is the luminosity of a galaxy with $M_r = -20$. We can then use the virial radius to scale the distance between two galaxies as a fraction of the neighbor's virial radius.

Rather than using a measure of the virial radius for the group analysis, we scale the distance as a fraction of the group's root mean square (rms) radius.

5.2.4 Absolute distance to nearest neighbor

We can also calculate the distance between two galaxies by ignoring the effects of their relative velocities. Instead of projecting both galaxies onto a sphere with radius \bar{r} , we instead project each onto its own sphere of radius

$$r = \frac{cz}{H_0} \quad (5.5)$$

We then convert to Cartesian coordinates and use the three-dimensional Pythagorean theorem to calculate the distance between the two galaxies.

5.3 SDSS Data and galaxy selection

The Sloan Digital Sky Survey Data Release 7 (SDSS DR7; Abazajian et al., 2009) is a wide-field multiband imaging and spectroscopic survey which maps approximately one-quarter of the northern sky using a drift scanning technique. Photometric data in the five-band SDSS system — u , g , r , i , and z — is taken on a dedicated 2.5m telescope at the Apache Point Observatory in New Mexico (Fukugita et al., 1996; Gunn et al., 1998). Galaxies with Petrosian r -band magnitudes $m_r < 17.77$ are selected for follow-up spectroscopic analysis (Lupton et al., 2001; Strauss et al., 2002). The galaxy colors are taken from the Korean Institute for Advanced Study Value-Added Galaxy Catalog (KIAS-VAGC; Choi et al., 2010), which contains galaxies from the SDSS DR7 main sky survey based on the New York University Value-Added Galaxy Catalog Data Release 7 (NYU-VAGC; Blanton et al., 2005). Total star formation rates (SFR) and total specific star formation rates (sSFR) are from the MPA-JHU value-added catalog¹, calculated using the technique described in Brinchmann et al. (2004). The gas-phase chemical abundances used are from Douglass & Vogeley (2017, in prep.), which are calculated using the Direct T_e method. The galaxies' large-scale environments are based on the void catalog compiled by Pan et al. (2012), which is constructed from SDSS DR7 using the VoidFinder algorithm of Hoyle & Vogeley (2002). Galaxies which are located within identified voids are labeled as void galaxies, and those which do not fall within a void are designated as a wall galaxy. The large-scale environment within $5 h^{-1}\text{Mpc}$ of the edge of the main SDSS DR7 footprint cannot be described using the VoidFinder algorithm because the minimum diameter of a void is $10 h^{-1}\text{Mpc}$. Therefore, the large-scale environment for galaxies within $5 h^{-1}\text{Mpc}$ of the edge of the main footprint in SDSS DR7 is designated as unknown.

5.3.1 Various samples

Two galaxy samples are used in this analysis. The largest one contains the 11,845 dwarf galaxies spectroscopically observed in SDSS DR7. The second sample contains those star-forming dwarf galaxies from the first set which have gas-phase chemical abundances in Douglass & Vogeley (2017, in prep.), totaling 2506 dwarf galaxies. While this subset of galaxies contains only star-forming

¹Available at <http://www.mpa-garching.mpg.de/SDSS/DR7/>

galaxies and is not representative of all dwarf galaxies, we show in Section 5.4.3 that this does not affect our results.

5.3.2 Group catalog

In addition to comparing the target galaxies to their nearest neighbor, we also look at the relationship between the dwarf galaxies' properties and their proximity to the nearest galaxy group. We use the Mr18 Berlind group catalog Berlind et al. (2006) as our source of groups, which is built on the galaxies in the NYU-VAGC. The catalog identifies groups using a friends-of-friends algorithm (Huchra & Geller, 1982) to connect galaxies with $M_r < -18$.

5.4 Distance analysis and results

Our primary objective is to compare various physical characteristics of dwarf galaxies against their nearest neighbors or groups to discern how the small-scale environment affects their evolution.

5.4.1 Parameter – distance relations

The relationships between various physical parameters and the distance to the nearest neighbor or group for our sample of star-forming dwarf galaxies are shown in Figs. 5.1–5.5. In each of the four plots within each figure, we bin the galaxies in distance-space and show the average parameter value in each bin, to see any overall trends in the data. We also fit a linear line to the data; the output of these fits are in Table 5.1. Each of these four plots probes this distance relationship from a different angle. The top left plots in Figs. 5.1–5.5 relate the target dwarf galaxy's parameter to the distance to its nearest neighbor, as defined by the closest galaxy on the sky in $h^{-1}\text{Mpc}$ with a velocity difference less than 300 km/s. The bottom left plots relate the target dwarf galaxy's parameter to the distance to its nearest neighbor, as defined by the closest galaxy on the sky in units of the virial radius of the neighbor galaxy with a velocity difference less than 300 km/s. The nearest galaxy is not necessarily the same for these two distance measurements, as explained in Sec. 5.2.

We repeat this same analysis on the nearest groups to the target dwarf galaxy. The top right plots in Figs. 5.1–5.5 relate the target dwarf galaxy's parameter to the distance to the center of the nearest group, as defined as the closest group in the sky in $h^{-1}\text{Mpc}$ with a velocity difference less

than 300 km/s. The bottom right plots in Figs. 5.1–5.5 relate the target dwarf galaxy’s parameter to the distance to the nearest group as defined by the closest group on the sky in units of the group’s rms radius with a velocity difference of less than 300 km/s. Groups are very rare in the void environment (by nature of the void environment), so the uncertainty in the binned values shown in these plots is much larger than in the galaxy neighbor plots.

These figures reveal influences from both the large-scale and small-scale environments, since we are identifying which galaxies reside in void regions and which do not.

Color

Because of the known morphology-density relation, we expect to find that a dwarf galaxy’s color became more blue as the distance to its nearest neighbor increased. Fig. 5.1 shows very little relationship between the distance and color, except at the smallest distance bin. The linear fits quantify this observation — the slopes are on the order of 10^{-3} . However, within a distance of $0.05 h^{-1}\text{Mpc}$ or $0.05r_{vir}$, dwarf galaxies tend to be bluer than at further distances from their nearest neighbor. At distances less than $0.1 h^{-1}\text{Mpc}$ from the center of the nearest groups, the dwarf galaxies are redder than average. However, there does not appear to be any relationship between a dwarf galaxy’s color and its distance to the center of the nearest group in units of the group’s rms radius. It has been well-established that void galaxies tend to be bluer than galaxies in denser environments (Grogin & Geller, 1999; Rojas et al., 2004; Patiri et al., 2006; von Benda-Beckmann & Müller, 2008; Hoyle et al., 2012); this shift is apparent in Fig. 5.1, where the void dwarf galaxies are slightly bluer than the wall dwarf galaxies.

sSFR

Following our prediction for the color-distance relations, we expect that the sSFR to increase with distance from the nearest neighbor. We also see very little relationship between the distance and sSFR in Fig. 5.2, except in the smallest distance bin. The linear fits quantify this observation — the slopes are on the order of 10^{-3} . Within a distance of $0.05 h^{-1}\text{Mpc}$ or $0.05r_{vir}$, dwarf galaxies tend to have higher sSFRs than at further distances from their nearest neighbor. There does not appear to be any relationship between a dwarf galaxy’s sSFR and its distance to the center of the nearest

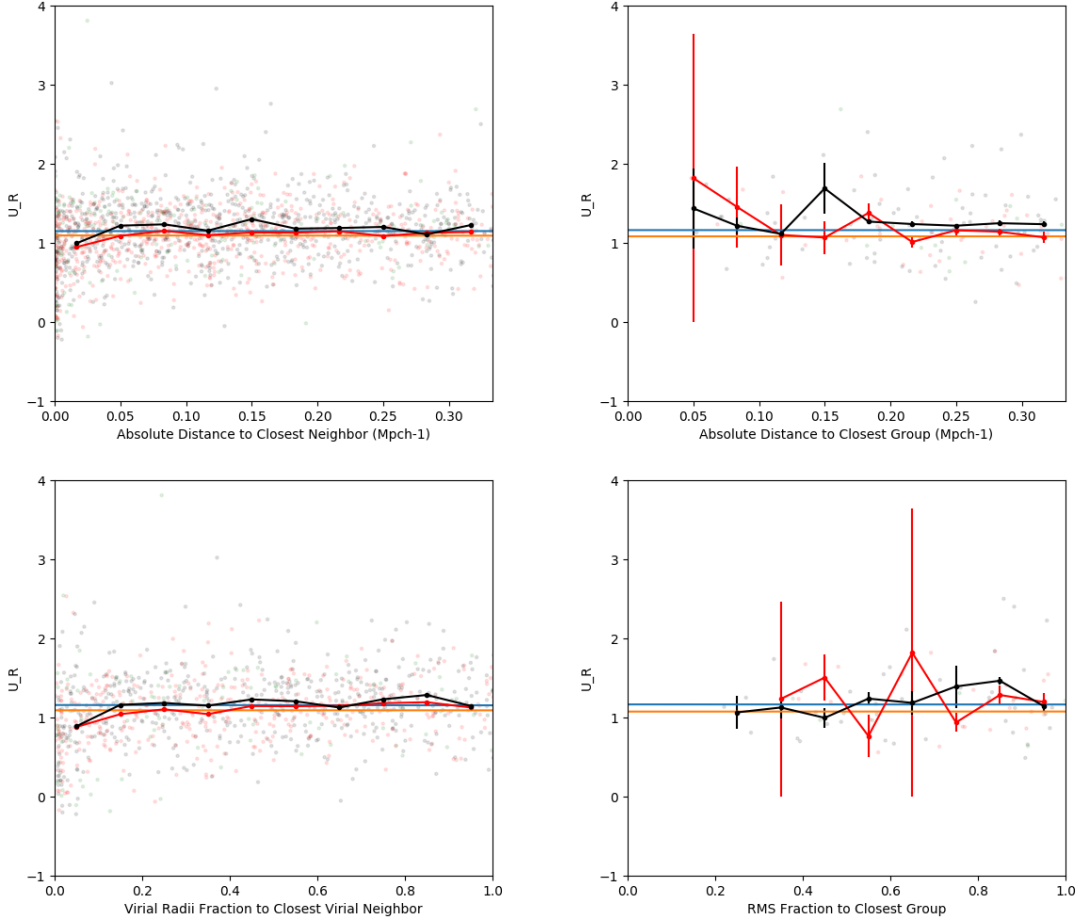


Figure 5.1: Color ($u - r$) versus distance to the nearest galaxy (on the left) and nearest group (on the right). The top panel shows the color as a function of the sky separation in $h^{-1}\text{Mpc}$ between the target dwarf galaxy and the neighbor, while the bottom panel shows the color as a function of the closest virial neighbor. Void galaxies are shown in red, while wall galaxies are shown in black and unknown in green. We have also included the average color for the galaxies after binning by distance, to discern any finer behavior in the relationships. Linear fits to the void and wall galaxies are shown in orange and blue, respectively. It is clear that the void dwarf galaxies are bluer than the wall dwarf galaxies. The nearest galaxies appear to only have some affect on the dwarf galaxy's color at separations less than $0.05 h^{-1}\text{Mpc}$, or $0.05r_{vir}$. The closest group appears to have some affect on the target dwarf galaxy's color at distances less than $0.1 h^{-1}\text{Mpc}$ to the group's center; there appears to be no relationship between a dwarf galaxy's color and its distance to the nearest group as represented by the fraction of the group's radius.

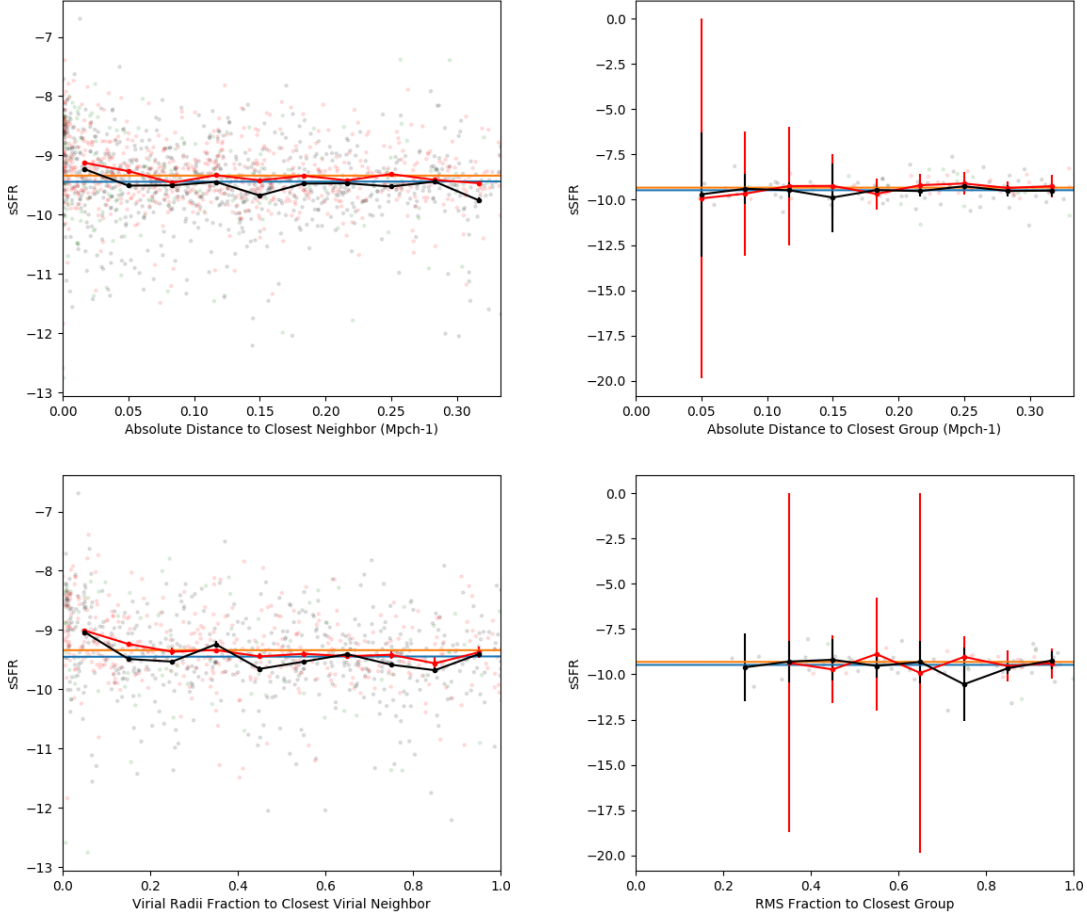


Figure 5.2: sSFR versus distance to the nearest galaxy (on the left) and nearest group (on the right). The top panel shows the sSFR as a function of the sky separation in $h^{-1}\text{Mpc}$ between the target dwarf galaxy and the neighbor, while the bottom panel shows the sSFR as a function of the closest virial neighbor. Void galaxies are shown in red, while wall galaxies are shown in black and unknown in green. We have also included the average sSFR for the galaxies after binning by distance, to discern any finer behavior in the relationships. Linear fits to the void and wall galaxies are shown in orange and blue, respectively. It is clear that the void dwarf galaxies have higher sSFRs than the wall dwarf galaxies. Only the neighbor galaxies at separations less than $0.05 h^{-1}\text{Mpc}$ or $0.05r_{vir}$ appear to have some affect on the dwarf galaxies' sSFR. There appears to be no relationship between a dwarf galaxy's sSFR and its distance to the nearest group.

group in either distance metric. In these distance comparisons, there is a shift towards higher sSFRs in the void dwarf galaxies when compared to the wall dwarf galaxies, as has been observed many times before (Rojas et al., 2005; von Benda-Beckmann & Müller, 2008; Moorman et al., 2015; Beygu et al., 2016).

Metallicity

Based on our hypothesis that galaxies would be redder and have lower sSFRs at small distances to their nearest neighbors, we anticipated that the metallicity of the galaxies would decrease with increasing distance. As before, we only see a relationship between the distance and metallicity in the smallest distance bin in Fig. 5.3. The linear fits quantify this observation — the slopes are on the order of 10^{-2} . Within a distance of $0.05 h^{-1}\text{Mpc}$ or $0.05r_{vir}$, dwarf galaxies tend to have higher metallicities than at further distances from their nearest neighbor. At distances less than $0.1 h^{-1}\text{Mpc}$ from the center of the nearest group, dwarf galaxies might have lower than average metallicities. However, this could be an erroneous conclusion due to low-number statistics. In these distance comparisons, there is a shift towards higher metallicities in the void dwarf galaxies when compared to the wall dwarf galaxies, as has been observed by Douglass & Vogeley (2017b) and Douglass & Vogeley (2017, in prep).

Nitrogen abundance

It was expected that the gas-phase nitrogen abundance would follow the same trend as the metallicity, to decrease with increasing distance. As observed with the other parameters, Fig. 5.4 shows very little relationship between the distance and N/H, except in the smallest distance bin for the closest virial neighbor. The linear fits quantify this observation — the slopes are on the order of 10^{-2} . Within a distance of $0.05r_{vir}$, dwarf galaxies tend to have higher nitrogen abundances than at distances further from their nearest neighbor. There does not seem to be any relationship between the nitrogen abundance of the star-forming dwarf galaxies and distance to the center of the nearest group. Unlike the shifts seen with the other parameters and what is observed in Douglass & Vogeley (2017b) and Douglass & Vogeley (2017, in prep), we see no significant difference in the nitrogen abundance resulting from the large-scale environment.

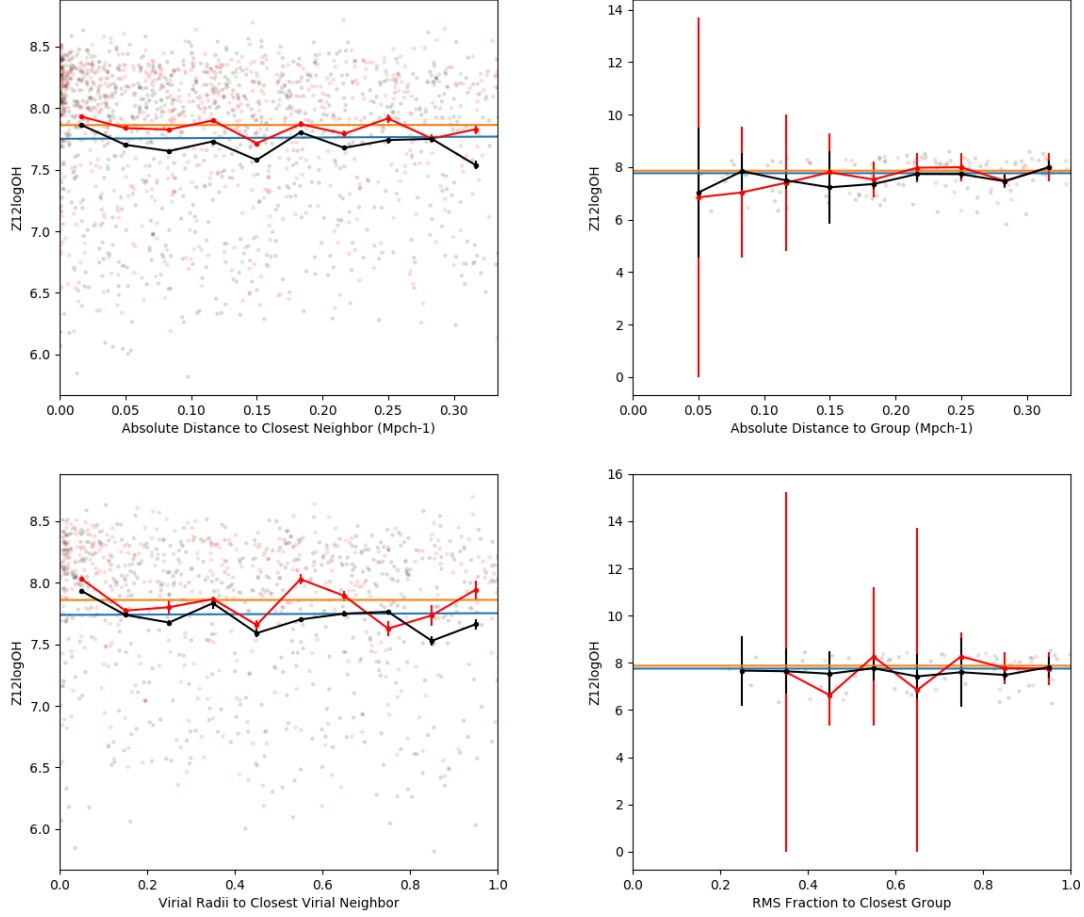


Figure 5.3: Metallicity versus distance to the nearest galaxy (on the left) and nearest group (on the right). The top panel shows the metallicity as a function of the sky separation in $h^{-1}\text{Mpc}$ between the target dwarf galaxy and the neighbor, while the bottom panel shows the metallicity as a function of the closest virial neighbor. Void galaxies are shown in red, while wall galaxies are shown in black and unknown in green. We have also included the average metallicity for the galaxies after binning by distance, to discern any finer behavior in the relationships. Linear fits to the void and wall galaxies are shown in orange and blue, respectively. It is clear that the void dwarf galaxies have higher metallicities than the wall dwarf galaxies. Only the neighbor galaxies at separations less than $0.05 h^{-1}\text{Mpc}$ or $0.05r_{vir}$ appear to have some affect on the dwarf galaxies' metallicity. When measuring the distance to the nearest group in $h^{-1}\text{Mpc}$, it appears that the dwarf galaxies have lower metallicities at distances less than $0.1 h^{-1}\text{Mpc}$ from their nearest group.

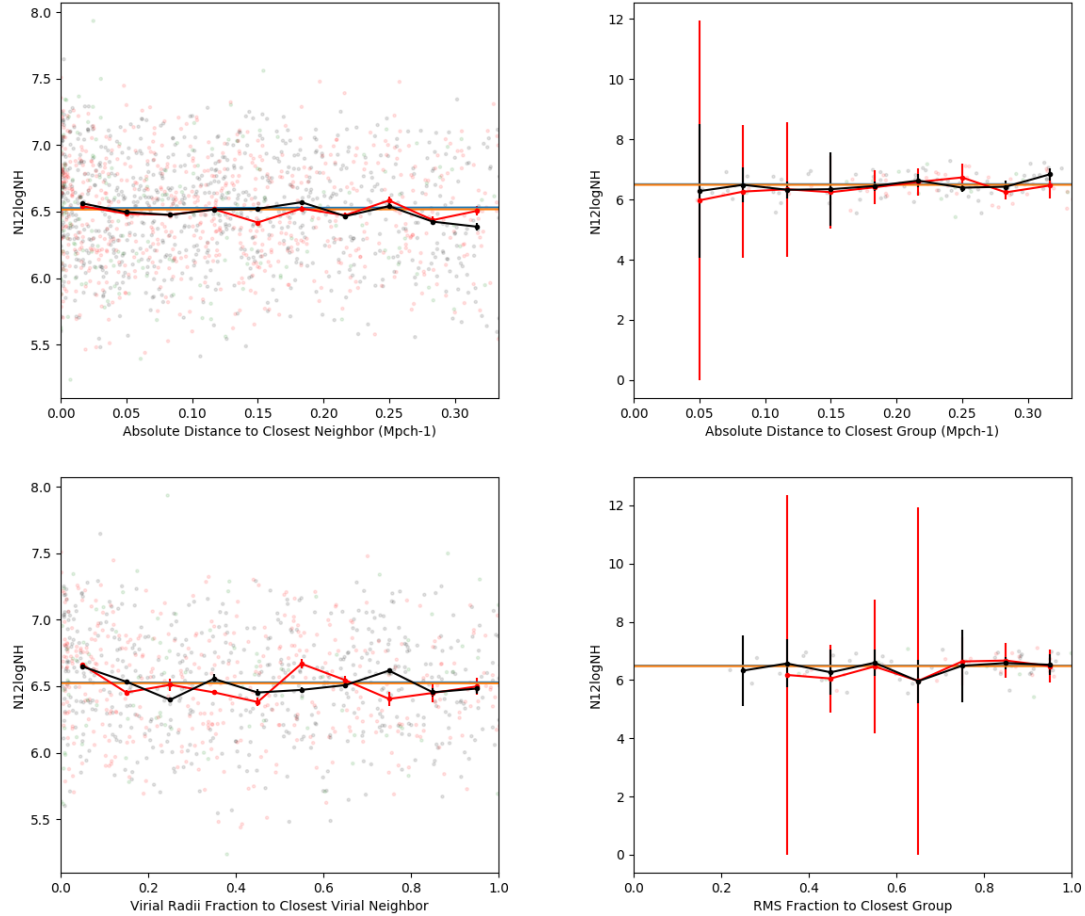


Figure 5.4: Gas-phase nitrogen abundance versus distance to the nearest galaxy (on the left) and nearest group (on the right). The top panel shows N/H as a function of the sky separation in $h^{-1}\text{Mpc}$ between the target dwarf galaxy and the neighbor, while the bottom panel shows N/H as a function of the closest virial neighbor. Void galaxies are shown in red, while wall galaxies are shown in black and unknown in green. We have also included the average nitrogen abundance for the galaxies after binning by distance, to discern any finer behavior in the relationships. Linear fits to the void and wall galaxies are shown in orange and blue, respectively. There is very little difference in N/H between the two large-scale environments. Only the neighbor galaxies at separations less than $0.05r_{vir}$ appear to have some affect on the dwarf galaxies' nitrogen abundance. There does not appear to be any relationship between the dwarf galaxies' nitrogen abundance and the distance to their nearest group.

N/O ratio

We do not expect any influence on the relative synthesis of oxygen and nitrogen from the proximity to a nearest neighbor. Unlike the other parameters studied, Fig. 5.5 shows that the N/O ratio does not have any relationship with the distance to a nearest neighbor at any separation. This is reflected in the linear fits to the data — the slopes are on the order of 10^{-2} and smaller. When looking at the relationship between the N/O ratio and the distance to the nearest group, though, the N/O ratio might be higher than average in galaxies within $0.1 h^{-1}\text{Mpc}$ of the group’s center. The shift towards lower N/O ratios in star-forming void dwarf galaxies is readily apparent, as Douglass & Vogeley (2017b) and Douglass & Vogeley (2017, in prep) find.

5.4.2 Linear fit parameters

To quantify the results shown in Figs. 5.1–5.5, we calculate the parameters for the best fit linear line. Any slope of significant magnitude shows an overall correlation between a given physical parameter and the galaxy’s distance to its nearest neighbor or group. The results of this analysis are listed in Table 5.1. These slopes reflect the observations described in Section 5.4.1: there is no correlation between the distance to the nearest neighbor and a galaxy’s color, sSFR, or gas-phase chemical abundances. This analysis does not capture any variations within the range of distances for all dwarf galaxies included in this study.

5.4.3 Selection effects

We test two components of our nearest neighbor criteria to understand how sensitive our results are to any initial conditions. The first parameter we discuss is the sensitivity of our results on the maximum peculiar velocity to define a match. Throughout our analysis, we use 300 km/s as the maximum velocity separation allowed between the target galaxy and its nearest neighbor or group. We look at how this affects our results by repeating the analysis with maximum velocities of 150 km/s and 600 km/s. The results of this comparison on the color of the galaxies can be seen in Fig. 5.6. The nearest neighbors in the left-hand panel are restricted to a maximum peculiar velocity of 150 km/s, while those in the right panel are restricted to 600 km/s. When compared to each other

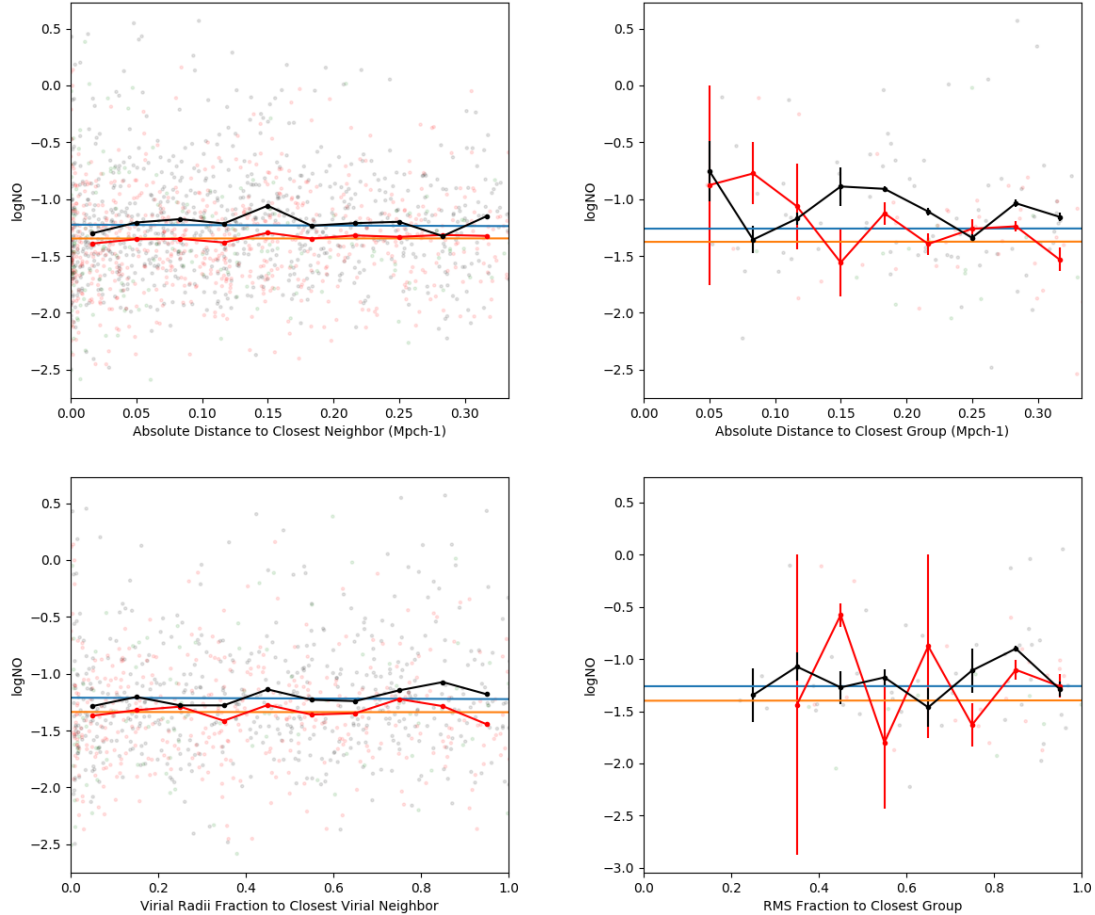


Figure 5.5: N/O ratio versus distance to the nearest galaxy (on the left) and nearest group (on the right). The top panel shows the N/O ratio as a function of the sky separation in $h^{-1}\text{Mpc}$ between the target dwarf galaxy and the neighbor, while the bottom panel shows N/O as a function of the closest virial neighbor. Void galaxies are shown in red, while wall galaxies are shown in black and unknown in green. We have also included the average nitrogen abundance for the galaxies after binning by distance, to discern any finer behavior in the relationships. Linear fits to the void and wall galaxies are shown in orange and blue, respectively. The void dwarf galaxies have lower N/O ratios than the wall dwarf galaxies, but there is no distinct relationship between the distance to the nearest neighbor and the N/O ratio. The N/O ratio might be higher in dwarf galaxies within 0.05 $h^{-1}\text{Mpc}$ of the center of the closest group.

Table 5.1: Linear fit parameters to various properties of the target dwarf galaxies by their distances to the nearest galaxy in units of $h^{-1}\text{Mpc}$, the nearest galaxy in units of the neighbor's virial radius, the center of the nearest group in units of $h^{-1}\text{Mpc}$, and the nearest group in units of the group's rms radius; all objects must be within 300 km/s of the target galaxy. The slopes are all negligible, quantifying the observations made that the proximity to a galaxy or group has little influence on a dwarf galaxy's evolution.

Property	Slope (wall)	Slope (void)	Intercept (wall)	Intercept (void)
Nearest galaxy by distance				
$u - r$	$1.25 \pm 1.17 \times 10^{-3}$	$-9.14 \pm 0.56 \times 10^{-3}$	1.15 ± 0.00076	1.09 ± 0.00049
sSFR	$2.07 \pm 0.18 \times 10^{-2}$	$-0.16 \pm 0.08 \times 10^{-3}$	-9.45 ± 0.001	-9.34 ± 0.0007
$12 + \log(\text{O/H})$	$5.35 \pm 0.17 \times 10^{-2}$	$0.33 \pm 0.08 \times 10^{-2}$	7.75 ± 0.0011	7.86 ± 0.0007
$12 + \log(\text{N/H})$	$1.64 \pm 0.11 \times 10^{-2}$	$0.62 \pm 0.06 \times 10^{-2}$	6.53 ± 0.0007	6.52 ± 0.0006
$\log(\text{N/O})$	$-3.70 \pm 0.13 \times 10^{-2}$	$0.29 \pm 0.07 \times 10^{-2}$	-1.23 ± 0.0009	-1.35 ± 0.0006
Nearest galaxy by fraction of virial radius				
$u - r$	$-3.81 \pm 0.04 \times 10^{-3}$	$-0.46 \pm 0.01 \times 10^{-3}$	1.16 ± 0.00014	1.09 ± 0.00008
sSFR	$5.96 \pm 0.06 \times 10^{-3}$	$-0.41 \pm 0.02 \times 10^{-3}$	-9.45 ± 0.0002	-9.33 ± 0.0001
$12 + \log(\text{O/H})$	$1.41 \pm 0.005 \times 10^{-2}$	$0.12 \pm 0.08 \times 10^{-2}$	7.74 ± 0.0002	7.86 ± 0.0001
$12 + \log(\text{N/H})$	$1.82 \pm 0.11 \times 10^{-3}$	$-1.14 \pm 0.002 \times 10^{-3}$	6.53 ± 0.0001	6.52 ± 0.0001
$\log(\text{N/O})$	$-1.22 \pm 0.004 \times 10^{-2}$	$-0.41 \pm 0.02 \times 10^{-3}$	-1.21 ± 0.0002	-1.33 ± 0.0001
Nearest group by distance				
$u - r$	$-2.53 \pm 0.01 \times 10^{-3}$	$1.34 \pm 0.01 \times 10^{-3}$	1.16 ± 0.00008	1.08 ± 0.0001
sSFR	$7.77 \pm 0.02 \times 10^{-3}$	$-1.68 \pm 0.02 \times 10^{-3}$	-9.48 ± 0.001	-9.33 ± 0.0001
$12 + \log(\text{O/H})$	$3.65 \pm 0.16 \times 10^{-4}$	$2.06 \pm 0.19 \times 10^{-4}$	7.77 ± 0.0001	7.86 ± 0.0001
$12 + \log(\text{N/H})$	$4.84 \pm 0.01 \times 10^{-3}$	$6.30 \pm 0.01 \times 10^{-3}$	6.51 ± 0.00008	6.49 ± 0.0001
$\log(\text{N/O})$	$4.47 \pm 0.01 \times 10^{-3}$	$6.09 \pm 0.01 \times 10^{-3}$	-1.26 ± 0.0001	-1.38 ± 0.0001
Nearest group by fraction of group radius				
$u - r$	$-1.00 \pm 0.002 \times 10^{-3}$	$0.90 \pm 0.002 \times 10^{-3}$	1.16 ± 0.00003	1.07 ± 0.00003
sSFR	$2.70 \pm 0.002 \times 10^{-3}$	$-1.71 \pm 0.002 \times 10^{-3}$	-9.48 ± 0.00005	-9.31 ± 0.00005
$12 + \log(\text{O/H})$	$8.81 \pm 0.02 \times 10^{-4}$	$-8.74 \pm 0.19 \times 10^{-4}$	7.76 ± 0.00005	7.88 ± 0.00005
$12 + \log(\text{N/H})$	$2.31 \pm 0.001 \times 10^{-3}$	$2.47 \pm 0.001 \times 10^{-3}$	6.49 ± 0.00003	6.47 ± 0.00004
$\log(\text{N/O})$	$1.43 \pm 0.002 \times 10^{-3}$	$3.35 \pm 0.002 \times 10^{-3}$	-1.26 ± 0.00005	-1.40 ± 0.00005

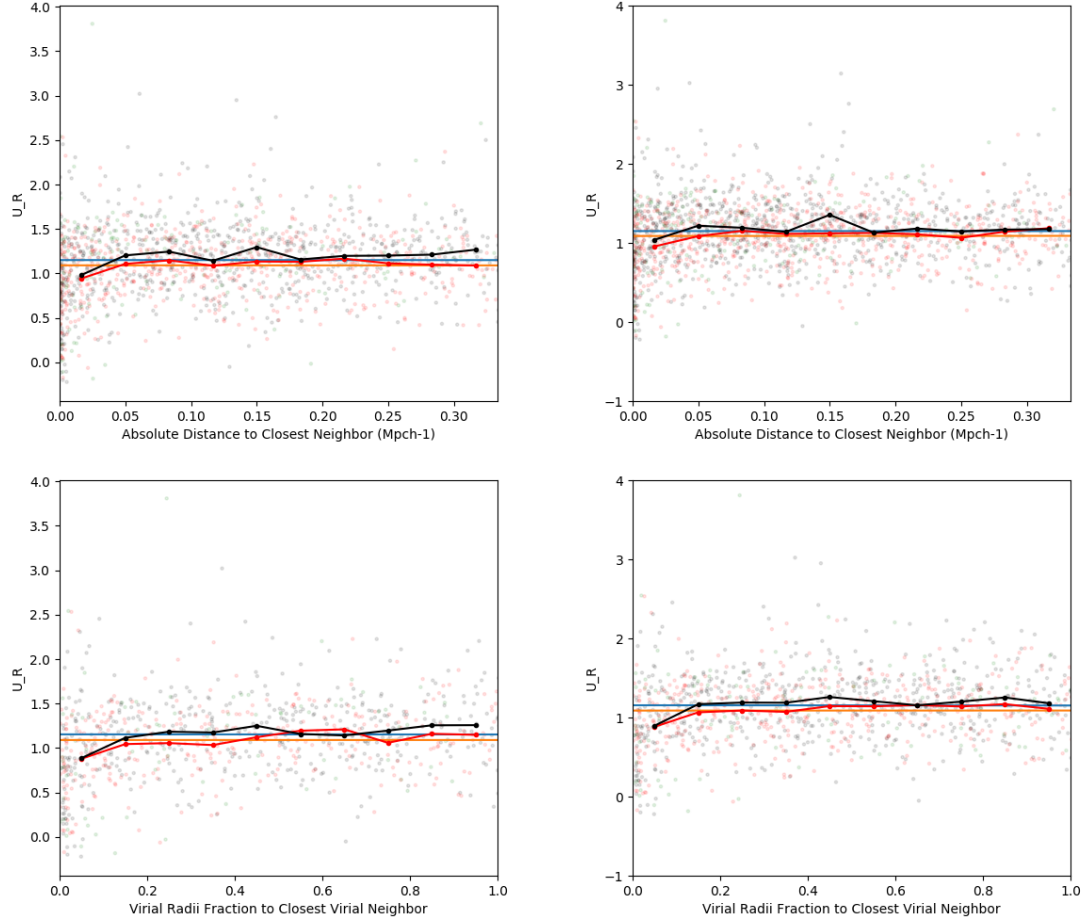


Figure 5.6: Color versus distance to nearest galaxy (in units of $h^{-1}\text{Mpc}$ on top and virial radii on bottom), with a maximum allowed peculiar velocity of 150 km/s in the left panel and 600 km/s in the right panel. Void galaxies are shown in red, wall in black, and unknown in green. The galaxies are binned by distance to tease out any trends at smaller distance scales; linear fits to the void and wall galaxies are shown in orange and blue, respectively. When compared with the two plots in the left panel of Fig. 5.1, we see that there is no significant influence on our results from the choice of maximum peculiar velocity allowed.

and to the left-hand panel of Fig. 5.1, it is clear that our choice of maximum peculiar velocity has no affect on the results of the study.

We also test the sensitivity of our results to the population of galaxies being studied. Because we want to look at the relationship between distance and the gas-phase chemical abundances of the dwarf galaxies, our sample is limited to star-forming dwarf galaxies with detected emission lines necessary for estimation of the chemical abundances with the Direct T_e method (see Douglass & Vogeley, 2017a, for more details). We perform the same distance analysis on all dwarf galaxies detected in SDSS DR7 with respect to their color, to understand how our results depend on our sample. When we compare Fig. 5.7 with the left-hand panel of Fig. 5.1, we see that there is no difference in the correlation between color and distance to the nearest neighbor. It is clear that our selection bias to star-forming dwarf galaxies does not influence any trends we observe in our analysis.

For about 41% of our dwarf galaxy sample, the two different metrics by which to define the nearest neighbor (minimum in units of $h^{-1}\text{Mpc}$ or virial radius of the nearest neighbor) return different neighboring galaxies. Fig. 5.8 compares the absolute magnitude distributions of these two nearest neighbor populations. The left panel shows the distribution of the absolute magnitudes of the nearest neighbor galaxies, while the right panel shows the distribution in absolute magnitude of the nearest neighbor galaxy relative to its target galaxy. The top row includes those nearest neighbors in units of $h^{-1}\text{Mpc}$, and the bottom row consists of the nearest neighbors in units of the neighbor's virial radius. Comparing the two plots in the right panel, we see that the closest galaxy to the target dwarf galaxy is often of equal or fainter magnitude than the target galaxy. Alternatively, using the virial radius of the neighbor galaxy as a measure of the distance often finds a brighter galaxy than the target galaxy, as the bottom right plot in Fig. 5.8 shows. By using these two different distance metrics, we are able to probe the relationship between a dwarf galaxy and its nearest neighbor and nearest dark matter halo.

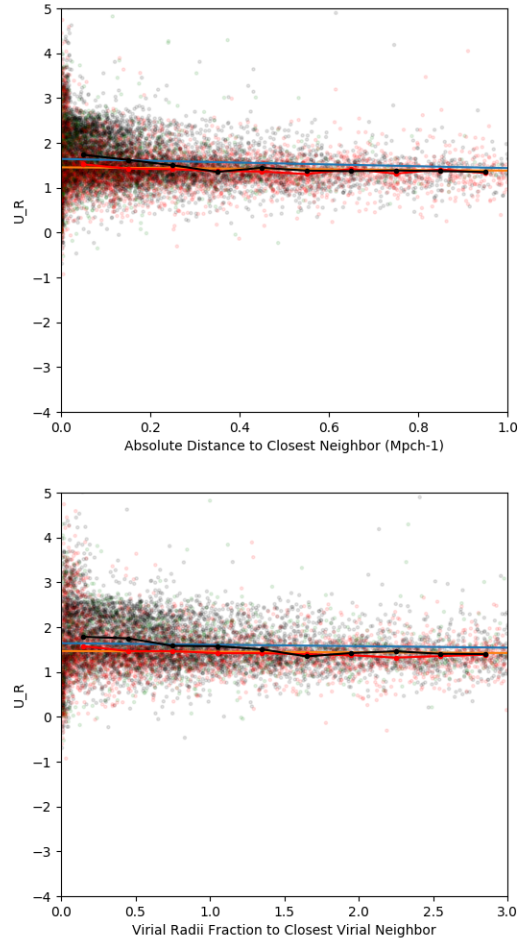


Figure 5.7: Color versus distance to the nearest galaxy (in units of $h^{-1}\text{Mpc}$ on top and virial radii on the bottom) for the entire dwarf galaxy population in SDSS DR7. When compared to the left-hand panel of Fig. 5.1, we see that there is no difference in the results of the analysis by studying only star-forming galaxies with sufficient detection of the various emission lines necessary to estimate the gas-phase chemical abundances.

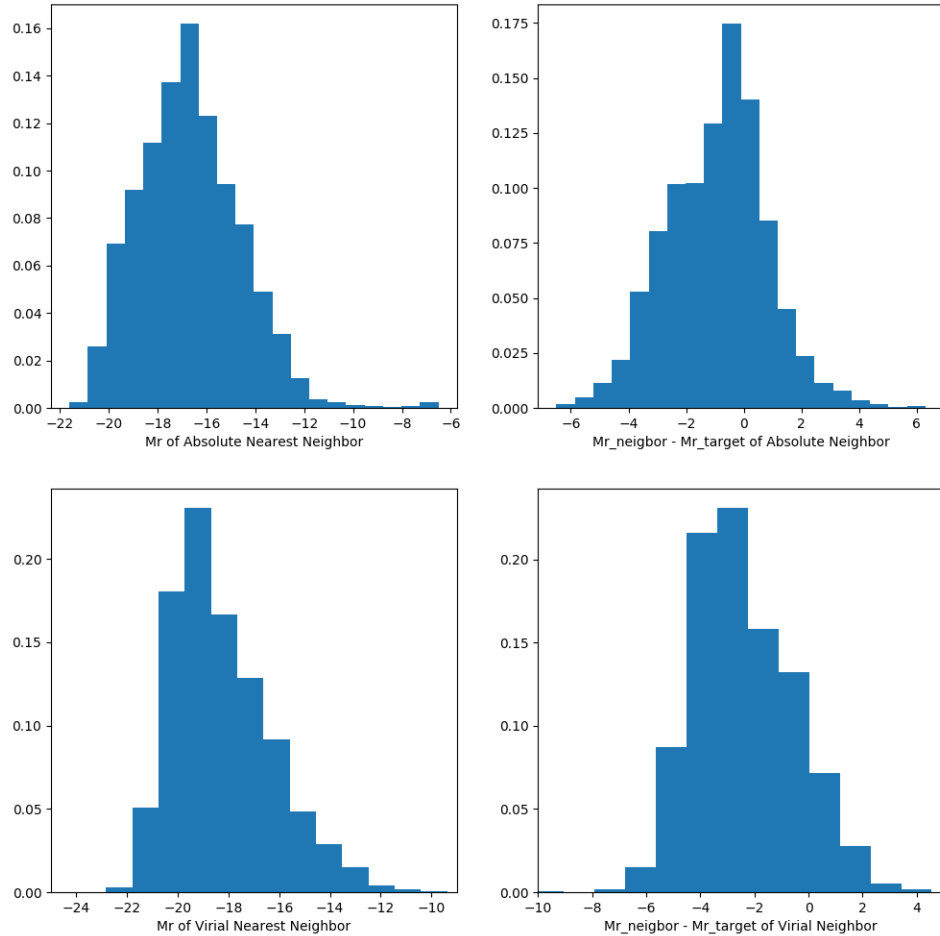


Figure 5.8: The distributions in absolute magnitude (left panel) and absolute magnitude relative to the target galaxy (right panel) of the nearest neighbor galaxies. The top row includes those nearest neighbors in units of $h^{-1}\text{Mpc}$, and the bottom row consists of the nearest neighbors in units of the neighbor’s virial radius. Comparing the two plots in the right panel, we see that the closest galaxy to the target dwarf galaxies is often of equal or fainter magnitude than the target galaxy. Alternatively, using the virial radius of the neighbor galaxy as a measure of distance often finds a brighter galaxy than the target galaxy, as the bottom right plot shows.

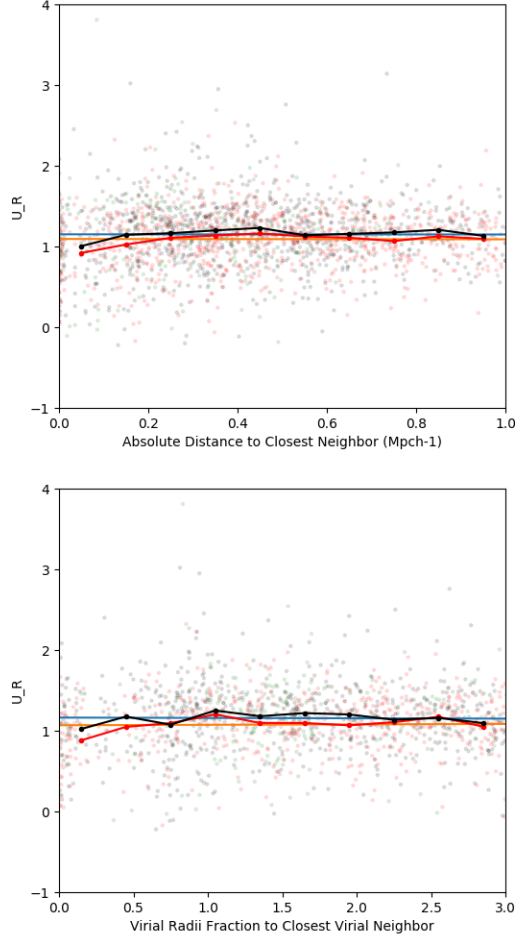


Figure 5.9: Color versus distance to the nearest galaxy (in units of $h^{-1}\text{Mpc}$ on top and virial radii on the bottom) for the star-forming dwarf galaxies. The redshift is included when calculating the distance to the nearest neighbor. While there is still no correlation between distance and color, we do note that there is a gap in the distribution of galaxies around a distance of $0.05 h^{-1}\text{Mpc}$ or $0.5r_{vir}$ from the nearest neighbor.

5.4.4 Including redshift in the distance

Realizing that the peculiar velocity, which is included in a galaxy's redshift, is not insignificant at the smaller scales, we have been careful to avoid calculating the distance between objects with the redshift. However, we are interested to see how the inclusion of redshift in the distance calculations affects the results of our analysis. Therefore, we repeat the same analysis on the relationship between color and distance, but this time we include redshift as a third component in the distance calculations. Consequently, we no longer limit our sample by a peculiar velocity separation. Fig. 5.9 shows the relationship between these distances and the color of the star-forming dwarf galaxies. When compared to Fig. 5.1, we see that there is no change in the correlation between distance and color for the galaxies.

We note the existence of a gap in the distribution of galaxies around a distance of $0.05 h^{-1}\text{Mpc}$ or $0.5r_{vir}$ from the nearest neighbor that is not present in Fig. 5.1. When we incorporate the redshift into the distance calculations, the resulting distance between galaxies which have small sky separations but larger redshift separations is much larger than those with larger sky separations and little redshift separation. As a result, galaxies which were originally close to the color axis in Fig. 5.1 will be moved to much larger distances, while the locations of those which were originally further from the color axis will change much less. The dwarf galaxies which remain close to the color axis in Fig. 5.9 must, therefore, have small sky separation and almost no difference in their peculiar velocities. We surmise that these represent merging systems, which future visual inspection will help to confirm.

5.5 Discussion

We see no relationship between a dwarf galaxy's color, sSFR, or gas-phase chemical abundances and its distance to the nearest galaxy or group beyond the target galaxy's immediate vicinity, implying that the small-scale environment does not significantly influence a dwarf galaxy's evolution. This is in contrast to the large-scale environment, which we have seen to influence the formation and evolution of dwarf galaxies.

Only those galaxies within $0.05 h^{-1}\text{Mpc}$ and $0.05r_{vir}$ of a nearest neighbor, or those within $0.1 h^{-1}\text{Mpc}$ of the nearest group appear to deviate from the average galaxy values. The target galaxies within this proximity of their nearest neighbor tend to be bluer, have a higher sSFR, and have higher oxygen and nitrogen abundances. Based on the shift in the distribution of galaxies seen in Fig. 5.9, these galaxies might be merging or strongly interacting with their nearest neighbor. If so, this provides evidence that galaxy interactions result in a burst of star formation that increases the gas-phase chemical abundances of the dwarf galaxies. Because merging galaxies share the same dark matter halo, it appears that the sharing of a dark matter halo has more influence on the evolution of a galaxy than the distance to its nearest neighbor.

In contrast, dwarf galaxies within $0.1 h^{-1}\text{Mpc}$ of the center of the nearest group are redder, have lower oxygen abundances (O/H), and have higher N/O ratios than average. Being so close to the center of a group seems to prevent more recent episodes of star formation. Due to their proximity to the group center, it is also likely that these dwarf galaxies are not able to retain as much of their heavy elements as a more isolated galaxy, thereby reducing their gas-phase oxygen abundance (and increasing their N/O ratio).

5.5.1 Comparison to literature results

The influence on the gas-phase oxygen abundance within $0.05 h^{-1}\text{Mpc}$ and $0.05r_{vir}$ agrees with the results of Shields et al. (1991); Pustilnik et al. (2006); Cooper et al. (2008); Ellison et al. (2009); Pustilnik et al. (2011b); Pustilnik (2014), and Sánchez Almeida et al. (2016), which all find that galaxies with higher metallicities preferentially reside in denser regions. Work by Rupke et al. (2008) finds that interacting galaxies have suppressed metallicities due to interaction- or merger-induced gas flows into the galaxy centers.

A study combining the effects of interactions and the large-scale environment is explained in Park & Choi (2009). They find two characteristic distances within which the behavior of the target galaxy changes: $0.05r_{vir}$ and r_{vir} of the neighboring galaxy. Our results seem to confirm the significance of distances out to $0.05r_{vir}$, while we see no significant change around the virial radius of the neighboring galaxy. While they only look at galaxies with $M_r < -19$ and limit the neighbors to be

at least half a magnitude brighter than the target, Park & Choi (2009) find that the morphology and luminosity play a significant role in these relationships. Of particular note is their observation that star formation increases in late type galaxies when their nearest neighbor is also of late type. This is the same behavior we see in our sample of dwarf galaxies at distances less than $0.05r_{vir}$. With all our target galaxies actively forming stars, and more than half of their nearest neighbors also dwarf galaxies, it is most likely that our galaxy pairs are also of the late-late type. Based on the results of Park & Choi (2009), the deviations we see for those galaxies with nearest neighbors within $0.05 h^{-1}\text{Mpc}$ and $0.05r_{vir}$ warrant further study.

5.6 Conclusions

Using the star-forming dwarf galaxies in the SDSS DR7 sample with gas-phase chemical abundances from Douglass & Vogeley (2017, in prep), we investigate the influence of the small-scale environment on the evolution of dwarf galaxies. From the \sim 2000 galaxies in the sample, there only appears to be an effect from a neighboring galaxy within $0.05 h^{-1}\text{Mpc}$ or $0.05r_{vir}$. The proximity of a group seems to only affect the target dwarf galaxy if it is within $0.1 h^{-1}\text{Mpc}$. Thus, the small-scale ($\sim 1 h^{-1}\text{Mpc}$) environment does not appear to strongly influence the evolution of dwarf galaxies.

We examine the relationship between distance to the nearest neighbor or group and the target galaxy's color, sSFR, and gas-phase chemical abundances. We find that, for those galaxies with a neighbor within $0.05 h^{-1}\text{Mpc}$ or $0.05r_{vir}$, the dwarf galaxies are bluer, have a higher sSFR, and have higher oxygen and nitrogen abundances than average. In contrast, dwarf galaxies within $0.1 h^{-1}\text{Mpc}$ of the center of the closest group are redder, have lower oxygen abundances, and have higher N/O ratios than average. These results do not depend on the maximum peculiar velocity difference or on the sample (star-forming versus all galaxies).

When we incorporate the redshift into the distance calculations, we find that those galaxies within $0.05r_{vir}$ are most likely mergers or strongly interacting with their nearest neighbor. This matches the results of Park & Choi (2009), who find that late-late type galaxy pairs within $0.05r_{vir}$ are bluer and have higher star formation rates. These merging galaxies likely share the same dark matter halo, indicating that the dark matter halo is more influential on a galaxy's evolution than

its distance to the nearest neighbor.

Further analysis of this study should include comparing the properties of the target galaxies with the nearest neighbors' properties as a function of distance ("galactic conformity"). The gas-phase chemical abundances between a galaxy and its nearest neighbor could be strongly correlated.

Chapter 6: Identifying green valley galaxies

This work was done in collaboration with Jinfu Dai for his senior thesis “Exploring the green valley.”

6.1 Introduction

The enrichment of the interstellar medium (ISM) and circumgalactic medium (CGM) of a galaxy involves many complicated astrophysical processes, the interplay of which is not yet well understood. A critical problem in galaxy formation is to understand how galaxies transition from the blue sequence to the red cloud of the optical color-magnitude diagram. Star formation is thought to be quenching in galaxies moving through the green valley, but the relevant baryonic processes (gas cooling, feedback, etc.) are very complex and heavily interdependent. Investigating the star formation history and chemical evolution of galaxies in the green valley should provide clues as to the evolution of a galaxy through the color-magnitude diagram.

Large galaxy surveys (like the Sloan Digital Sky Survey; York et al., 2000) revealed the structure of the color-magnitude diagram (CMD). As seen in Fig. 6.1, the $u - r$ CMD is dominated by two major subgroups of galaxies: the red cloud and the blue sequence (Strateva et al., 2001; Baldry et al., 2004). Most galaxies that reside in the red cloud appear to be older, elliptical galaxies that are no longer making stars (“red and dead”). On the other hand, the blue sequence consists of mostly spiral and irregular galaxies which are actively forming stars.

There are a number of different astrophysical processes which simultaneously evolve a galaxy’s stellar and gas content. AGN feedback strongly affects massive galaxies, while dwarf galaxy feedback is dominated by supernovae. Both AGN and supernovae can inject enough energy into a galaxy’s ISM to prevent its cooling, thereby quenching star formation. In addition to internal mechanisms, galaxies will often experience interactions in denser environmental regions. Depending on the properties of the galaxies involved (mass, speed, etc.), these interactions can either strip gas from the galaxy (removing a primary source of fuel for future star formation), or they can trigger a burst of star

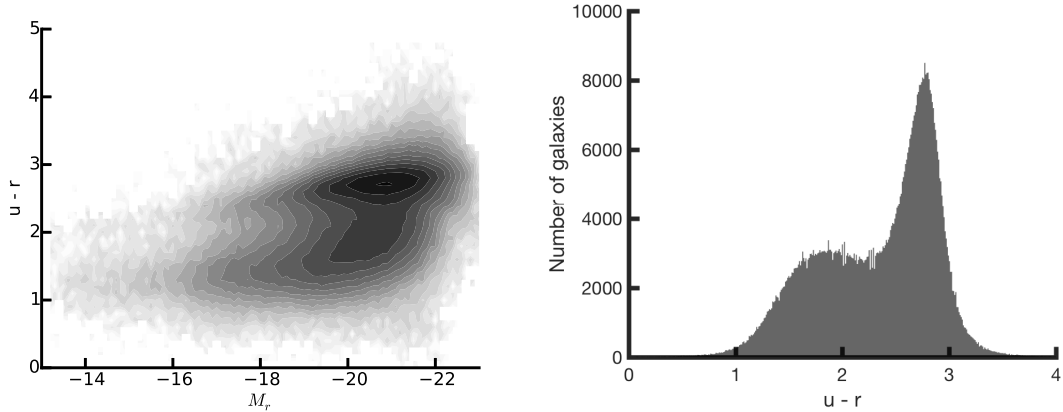


Figure 6.1: The optical color-magnitude diagram (left) and histogram of $u - r$ colors (right) of galaxies in SDSS DR7. There are two groups of galaxies, the populations of which are well fit by the sum of two Gaussians. They are aptly named the “red cloud” and the “blue sequence.”

formation.

Our current theory of galactic evolution necessitates the existence of a transition period in a galaxy’s lifetime, when the galaxy migrates from the star-forming blue sequence to the red cloud on the optical CMD. However, the $u - r$ CMD is very well fit by the sum of only two Gaussians (Strateva et al., 2001; Baldry et al., 2004); an intermediate population is not present in the optical CMD. Early explanations developed to reconcile this apparent discrepancy between theory and observation included a sudden transition from the blue sequence to the red cloud, often associated with some star-formation quenching mechanism.

Dubbed the “green valley,” it is thought that star formation is being quenched in the galaxies moving through the green valley (Martin et al., 2007). So far, results of studies done with these green valley galaxies have been inconclusive as to why or how this occurs.

6.2 Calculating the color of a galaxy

A galaxy’s color is the ratio of the flux emitted by the galaxy in two different bands. The stellar population of a galaxy will determine its color — redder galaxies contain much older, cooler stars, while the spectrum of a bluer galaxy is produced by light from much younger, hotter stars. A galaxy’s color is independent of its redshift, so only photometry is needed to calculate the ratio.

While the KIAS-VAGC catalog (described below in Section 6.3.1) provides the $u - r$ color for all galaxies in SDSS, we make use of the Petrosian fluxes in the NSA (described in Section 6.3.2) to calculate the UV-optical color. The NUV- r color is calculated by

$$\text{NUV} - r = -2.5 \log \left(\frac{f_{\text{NUV}}}{f_r} \right) \quad (6.1)$$

where f_{NUV} is the Petrosian flux in the NUV-band of GALEX, and f_r is the Petrosian flux in the r -band of SDSS.

6.3 SDSS and GALEX data

We use the photometric data from SDSS (optical) and GALEX (ultraviolet) as cross-matched in the NSA.

6.3.1 Optical data — SDSS

The SDSS Data Release 7 (Abazajian et al., 2009, DR7) is a wide-field multi-band imaging and spectroscopic survey that uses drift scanning to map approximately one-quarter of the northern sky. A dedicated 2.5-meter telescope at the Apache Point Observatory in New Mexico takes photometric data in the five-band SDSS system — u , g , r , i , and z (Fukugita et al., 1996; Gunn et al., 1998). Galaxies with a Petrosian r -band apparent magnitude $m_r < 17.77$ are selected for spectroscopic analysis (Lupton et al., 2001; Strauss et al., 2002). Gas-phase chemical abundances are calculated via the Direct T_e method using emission-line fluxes measured by the MPA-JHU catalog¹ and published in Douglass & Vogeley (2017, in prep). The large-scale environment of the galaxies is based on the void catalog compiled by Pan et al. (2012). This void catalog is constructed from SDSS DR7 using the VoidFinder algorithm of Hoyle & Vogeley (2002). Galaxies which are located within the identified voids are labeled as void galaxies; those which do not reside in a void are designated as wall galaxies. Because the minimum diameter of a void is defined as $10 h^{-1}\text{Mpc}$, the large-scale environment of galaxies within $5 h^{-1}\text{Mpc}$ of the edge of the SDSS DR7 footprint cannot be described, so their environment is labeled as unknown.

¹ Available at <http://www.mpa-garching.mpg.de/SDSS/DR7>

The Korea Institute for Advanced Study Value-Added Galaxy Catalog (Choi et al., 2010, KIAS-VAGC) contains galaxies from the SDSS DR7 main sky survey based on the New York University Value-Added Galaxy Catalog Data Release 7 (Blanton et al., 2005, NYU-VAGC). It provides a morphological class and type following the automated morphology classification scheme of Park & Choi (2005), using the color $u - r$, color gradient $\Delta(g - r)$, and inverse concentration index. We use the absolute magnitudes as listed in the KIAS-VAGC.

6.3.2 UV data — GALEX

The Galaxy Evolution Explorer (Martin et al., 2005, GALEX) is an orbiting space telescope conducting an extra-galactic ultraviolet all-sky survey. The instrument allows imaging and spectroscopic observations in two ultraviolet bands — Far UV (FUV, 1350–1780Å) and Near UV (NUV, 1770–2730Å) (Morrissey et al., 2007). The NUV- r colors used in this study are calculated from the azimuthally-averaged SDSS-style Petrosian fluxes provided in the NASA-Sloan Atlas version 0.1.2 (Blanton et al., 2011, NSA).

6.4 Classification of galaxies in the color-magnitude diagram

Combining the results of GALEX with the optical photometry of SDSS, we construct a NUV- r CMD. Probing light from even younger stars in the galaxies, GALEX is able to increase the separation of the blue sequence and red cloud populations of the optical CMD, revealing a third, smaller population of galaxies (Wyder et al., 2007).

This analysis reveals a population of galaxies that lie in the Green Valley on the NUV- r color-magnitude diagram, identified independent of their location on the diagram. Rather than being classified based on arbitrary limits placed on the NUV- r values (as done by Schawinski et al., 2014; Salim, 2014), the galaxies can be easily separated into three distinct populations based on the galaxies’ morphological types as calculated in the KIAS-VAGC; this can be seen in Fig. 6.2. Defined by the $u - r$ color and the color gradient $\Delta(g - i)$, it is novel that an estimate of the morphological type of the galaxies is an adequate classification for the three populations of the NUV- r CMD. In addition, Fig. 6.3 shows a histogram of the galaxies which overlap in both

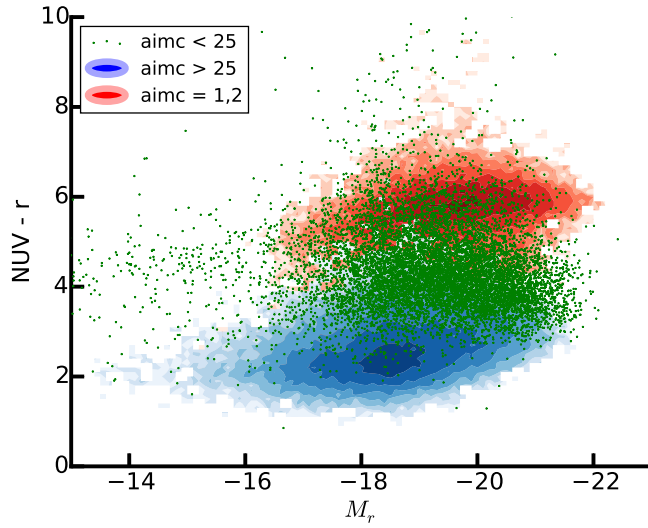


Figure 6.2: The NUV $-r$ color-magnitude diagram of galaxies in SDSS DR7. Those galaxies in the red contours have morphological classifications of either normal early types (aimc = 1) or blue early types (aimc = 2), as determined by the KIAS-VAGC. The green points represent a subset of the normal late type galaxies (aimc less than 25, excluding those with values of 1 or 2), and the blue contours represents the remaining normal late type galaxies (aimc greater than 25). It is clear that this morphological classification defines those galaxies that are transitioning from the blue sequence to the red cloud.

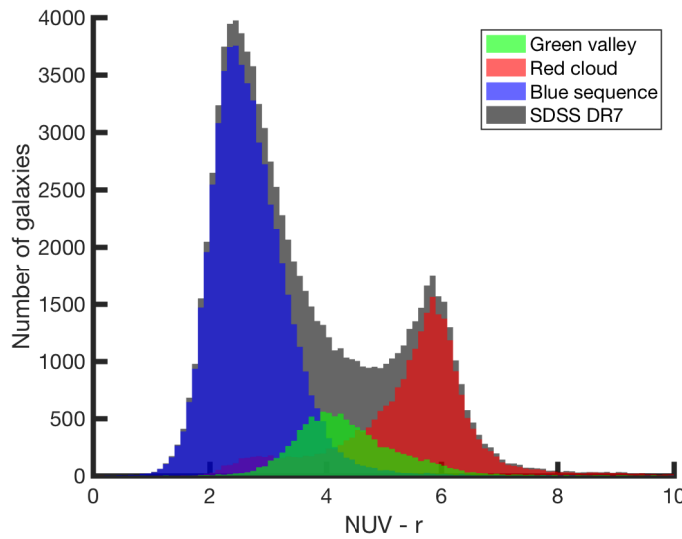


Figure 6.3: A histogram of the NUV $-r$ color of those SDSS DR7 galaxies which are also detected in GALEX. The red cloud, blue sequence, and green valley populations are separated by the morphological types as defined by the KIAS-VAGC. It is readily apparent that the green valley galaxies exist in the space between the red cloud and blue sequence.

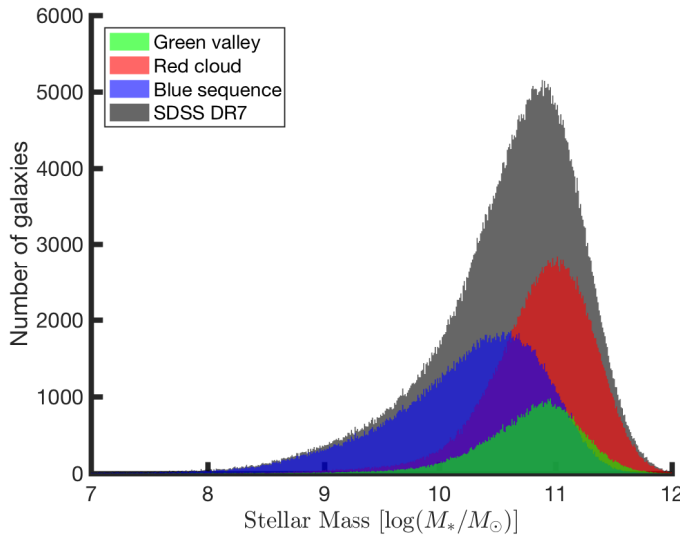


Figure 6.4: The distribution of stellar mass for all galaxies in SDSS DR7, separated by their morphological type. The galaxies in the green valley have stellar masses comparable to those in the red cloud. The stellar masses of those galaxies in the blue sequence range from the lowest mass objects up through the stellar masses of the green valley galaxies.

GALEX and SDSS, separated by their morphological classification from the KIAS-VAGC. It shows that the three populations are well fit by three Gaussians — the new population in the middle is the transient galaxy population originally “missing” from the optical CMD.

The morphological classification that we use to isolate the green valley population is relatively unique in that it is analytic; morphological classification attempts are often completed in a more subjective manner (such as the GalaxyZoo, Lintott et al., 2011). In particular, the morphological type provided in KIAS-VAGC is a combination of the color $u - r$ and the color gradient $\Delta(g - i)$. Both these quantities are independent of the NUV– r CMD, which is part of the novelty behind why this measure separates the galaxies into the three evolutionary stages of the CMD so well.

6.4.1 Properties of the Green Valley Galaxies

Stellar mass

If the green valley galaxies represent those galaxies transitioning between the blue sequence and red cloud, then their stellar masses should overlap the masses in both these populations. The distribution of the stellar masses for the galaxies in SDSS DR7 is shown in Fig. 6.4. We can see

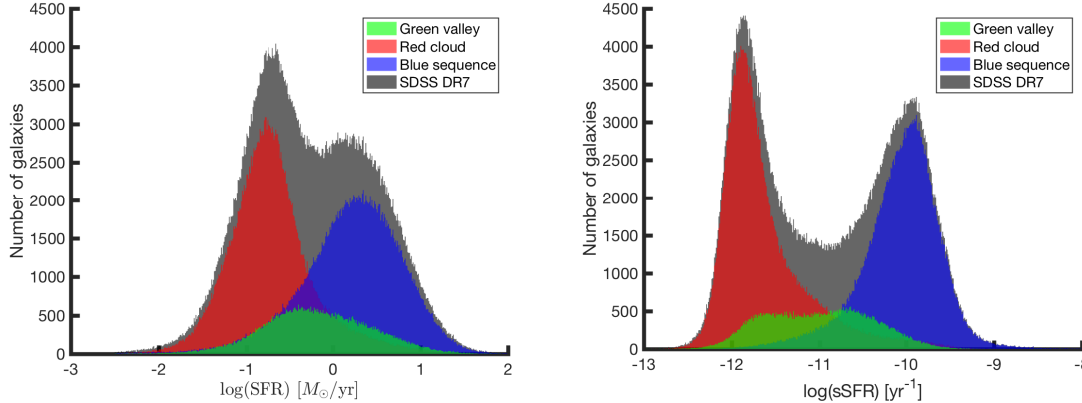


Figure 6.5: The distribution of SFR (left panel) and sSFR (right panel) for all galaxies in SDSS DR7, separated by their morphological type. The green valley galaxies occupy the intermediate SFRs, while galaxies in the red cloud have low SFRs and galaxies in the blue sequence have higher SFRs. The same ranges exist for the sSFRs, although the green valley galaxies extend well into the range of sSFRs occupied by the galaxies in the red cloud.

that the galaxies in the green valley have stellar masses comparable to those in the red cloud. The stellar masses of those galaxies in the blue sequence range from the lowest mass objects up through the stellar masses of the green valley galaxies. The distribution of stellar masses of blue sequence galaxies should be much broader than the range of masses seen in the red cloud galaxies, since those in the blue sequence are slowly building up their stellar mass by forming stars from both their gas reservoirs and cool gas falling onto the galaxy. Galaxies in the red cloud are fairly stagnant in their star formation, so the range of stellar masses of these galaxies will be more narrow than that of the blue sequence. If the green valley galaxies are transitioning between the two populations due to a quenching of star formation or a sudden burst of star formation, then we would expect their mass range to cover the high-mass end of the blue sequence and most of the red cloud. These expectations are met in Fig. 6.4.

Star formation rates

If green valley galaxies are transitioning between the blue sequence and red cloud, then they should have intermediate (s)SFRs. The distribution of SFR and sSFR for the galaxies in SDSS DR7 are shown in Fig. 6.5, with the galaxies separated by their morphological types. We see that the distribution of SFRs for galaxies in the green valley peaks around $\log(\text{SFR}) \sim -0.5$, in between the

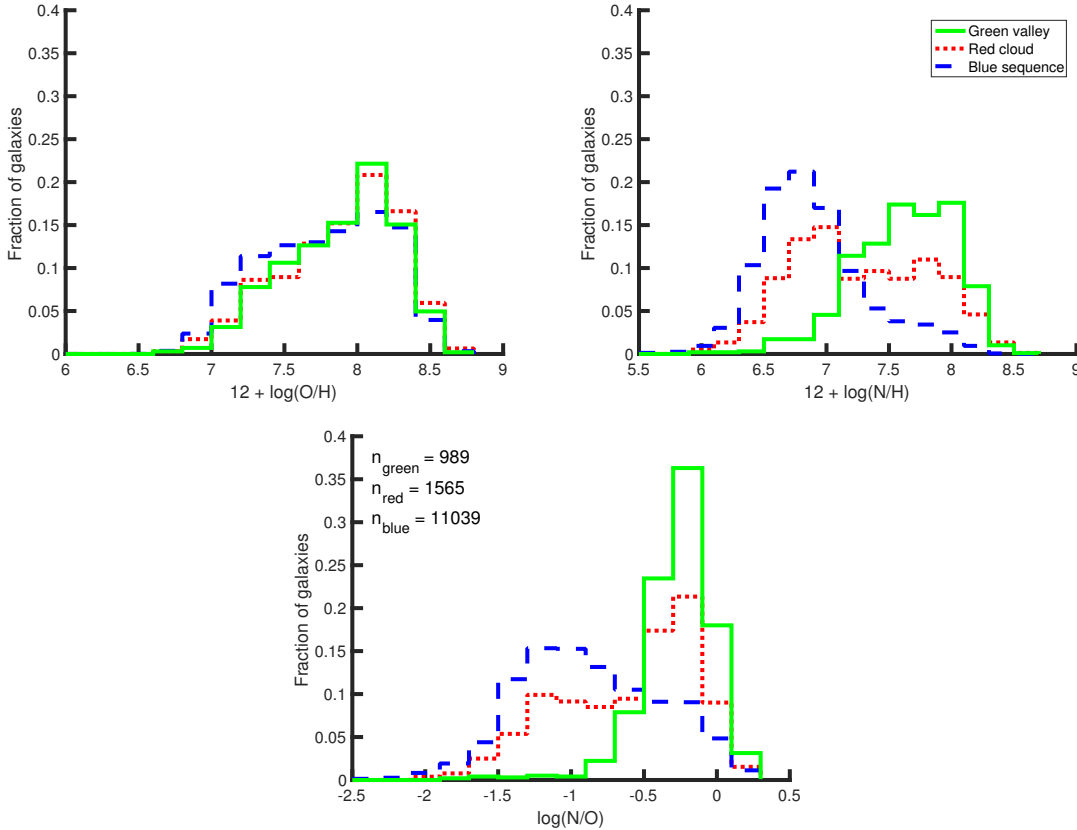


Figure 6.6: Histograms of the oxygen abundance (top left), nitrogen abundance (top right), and N/O ratio (bottom center) of the cross-matched SDSS DR7 – GALEX galaxies, separated into their locations on the $\text{NUV} - r$ color-magnitude diagram according to the morphological type listed in the KIAS-VAGC. It is readily apparent that the green valley galaxies have higher nitrogen abundances than those in the blue sequence (and some of the red cloud). This, therefore, corresponds to them having high N/O ratios.

ranges occupied by the red cloud and blue sequence galaxies. A similar distribution is shown for the sSFRs, although the green valley galaxies extend well into the range of sSFRs occupied by the galaxies in the red cloud. Salim (2014) describes transitional galaxies (those in the green valley) to have lower sSFRs than galaxies in the blue sequence, specifically $-11.8 < \log(\text{sSFR}) < -10.8$. While our results do indicate that green valley galaxies have lower sSFRs than those in the blue sequence, we find that their range of sSFR is almost double the width of that described in Salim (2014). The green valley galaxies have a sSFR within the range $-12 \lesssim \log(\text{sSFR}) \lesssim -10$.

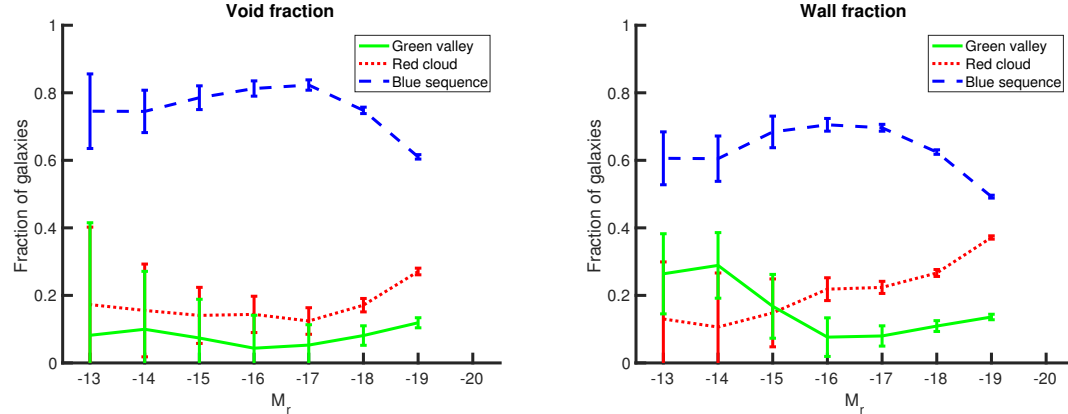


Figure 6.7: Fraction of void (left) and wall (right) galaxies in each of the three CMD populations, classified by the morphological type listed in the KIAS-VAGC. There is a higher fraction of green valley dwarf galaxies ($M_r > -17$) found in the more dense environments than in the voids. This would indicate that void galaxies are slightly behind wall galaxies in their evolution, matching predictions based on the Λ CDM cosmology.

Gas-phase chemical abundances

Estimates of the gas-phase chemical abundances of galaxies probe their integrated star formation histories, which can provide insight into the enrichment of the ISM and CGM. A few of the galaxies for which Douglass & Vogeley (2017, in prep) are able to estimate metallicities reside in the green valley. When compared with the metallicities of galaxies in the blue sequence and red cloud, Fig. 6.6 shows that the green valley galaxies have higher nitrogen abundances than star-forming galaxies in the blue sequence (and some of the red cloud). With oxygen abundances that fall within the same range as the other two galaxy populations, this shift causes the N/O ratio to be much higher in green valley galaxies than in the blue sequence.

Large-scale environment

When we separate the galaxies in each of the three populations by their large-scale environment, we discover a variation in these populations as a function of luminosity. As we see in Fig. 6.7, the fraction of galaxies in the green valley depends on the large-scale environment, even at fixed stellar mass or luminosity. A larger fraction of faint wall galaxies are found in the green valley than for faint void galaxies.

6.5 Understanding green valley galaxies

Galaxies in the green valley are described to be in a transitional period of the galaxy's life cycle, where they are being quenched in their star formation or are beginning to form stars after being quiescent. Here, we are able to quantitatively define galaxies in the green valley of the UV-optical CMD. We find them to be of comparable stellar mass to galaxies in the red cloud, have intermediate SFRs and intermediate-to-low sSFRs, and have higher gas-phase nitrogen abundances and N/O ratios than galaxies in the blue sequence.

The range of stellar masses in galaxies from the green valley in Fig. 6.4 shows us that these galaxies have completed most of their star formation. They have acquired enough stars to have converted much of their gas into heavier elements. Combined with the intermediate SFRs and intermediate-to-low sSFRs seen in Fig. 6.5, this tells us that these galaxies are no longer forming stars at a high rate. This is most likely due to an extinction of available cool gas from which to form stars. These galaxies are reaching a natural point in their evolution where they transition from an active star formation period to a quieter, more quiescent lifestyle.

As explained in Douglass & Vogeley (2017b), nitrogen is thought to be produced in both a primary and secondary stage, depending on the presence of other heavy elements. The fact that the galaxies in the green valley have higher nitrogen abundances compared to those in the blue sequence indicate that they are building up a surplus of nitrogen, most likely due to the presence of heavier elements at the later star formation episodes. The surplus of heavier elements allows the CNO cycle to commence earlier in the stars' lifetimes, producing nitrogen at a higher rate than oxygen. It is also possible that the higher nitrogen abundances are a sign that the galaxies' intermediate mass stars (those primarily responsible for nitrogen synthesis) have expired. This surplus of nitrogen results in the high N/O ratios seen for the green valley galaxies in Fig. 6.6.

Fig. 6.7 shows a higher fraction of faint wall galaxies than faint void galaxies are in the green valley. This would indicate that void galaxies are slightly behind wall galaxies in their evolution, matching predictions based on the Λ CDM cosmology. These results also coincide with the observations of Douglass & Vogeley (2017b) and Douglass & Vogeley (2017, in prep). They find that, for

dwarf galaxies ($M_r > -17$), those which exist in voids may have commenced their star formation at a later time and have not experienced the same cosmic downsizing as dwarf galaxies residing in denser regions. The higher fraction of wall dwarf galaxies in the green valley might also point to an environmental influence on the reason for transitioning through the green valley, such as ram pressure stripping, which would occur much less frequently in the void environment. However, the existence of void galaxies in the green valley indicate that galaxy interactions cannot be the only star formation quenching mechanism.

6.5.1 Gas content indicators

If a galaxy's star formation is quenched due to a loss of cold gas, then its HI content will be lower than other galaxies of a similar stellar mass and large-scale environment. Schawinski et al. (2014) finds that 48% of the late-type galaxies they define to be in the green valley have H I detections in the ALFALFA survey, consistent with a high probability of gas reservoir retention. Likewise, Catinella et al. (2012) shows that the gas fraction (M_{HI}/M_*) correlates with the NUV– r color, suggesting that the transition of galaxies into the green valley is not due to an abrupt change in the galaxy's neutral gas supply. If it is quenched due to a high gas temperature (from AGN or supernovae feedback), then the temperature of the gas will be higher than others of a similar size. These factors will also help to determine when and why a galaxy transitions from star-forming to quiescent (and maybe back to star-forming).

6.5.2 Evidence of AGN feedback

To understand the gas-phase chemical abundances of the green valley galaxies, we compare Fig. 6.6 with the distribution of the gas-phase chemical abundances of star-forming and composite galaxies and galaxies with an AGN shown in Fig. 6.8. We see that the galaxies with an AGN have the most similar distributions in the three abundance ratios as the green valley galaxies: both groups have similar oxygen abundances (O/H) and higher nitrogen abundances (N/H) and N/O ratios than the star-forming galaxies. This might indicate a link between green valley galaxies and a host AGN. The presence of an AGN in green valley galaxies would support other studies of the transition of

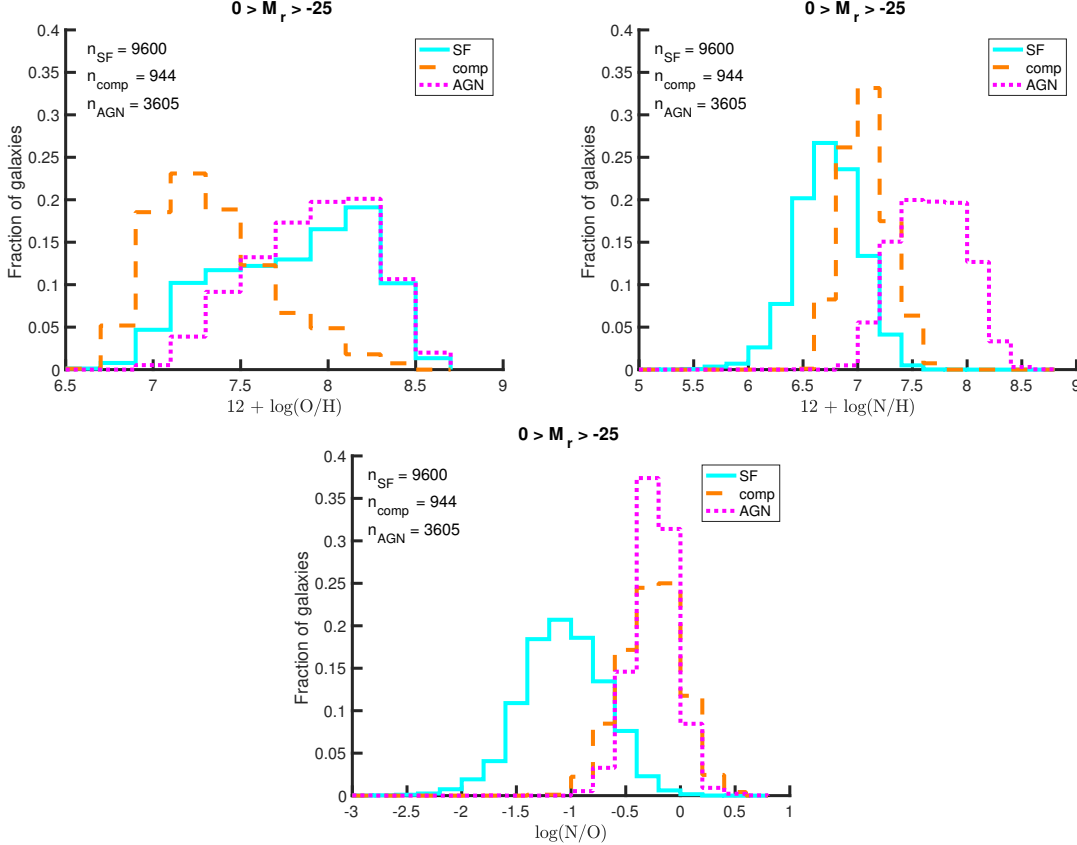


Figure 6.8: Distribution of the gas-phase oxygen abundance (O/H, top left), nitrogen abundance (N/H, top right), and N/O ratio (bottom center) of the SDSS DR7 galaxies with detectable emission lines for abundance calculations with the Direct T_e method. Star-forming galaxies are shown with a solid cyan line, while composite galaxies are a dashed orange line and galaxies with an AGN are represented as a dotted magenta line. Composite galaxies have lower oxygen abundances than both star-forming galaxies and those with an AGN. The nitrogen abundance range is different for each of the three classes, with star-forming galaxies having the lowest nitrogen abundances, AGN having the highest, and composite galaxies in the middle. Therefore, star-forming galaxies have N/O ratios < 0 , while composite galaxies and galaxies with an AGN have N/O ratios between -1 and 0.5.

galaxies from the blue sequence to the red cloud, which attribute the quenching of star formation to accretion of a central black hole (e.g., Croton et al., 2006; Stasińska et al., 2008).

6.6 Conclusions

We can define galaxies which are transitioning through the green valley of the color-magnitude diagram by combining the galaxy's color, color gradient, and inverse concentration index. Galaxies with a magnitude less than 25 for the morphological type as calculated in the KIAS-VAGC exist in the green valley portion of the UV-optical color magnitude diagram. Galaxies defined as early types (morphological type values equal to 1 or 2) are in the red cloud, while those with morphological type values greater than 25 are in the blue sequence. With this quantitative definition for galaxies transitioning through the green valley, we can begin to understand the properties of green valley galaxies and the evolution of galaxies.

Based on our analysis, green valley galaxies have stellar masses comparable to those in the red cloud. They have intermediate SFRs, and low-to-intermediate sSFRs. Green valley galaxies also have high gas-phase nitrogen abundances (N/H), resulting in high N/O ratios. While their SFRs show that something has quenched their star formation, their stellar masses inform us that this is not due to any premature quenching mechanism. The high nitrogen abundances in the green valley galaxies indicate that the galaxies are either no longer forming stars (since nitrogen is produced in lower mass stars than oxygen), or that the galaxies were able to produce both primary and secondary nitrogen (heavy elements were present during the last few star formation episodes to permit the CNO cycle to commence earlier). This chemical abundance pattern (normal oxygen, high nitrogen, and high N/O ratio) is also seen in galaxies classified as AGN, indicating that the galaxies in the green valley have an AGN.

There is a higher fraction of faint wall galaxies than faint void galaxies in the green valley. In conjunction with the conclusions of Douglass & Vogeley (2017b) and Douglass & Vogeley (2017, in prep), this indicates that void dwarf galaxies are less evolved than dwarf galaxies in denser environments. It would be beneficial to investigate the small-scale ($\sim 1 h^{-1}\text{Mpc}$) environment of galaxies in the green valley, to determine if any interactions are responsible for the transitional state.

Chapter 7: Conclusions and suggestions for future work

7.1 Large-scale environmental influence on the gas-phase chemical abundances in dwarf galaxies

We find that the large-scale environment influences the chemical evolution of dwarf galaxies by estimating the gas-phase oxygen (O/H) and nitrogen (N/H) abundances and the N/O ratio of star-forming dwarf galaxies in SDSS DR7 using the Direct T_e method and spectroscopic line flux measurements as reprocessed in the MPA-JHU catalog (Douglass & Vogeley, 2017a,b, Douglass et al., 2017, in prep). Due to the minimum redshift limit for detecting the [O II] $\lambda 3727$ emission line in SDSS DR7 spectra, only 135 star-forming dwarf galaxies are available for analysis with the Direct T_e method. With this sample, we see no difference in the metallicity (O/H) between dwarf galaxies in voids and denser regions (Douglass & Vogeley, 2017a). Upon closer inspection, we find minor shifts in the distributions of gas-phase chemical abundances for void dwarf galaxies when compared to dwarf galaxies in denser regions: star-forming void dwarf galaxies have higher oxygen abundances (O/H), lower nitrogen abundances (N/H), and lower N/O ratios (Douglass & Vogeley, 2017b).

By deriving a relation between the doubly-ionized oxygen and total oxygen abundance in star-forming galaxies, we can expand our sample to consist of 1920 star-forming dwarf galaxies by removing the dependence on the [O II] $\lambda 3727$ doublet. This larger sample exhibits the same shifts in the gas-phase chemical abundances as the smaller, 135 star-forming dwarf galaxy sample, but with a much higher statistical significance. We find that star-forming void dwarf galaxies have, on average, 7% higher oxygen abundances, 10% lower nitrogen abundances, and 17% lower N/O ratios than star-forming dwarf galaxies in denser regions. The large-scale ($\sim 10 h^{-1}\text{Mpc}$) environment influences the chemical evolution of star-forming dwarf galaxies.

In addition to studying the large-scale environmental influence on the distribution of gas-phase chemical abundances in star-forming dwarf galaxies, we also investigate if and how the large-scale environment affects relationships between the chemical abundances and various other physical prop-

erties of the galaxies. We find that the N/O ratio decreases with increasing metallicity rather than a constant value for the N/O ratio as a function of O/H as observed in other studies. This is contrary to what we see in the M_* -N/O relationship, where we find that some of the star-forming dwarf galaxies have a constant value of N/O for a range of masses while the remainder exhibit a positive relationship between the stellar mass and N/O ratio. We make note of a different critical mass in the M_* -N/O relationship in the two environments, where the void dwarf galaxies begin to show evidence of secondary nitrogen synthesis at a stellar mass \sim 0.4 dex lower than for the galaxies in denser regions. Most of our star-forming dwarf galaxies follow the established mass-metallicity relation (e.g., Tremonti et al., 2004).

No relationship is observed between the metallicity and H I mass in our sample of star-forming dwarf galaxies, but we find that the N/O ratio decreases with increasing H I mass for a given stellar mass. The star-forming dwarf galaxies also exhibit an increase in the metallicity and N/O ratio with increasing color (both $u - r$ and $g - r$). We see very little correlation with SFR for either metallicity or the N/O ratio in dwarf galaxies, but the metallicity and N/O ratio decrease with increasing sSFR. Beyond the large-scale environmental influence on the distributions of the gas-phase chemical abundances and the critical mass in the M_* -N/O relationship, we do not observe any significant differences between the star-forming void and wall dwarf galaxies in any of these relationships.

We surmise that the differences in the distributions of metallicity and the N/O ratio seen in the sample of star-forming dwarf galaxies are due to a large-scale environmental influence on their star formation history and evolution. The shift in the gas-phase oxygen abundance distribution could be observational evidence for delayed star formation in void galaxies when compared to those in denser regions. This would result in a smaller ratio of stellar mass to dark matter halo mass in void galaxies than in dwarf galaxies in denser regions, as predicted in simulations by Jung et al. (2014) and Tonnesen & Cen (2015). If the void galaxies are retaining more oxygen as a result of their deeper potential wells, then they would be able to commence secondary nitrogen synthesis earlier, as seen in the M_* -N/O relation in Fig. ???. In addition, the shift towards lower N/O ratios in the star-forming dwarf galaxies might be evidence that cosmological downsizing is environmentally dependent as

predicted by Cen (2011). Our results provide evidence for delayed, ongoing star formation in void dwarf galaxies whose dark matter halos ceased coalescing earlier than for dwarf galaxies in denser regions.

It has been hypothesized that a special population of extremely metal-poor galaxies exist in void regions. We find no evidence for a special population of extremely metal-poor star-forming dwarf galaxies in the voids, as we note an equal fraction of low metallicity dwarf galaxies in both the void and denser regions. Due to their low gas-phase oxygen abundances, these 287 dwarf galaxies have some of the larger N/O ratios of the star-forming dwarf galaxies sample studied. While the metallicities of these galaxies cause them to stand out in the relationships between metallicity and other physical quantities (stellar mass, color, (s)SFR), they are not unusual when studying the relationships between the N/O ratio and these other quantities.

7.2 Small-scale environmental influence on dwarf galaxy evolution

In addition to the influence of the large-scale environment on the evolution of dwarf galaxies, we also study the effects of the small-scale environment on dwarf galaxies. We find that only the presence of a neighboring galaxy within $0.05 h^{-1}\text{Mpc}$ or $0.05r_{vir}$, or the presence of a group within $0.1 h^{-1}\text{Mpc}$ influences a dwarf galaxy's evolution. Dwarf galaxies with a nearest neighbor galaxy within $0.05 h^{-1}\text{Mpc}$ or $0.05r_{vir}$ are bluer, have a higher sSFR, and have higher oxygen and nitrogen abundances than average. This matches the results of Park & Choi (2009), who find that late-late type galaxy pairs within $0.05r_{vir}$ are bluer and have higher SFRs. In contrast, dwarf galaxies within $0.1 h^{-1}\text{Mpc}$ of the center of the closest group are redder, have lower oxygen abundances, and have higher N/O ratios than average. These results are independent of both the maximum relative velocity required to define a nearest neighbor and the sample (star-forming versus all dwarf galaxies).

When we incorporate the redshift into the distance calculations, we find that the galaxies within $0.05r_{vir}$ are most likely strongly interacting or merging with their nearest neighbor. These merging galaxies likely share the same dark matter halo, suggesting that the dark matter halo is more influential on a galaxy's evolution than the distance between a galaxy and its nearest neighbor.

7.3 Properties of green valley galaxies

Finally, we also investigate the properties of galaxies residing in the green valley of the color-magnitude diagram (CMD) in an effort to understand the role of the environment on a galaxy's evolution through the color-magnitude diagram. We discover that we can define galaxies which are transitioning through the green valley of the CMD by combining the galaxy's color, color gradient, and inverse concentration index. Galaxies with a value less than 25 for the morphological type as calculated in the KIAS-VAGC exist in the green valley portion of the UV-optical CMD. Galaxies defined as early types (morphological type values equal to 1 or 2) are in the red cloud, while those with morphological type values greater than 25 are in the blue sequence. With this quantitative definition for galaxies transitioning through the green valley, we can begin to understand the properties of green valley galaxies and their evolution.

Based on our analysis, green valley galaxies have stellar masses comparable to galaxies in the red cloud. They have intermediate SFRs and low-to-intermediate sSFRs. Green valley galaxies also have high gas-phase nitrogen abundances (N/H), resulting in high N/O ratios. While their SFRs show that their star formation has been quenched, their stellar masses inform us that this is not due to any premature quenching mechanism. The high nitrogen abundances in the green valley galaxies indicate that the galaxies are either no longer forming stars (since nitrogen is produced in lower mass stars than oxygen), or that the galaxies were able to synthesize both primary and secondary nitrogen (heavy elements were present during the last few star formation episodes to permit the CNO cycle to commence earlier). This chemical abundance pattern of normal oxygen (O/H), high nitrogen (N/H), and high N/O ratio is also seen in galaxies classified as AGN, indicating that galaxies in the green valley have an AGN.

There is a higher fraction of faint galaxies from denser regions than faint void galaxies in the green valley. Combined with the previous results about the large-scale environmental influence on the gas-phase chemical abundances, this indicates that void dwarf galaxies are less evolved than dwarf galaxies in denser environments.

7.4 Suggestions for future work

A critical problem in galaxy formation is understanding how galaxies transition from the blue sequence to the red cloud in the optical color-magnitude diagram. Star formation is thought to be quenching in galaxies moving through the green valley, but the relevant baryonic processes (gas cooling, feedback, etc.) are very complex and heavily independent. The enrichment of the interstellar medium (ISM) and circumgalactic medium (CGM) of a galaxy involves many complicated processes, the interplay of which is not yet well understood. Investigating the star formation history and chemical evolution of galaxies in the green valley should provide clues of the movement of a galaxy through the color-magnitude diagram.

With the advent of 2-dimensional spectroscopic data from SDSS MaNGA (Bundy et al., 2015; SDSS Collaboration et al., 2016), it is possible to examine how the ISM and CGM are enriched over time. MaNGA is the first large-scale survey using integral-field spectroscopy, which would permit the study of spatially-resolved physical properties of galaxies across many different environments, morphologies, and stages of evolution. In particular, it would be instructive to study the gradients of the gas-phase chemical abundances of galaxies in order to better understand their evolution through the CMD and also the influence of the environment in both large and small scales on the chemical evolution of these galaxies.

A better knowledge of the chemical abundances of galaxies with an AGN is also crucial to understanding the evolution of galaxies. Understanding how the presence of an AGN affects a galaxy's evolution is currently limited — at the moment, most research is concentrated on the physics within an AGN. Many simulations have been done to test different theories about the role of an AGN in a galaxy, and observations are now needed to test the results of the simulations.

The work done here on the small-scale environment is only the beginning of what can be done in this subject area. In addition to studying the relationship between a galaxy's physical parameters and its distance to the nearest neighbor, it is also important to look at the ratio of the galaxy's parameters to its neighbor's and the distance to the nearest neighbor — “galactic conformity.” These comparisons should include a morphological comparison, similar to the analysis done by

Park & Choi (2009). We also find evidence of possible mergers when studying the influence of the small-scale environment. Visual inspection of these dwarf galaxies is imperative to confirming this conclusion.

Bibliography

- Abazajian, K. N., Adelman-McCarthy, J., Agueros, M. A., et al. 2009, ApJS, 182, 543
- Ahn, C. P., Alexandroff, R., Allende Prieto, C., et al. 2012, ApJS, 203, 21
- Amorín, R. O., Pérez-Montero, E., & Vílchez, J. M. 2010, ApJL, 715, L128
- Andrews, B. H., & Martini, P. 2013, ApJ, 765, 140
- Ann, H. B., Park, C., & Choi, Y.-Y. 2008, MNRAS, 389, 86
- Asplund, M., Grevesse, N., Sauval, A. J., & Scott, P. 2009, ARA&A, 47, 481
- Baldry, I. K., Glazebrook, K., Brinkmann, J., et al. 2004, ApJ, 600, 681
- Bell, E. F., & de Jong, R. S. 2000, MNRAS, 312, 497
- Berg, D. A., Skillman, E. D., Marble, A. R., et al. 2012, ApJ, 754, 98
- Berlind, A. A., Frieman, J., Weinberg, D. H., et al. 2006, ApJS, 167, 1
- Beygu, B., Kreckel, K., van der Hulst, J. M., et al. 2016, MNRAS, 458, 394
- Beygu, B., Peletier, R. F., Hulst, J. M. v. d., et al. 2017, MNRAS, 464, 666
- Blanton, M. R., Kazin, E., Muna, D., Weaver, B. A., & Price-Whelan, A. 2011, AJ, 142, 31
- Blanton, M. R., Lin, H., Lupton, R. H., et al. 2003, AJ, 125, 2276
- Blanton, M. R., Schlegel, D. J., Strauss, M. A., et al. 2005, AJ, 129, 2562
- Bond, J. R., Kofman, L., & Pogosyan, D. 1996, Nature, 380, 603
- Brinchmann, J., Charlot, S., White, S. D. M., et al. 2004, MNRAS, 351, 1151
- Brisbin, D., & Harwit, M. 2012, ApJ, 750, 142
- Bundy, K., Bershady, M. A., Law, D. R., et al. 2015, ApJ, 798, 7
- Catinella, B., Schiminovich, D., Kauffmann, G., et al. 2012, A&A, 544, A65
- Cen, R. 2011, ApJ, 741, 99
- Choi, Y.-Y., Han, D.-H., & Kim, S. S. 2010, JKAS, 43, 191
- Contini, T., Treyer, M. A., Sullivan, M., & Ellis, R. S. 2002, MNRAS, 330, 75
- Cooper, M. C., Tremonti, C. A., Newman, J. A., & Zabludoff, A. I. 2008, MNRAS, 390, 245
- Croton, D. J., Farrar, G. R., Norberg, P., et al. 2005, MNRAS, 356, 1155
- Croton, D. J., Springel, V., White, S. D. M., et al. 2006, MNRAS, 365, 11
- Cybulski, R., Yun, M. S., Fazio, G. G., & Gutermuth, R. A. 2014, MNRAS, 439, 3564
- de Lapparent, V., Geller, M. J., & Huchra, J. P. 1986, ApJL, 302, L1
- De Robertis, M., Dufour, R., & Hunt, R. 1987, JRASC, 81, 195

- de Rossi, M. E., Tissera, P. B., & Scannapieco, C. 2007, MNRAS, 374, 323
- Deng, X.-F. 2011, AJ, 141, 162
- Dopita, M. A., Sutherland, R. S., Nicholls, D. C., Kewley, L. J., & Vogt, F. P. A. 2013, ApJS, 208, 10
- Douglass, K. A., & Vogeley, M. S. 2017a, ApJ, 834, 186
- . 2017b, ApJ, 837, 42
- Dressler, A. 1980, ApJ, 236, 351
- Ellison, S. L., Simard, L., Cowan, N. B., et al. 2009, MNRAS, 396, 1257
- Emsley, J. 2011, Nature's Building Blocks: An A-Z Guide to the Elements (OUP Oxford)
- Fakhouri, O., & Ma, C.-P. 2009, MNRAS, 394, 1825
- Filho, M. E., Sánchez Almeida, J., Muñoz-Tuñón, C., et al. 2015, ApJ, 802, 82
- Fukugita, M., Ichikawa, T., Gunn, J. E., et al. 1996, AJ, 111, 1748
- Gao, L., & White, S. D. M. 2007, MNRAS, 377, L5
- Garnett, D. R. 1992, AJ, 103, 1330
- Geha, M., Blanton, M. R., Yan, R., & Tinker, J. L. 2012, ApJ, 757, 85
- Goldberg, D. M., Jones, T. D., Hoyle, F., et al. 2005, ApJ, 621, 643
- Goldberg, D. M., & Vogeley, M. S. 2004, ApJ, 605, 1
- Gott, III, J. R., Miller, J., Thuan, T. X., et al. 1989, ApJ, 340, 625
- Gottlöber, S., Lokas, E. L., Klypin, A., & Hoffman, Y. 2003, MNRAS, 344, 715
- Gregory, S. A., & Thompson, L. A. 1978, ApJ, 222, 784
- Grogan, N. A., & Geller, M. J. 1999, AJ, 118, 2561
- . 2000, AJ, 119, 32
- Gunn, J. E., Carr, M., Rockosi, C., et al. 1998, AJ, 116, 3040
- Guseva, N., Papaderos, P., Meyer, H., Izotov, Y., & Fricke, K. 2009, A&A, 505, 63
- Henry, A., Martin, C. L., Finlator, K., & Dressler, A. 2013, ApJ, 769, 148
- Henry, R. B. C., Edmunds, M. G., & Köppen, J. 2000, ApJ, 541, 660
- Henry, R. B. C., Nava, A., & Prochaska, J. X. 2006, ApJ, 647, 984
- Hirschmann, M., De Lucia, G., Wilman, D., et al. 2014, MNRAS, 444, 2938
- Hoversten, E. A., & Glazebrook, K. 2008, ApJ, 675, 163
- Hoyle, F., Rojas, R. R., Vogeley, M. S., & Brinkmann, J. 2005, ApJ, 620, 618
- Hoyle, F., & Vogeley, M. S. 2002, ApJ, 566, 641
- Hoyle, F., Vogeley, M. S., & Pan, D. 2012, MNRAS, 426, 3041
- Hu, C.-Y., Naab, T., Walch, S., Glover, S. C. O., & Clark, P. C. 2016, MNRAS, 458, 3528

- Huchra, J. P., & Geller, M. J. 1982, *ApJ*, 257, 423
- Hughes, T. M., Cortese, L., Boselli, A., Gavazzi, G., & Davies, J. I. 2013, *A&A*, 550, A115
- Hwang, H. S., & Park, C. 2010, *ApJ*, 720, 522
- Izotov, Y. I., Stasińska, G., Meynet, G., Guseva, N. G., & Thuan, T. X. 2006, *A&A*, 448, 955
- Izotov, Y. I., & Thuan, T. X. 1999, *ApJ*, 511, 639
- Jones, M. G., Papastergis, E., Haynes, M. P., & Giovanelli, R. 2016, *MNRAS*, 457, 4393
- Jung, I., Lee, J., & Yi, S. K. 2014, *ApJ*, 794, 74
- Kauffmann, G., Heckman, T. M., White, S. D. M., et al. 2003, *MNRAS*, 341, 33
- Kennicutt, Jr., R. C., Bresolin, F., & Garnett, D. R. 2003, *ApJ*, 591, 801
- Kereš, D., Katz, N., Weinberg, D. H., & Davé, R. 2005, *MNRAS*, 363, 2
- Kewley, L. J., & Dopita, M. A. 2002, *ApJS*, 142, 35
- Kewley, L. J., & Ellison, S. L. 2008, *ApJ*, 681, 1183
- Kirshner, R. P., Oemler, Jr., A., Schechter, P. L., & Shectman, S. A. 1981, *ApJL*, 248, L57
- Kniazev, A. Y., Zijlstra, A. A., Grebel, E. K., et al. 2008, *MNRAS*, 388, 1667
- Kravtsov, A. 2009, in *Astronomical Society of the Pacific Conference Series*, Vol. 419, *Galaxy Evolution: Emerging Insights and Future Challenges*, ed. S. Jogee, I. Marinova, L. Hao, & G. A. Blanc, 283
- Kreckel, K., Croxall, K., Groves, B., van de Weygaert, R., & Pogge, R. W. 2015, *ApJL*, 798, L15
- Kreckel, K., Platen, E., Aragon-Calvo, M., et al. 2012, *AJ*, 144, 16
- Kroupa, P. 2001, *MNRAS*, 322, 231
- . 2002, *Science*, 295, 82
- Lackner, C. N., Cen, R., Ostriker, J. P., & Joung, M. R. 2012, *MNRAS*, 425, 641
- Lara-Lopez, M., Hopkins, A., Lopez-Sánchez, A., et al. 2013, *MNRAS*, 434, 451
- Lee, J. C., Salzer, J. J., & Melbourne, J. 2004, *ApJ*, 616, 752
- Lintott, C., Schawinski, K., Bamford, S., et al. 2011, *MNRAS*, 410, 166
- Lupton, R., Gunn, J. E., Ivezić, Z., Knapp, G. R., & Kent, S. 2001, in *Astronomical Society of the Pacific Conference Series*, Vol. 238, *Astronomical Data Analysis Software and Systems X*, ed. F. R. Harnden, Jr., F. A. Primini, & H. E. Payne, 269
- Luridiana, V., Morisset, C., & Shaw, R. A. 2015, *A&A*, 573, A42
- Mannucci, F., Cresci, G., Maiolino, R., Marconi, A., & Gnerucci, A. 2010, *MNRAS*, 408, 2115
- Marcolini, A., Brighenti, F., & D'Ercole, A. 2004, *MNRAS*, 352, 363
- Marino, R. A., Rosales-Ortega, F. F., Sánchez, S. F., et al. 2013, *A&A*, 559, A114
- Martin, D. C., Fanson, J., Schiminovich, D., et al. 2005, *ApJ*, 619, L1
- Martin, D. C., Wyder, T. K., Schiminovich, D., et al. 2007, *ApJSS*, 173, 342
- Matteucci, F. 1986, *MNRAS*, 221, 911

- Melioli, C., Brighenti, F., & D'Ercole, A. 2015, MNRAS, 446, 299
- Meurer, G. R., Wong, O. I., Kim, J. H., et al. 2009, ApJ, 695, 765
- Moorman, C. M., Moreno, J., White, A., et al. 2016, ApJ, 831, 118
- Moorman, C. M., Vogeley, M. S., Hoyle, F., et al. 2014, MNRAS, 444, 3559
- . 2015, ApJ, 810, 108
- Moran, S. M., Heckman, T. M., Kauffmann, G., et al. 2012, ApJ, 745, 66
- Morrissey, P., Conrow, T., Barlow, T. A., et al. 2007, ApJS, 173, 682
- Mouhcine, M., Baldry, I., & Bamford, S. 2007, MNRAS, 382, 801
- Muratov, A. L., Kereš, D., Faucher-Giguère, C.-A., et al. 2015, MNRAS, 454, 2691
- . 2017, MNRAS, 468, 4170
- Nava, A., Cassebeer, D., Henry, R. B. C., & Jevremovic, D. 2006, ApJ, 645, 1076
- Nicholls, D. C., Dopita, M. A., Sutherland, R. S., et al. 2014a, ApJ, 786, 155
- Nicholls, D. C., Jerjen, H., Dopita, M. A., & Basurah, H. 2014b, ApJ, 780, 88
- Osterbrock, D. E. 1989, *Astrophysics of Gaseous Nebulae and Active Galactic Nuclei* (Mill Valley, CA: University Science Books)
- Pan, D. C., Vogeley, M. S., Hoyle, F., Choi, Y.-Y., & Park, C. 2012, MNRAS, 421, 926
- Park, C., & Choi, Y.-Y. 2005, ApJ, 635, L29
- . 2009, ApJ, 691, 1828
- Park, C., Choi, Y.-Y., Vogeley, M. S., et al. 2007, ApJ, 658, 898
- Patiri, S. G., Prada, F., Holtzman, J., Klypin, A., & Betancort-Rijo, J. 2006, MNRAS, 372, 1710
- Pérez-Montero, E., & Contini, T. 2009, MNRAS, 398, 949
- Pérez-Montero, E., Contini, T., Lamareille, F., et al. 2013, A&A, 549, A25
- Pettini, M., & Pagel, B. E. 2004, MNRAS, 348, L59
- Pilyugin, L. S., Contini, T., & Vílchez, J. M. 2004, A&A, 423, 427
- Pilyugin, L. S., & Mattsson, L. 2011, MNRAS, 412, 1145
- Pilyugin, L. S., Mollá, M., Ferrini, F., & Vílchez, J. M. 2002, A&A, 383, 14
- Pilyugin, L. S., & Thuan, T. X. 2007, ApJ, 669, 299
- Pilyugin, L. S., Thuan, T. X., & Vílchez, J. M. 2006, MNRAS, 367, 1139
- Power, C., Wynn, G. A., Robotham, A. S. G., Lewis, G. F., & Wilkinson, M. I. 2014, ArXiv e-prints, arXiv:1406.7097
- Pustilnik, S. A. 2014, ArXiv e-prints, 1412.1316
- Pustilnik, S. A., Engels, D., Kniazev, A. Y., et al. 2006, AstL, 32, 228
- Pustilnik, S. A., Martin, J.-M., Lyamina, Y. A., & Kniazev, A. Y. 2013, MNRAS, 432, 2224
- Pustilnik, S. A., Martin, J.-M., Tepliakova, A. L., & Kniazev, A. Y. 2011a, MNRAS, 417, 1335

- Pustilnik, S. A., Tepliakova, A. L., & Kniazev, A. Y. 2011b, *Astrophysical Bulletin*, 66, 255
- Rojas, R. R., Vogeley, M. S., Hoyle, F., & Brinkmann, J. 2004, *ApJ*, 617, 50
- . 2005, *ApJ*, 624, 571
- Rupke, D. S. N., Veilleux, S., & Baker, A. J. 2008, *ApJ*, 674, 172
- Saintonge, A. 2007, PhD thesis, Cornell University
- Salim, S. 2014, *Serbian Astronomical Journal*, 189, 1
- Sánchez Almeida, J., Pérez-Montero, E., Morales-Luis, A. B., et al. 2016, *ApJ*, 819, 110
- Schawinski, K., Urry, C. M., Simmons, B. D., et al. 2014, *MNRAS*, 440, 889
- SDSS Collaboration, Albareti, F. D., Allende Prieto, C., et al. 2016, ArXiv e-prints, arXiv:1608.02013
- Shields, G. A., Skillman, E. D., & Kennicutt, Jr., R. C. 1991, *ApJ*, 371, 82
- Springel, V., White, S. D. M., Jenkins, A., et al. 2005, *Nature*, 435, 629
- Stasińska, G., Vale Asari, N., Cid Fernandes, R., et al. 2008, *MNRAS*, 391, L29
- Strateva, I., Željko Ivezić, Knapp, G. R., et al. 2001, *AJ*, 122, 1861
- Strauss, M. A., Weinberg, D. H., Lupton, R. H., et al. 2002, *AJ*, 124, 1810
- Sutter, P. M., Lavaux, G., Wandelt, B. D., et al. 2014, *MNRAS*, 442, 3127
- Thuan, T. X., Izotov, Y. I., & Lipovetsky, V. A. 1995, *ApJ*, 445, 108
- Tonnesen, S., & Cen, R. 2015, *ApJ*, 812, 104
- Tremonti, C. A., Heckman, T. M., Kauffmann, G., et al. 2004, *ApJ*, 613, 898
- van de Weygaert, R., & Platen, E. 2011, *IJMPS*, 1, 41
- van Zee, L., & Haynes, M. P. 2006, *ApJ*, 636, 214
- Vila Costas, M. B., & Edmunds, M. G. 1993, *MNRAS*, 265, 199
- von Benda-Beckmann, A. M., & Müller, V. 2008, *MNRAS*, 384, 1189
- Wilkinson, D. M., Maraston, C., Thomas, D., et al. 2015, *MNRAS*, 449, 328
- Wyder, T. K., Martin, D. C., Schiminovich, D., et al. 2007, *ApJSS*, 173, 293
- Xie, L., Gao, L., & Guo, Q. 2014, *MNRAS*, 441, 933
- Yin, S., Liang, Y., Hammer, F., et al. 2007, *A&A*, 462, 535
- York, D. G., Adelman, J., John E. Anderson, J., et al. 2000, *AJ*, 120, 1579

Appendix A: The physics of the Direct T_e method

The Direct T_e method is used to calculate the gas-phase chemical abundances (oxygen, nitrogen, etc. relative to hydrogen) in H II regions. It differs from other commonly-used methods by estimating the gas temperature and electron density of the region directly from the galaxy's spectrum. UV photons from young stars in an H II region keep the interstellar gas partially ionized. In an H II region, a photon with an energy $E_\gamma \gtrsim 13.6$ eV ionizes a hydrogen atom, producing an H^+ ion and an electron with some kinetic energy $K_{e^-} = E_\gamma - 13.6$ eV. As the free electron moves around in the gas, it loses some of its kinetic energy as it collisionally excites other ions in the gas. Because we are in a Strömgren sphere (an ionized region or an H II region), the cross-section for this electron scattering is much larger than the photoionization cross section, so the free electrons will thermalize quickly (De Robertis et al., 1987). Eventually, the free electron recombines with an H^+ ion, forming atomic hydrogen. The ions that are collisionally excited by the electron before its recombination eventually de-excite via forbidden transitions, emitting radiation that escapes the H II region.

In equilibrium, the total energy input into the gas via radiation from the star (that ionizes the hydrogen), $E_{\text{photoionization}}$, must be equal to the energy required to recombine the electron and the H^+ ion, $E_{\text{recombination}}$, and the energy radiated away from the H II region by the forbidden transitions, $E_{\text{radiation}}$. So

$$E_{\text{photoionization}} = E_{\text{recombination}} + E_{\text{radiation}} \quad (\text{A.1})$$

For radiative de-excitation to dominate over collisional de-excitation, the electron density $n_e \ll 10^{8-10} \text{ cm}^{-3}$ (De Robertis et al., 1987). Typical H II regions have an electron density $n_e \approx 100 \text{ cm}^{-3}$, so radiative de-excitation dominates; this is why we observe forbidden transitions in outer space but not here on Earth.

A.1 Forbidden transitions

Similar to a fingerprint, every element has a unique set of wavelengths seen in its spectrum that corresponds to the atom's different energy levels. Since electrons within an atom have discrete energy levels, transitions between levels result in either the emission (when decreasing in energy) or absorption (an increase in energy) of a photon of the same energy as the difference between the two levels. The separation between energy levels is unique for each element, so the photon energies either emitted or absorbed by each element are unique.

A.1.1 Time-dependent perturbation theory

A time-dependent potential is added to the Schrödinger equation in order to solve for the forbidden transition energies. We can assume that the time perturbation is a minor component of the potential and can thus treat it as a perturbation. For a simplified two-level system, the time-dependent wave function is

$$\Psi(t) = c_a(t)\psi_a e^{iE_a t/\hbar} + c_b(t)\psi(b)e^{-iE_b t/\hbar} \quad (\text{A.2})$$

To solve for the time-dependent coefficients, we substitute $\Psi(t)$ into the time-dependent Schrödinger equation

$$H\Psi = i\hbar \frac{\partial \Psi}{\partial t}, \quad \text{where } H = H^0 + H'(t) \quad (\text{A.3})$$

We find that

$$\dot{c}_a = -\frac{i}{\hbar} H'_{ab} e^{-i\omega_0 t} c_b \quad (\text{A.4})$$

$$\dot{c}_b = -\frac{i}{\hbar} H'_{ba} e^{-i\omega_0 t} c_a \quad (\text{A.5})$$

where

$$\omega_0 \equiv \frac{E_b - E_a}{\hbar} \quad (\text{A.6})$$

and

$$H_{ij} \equiv \langle \psi_i | H' | \psi_j \rangle \quad (\text{A.7})$$

The probability that transmission has occurred is $P_{b \rightarrow a} = |c_a(t)|^2$. The transmission rate $R_{a \rightarrow b} = dP/dt$.

For an electromagnetic wave, the atom experiences an oscillating electric field. For visible light, it is typically safe to assume that the spatial portion of the field does not change, since the wavelength is much longer than the size of the atom. However, if we consider a spatial variation of the field, we find that the true electric field is

$$\vec{E}(\vec{r}, t) = \vec{E}_0 \cos(\vec{k} \cdot \vec{r} - \omega t) \quad (\text{A.8})$$

Expanding this to first order, we find that

$$\vec{E}(\vec{r}, t) = \vec{E}_0 [\cos(\omega t) + (\vec{k} \cdot \vec{r} \sin(\omega t))] \quad (\text{A.9})$$

The first term in this approximation represents the electric dipole transitions (the canonical electron transitions). The second term leads to forbidden transitions (magnetic dipole and electric quadrupole).

A.2 Temperatures from the forbidden emission lines

Expanding the description in Sec. 2.2.2, we can define the ratio of the emission line strengths for [O III] $\lambda 4363$ and [O III] $\lambda\lambda 4959, 5007$ as

$$\frac{j_{4959} + j_{5007}}{j_{4363}} = \frac{\Omega(^3P, ^1D)}{\Omega(^3P, ^1S)} \left[\frac{A_{^1S, ^1D} + A_{^1S, ^3P}}{A_{^1S, ^1D}} \right] \frac{\bar{\nu}(^3P, ^1D)}{\nu(^1D, ^1S)} e^{\Delta E/kT} \quad (\text{A.10})$$

where

$$\bar{\nu}(^3P, ^1D) = \frac{A_{^1D_2, ^3P_2} \nu(\lambda 5007) + A_{^1D_2, ^3P_1} \nu(\lambda 4959)}{A_{^1D_2, ^3P_2} + A_{^1D_2, ^3P_1}} \quad (\text{A.11})$$

and j_λ is the emissivity of the emission line, $\Omega(i, j)$ is the collision strength between levels i and j , $A_{i,j}$ is the radiative transition probability between an upper level i and a lower level j , ν is the frequency of the transition, ΔE is the energy difference between the 1D_2 and 1S_0 levels, and T is

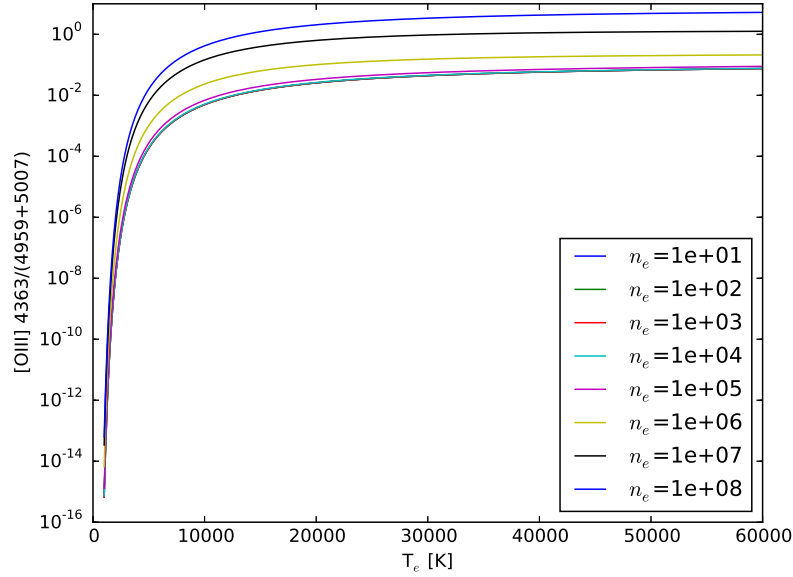


Figure A.1: The [O III] $\lambda 4363 / (\lambda 4959 + \lambda 5007)$ ratio as a function of temperature for various densities (Luridiana et al., 2015). Typical electron densities in H II regions are $\sim 100 \text{ cm}^{-3}$.

the electron temperature (Osterbrock, 1989). The transition probabilities $A_{i,j}$ do not depend on the temperature, but the collision strength $\Omega(i,j)$ is temperature-dependent. We can define

$$\bar{\nu}(^3\text{P}, ^1\text{D}) = \frac{A_{1\text{D}_2, ^3\text{P}_2}\nu(5007) + A_{1\text{D}_2, ^3\text{P}_1}\nu(4959)}{A_{1\text{D}_2, ^3\text{P}_2} + A_{1\text{D}_2, ^3\text{P}_1}} \quad (\text{A.12})$$

Inserting numerical values for the collision strengths and transition probabilities from Osterbrock (1989), the ratio becomes

$$\frac{j_{4959} + j_{5007}}{j_{4363}} = \frac{7.73 \exp[(3.29 \times 10^4)/T]}{1 + 4.5 \times 10^{-4}(N_e/T^{1/2})} \quad (\text{A.13})$$

Fig. A.1 shows how this ratio depends on the temperature. By measuring the flux of these emission lines, we can then solve for the temperature of the gas.

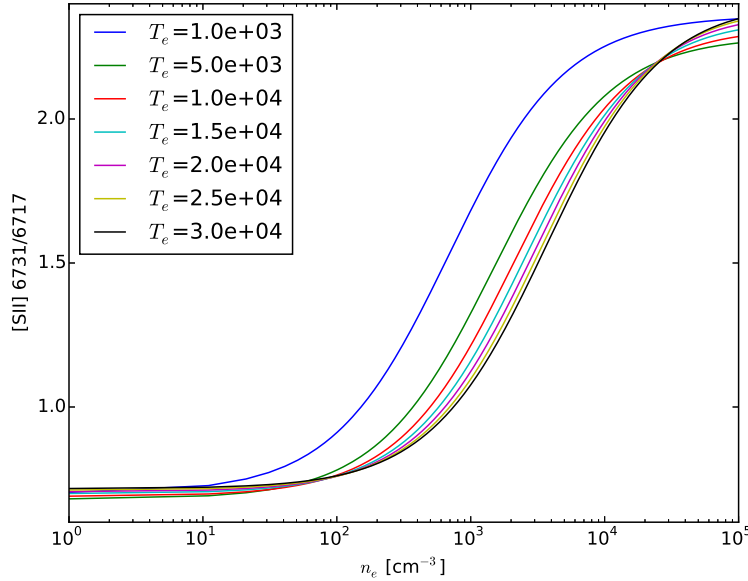


Figure A.2: The [S II] $\lambda 6731/\lambda 6717$ ratio as a function of density for various temperatures (Luridiana et al., 2015). The gas temperatures of H II regions are typically around 10^4 K.

A.3 [S II]

Similar to the sensitivity of the doubly-ionized oxygen ion transitions to the electron temperature of the surrounding gas, the transitions for singly-ionized sulfur are sensitive to electron number density. The relative excitation rates depend only on the ratio of the collision strengths when two emission lines (from the same ion) with nearly identical excitation energies are compared (Osterbrock, 1989). If the two levels have different transition probabilities and/or different collisional de-excitation rates, their ratio depends on the density.

The relative excitation rates of the two lines shown in Fig. 2.1 are proportional to their statistical weights; thus, the ratio of the line intensities is a constant in the low-density limit (Osterbrock, 1989). In the high-density regime, this ratio is best accurately described by a Boltzmann population ratio. There is a critical density for the energy levels which describes the turning point between these two extremes. A graphical representation of this ratio as a function of density can be seen in Fig. A.2. H II regions typically have densities well within the low-density regime, so we set the electron density for all our galaxies at 100 cm^{-3} .

Appendix B: Simulations of dwarf galaxy formation and evolution

Numerous simulations have been performed over the years in an attempt to understand the formation and evolution of our universe. As observers, it is important to connect our observations with the theory in order to grow our ideas about the universe.

B.1 Dwarf galaxy formation and evolution

It is impossible to directly observe the formation of a galaxy. Based on detected merging galaxies, the astronomical community has surmised that galaxies have increased their mass largely due to the merging of smaller galaxies. Λ CDM simulations of hierarchical galaxy formation by de Rossi et al. (2007) find that the growth of systems by aggregation is responsible for the mass-metallicity relation. Less massive systems tend to increase their stellar mass by either gas-rich mergers or secular evolution, resulting in a stronger correlation between stellar mass and metallicity. Evidence of this is seen in the mass-metallicity relation of Tremonti et al. (2004), where there is little relationship between stellar mass and the metallicity for massive systems, but at intermediate and lower masses the correlation is strong between the two quantities.

The inflow and outflow of gas in galaxies are aspects of galaxy evolution that are not yet well understood. This is especially important when studying dwarf galaxies, since their gravitational potential wells may be shallow enough to be strongly influenced by stellar winds and/or supernovae. Simulations by Marcolini et al. (2004) find that when ram pressure from the intergalactic medium (IGM) is comparable to the thermal pressure of the central interstellar medium (ISM), stripping and superwind influence each other and increase the gas removal rate. They find that the amount of metal-rich ejecta is sensitive to the ram pressure. Simulations by Power et al. (2014) and Melioli et al. (2015) show that supernovae contain sufficient energy to unbind the gas in a low mass halo. Hu et al. (2016) show that supernova-driven galactic outflows push metal-rich gas into the halo. A small fraction of the gas eventually escapes the halo, while most falls back onto the disc. This results in the

halo metallicity being about 20% higher than the disc metallicity. Likewise, Muratov et al. (2017) find that almost all metals produced in a Type II supernova are ejected from the galaxy. Unlike the supernovae, Melioli et al. (2015) finds that the ISM material does not have a strong likelihood of being expelled from a galaxy due to star formation. In contrast, Muratov et al. (2015) finds that a large portion of material is ejected in galactic outflows after a burst of star formation, which collects in the circumgalactic medium (CGM) and is sometimes recycled in later star formation episodes. In galaxies with $M_h < 10^{12} M_\odot$, a fraction of material is lost to the IGM.

Numerical simulations that study the properties of the ISM in an isolated, star-forming galaxy find that stellar feedback slowly increases the disc metallicity (Hu et al., 2016). The majority of outflows are enriched winds, which reduces the metallicity of the ISM. In dwarf galaxies at low redshifts, these outflows to the CGM are dominated by metal-poor gas (Muratov et al., 2017). While galaxies retain most of the metals they produce, a large fraction is in the CGM. By combining our observations with the results of these simulations, we can begin to understand how star formation and supernovae influence a dwarf galaxy's gas content.

B.2 Environmental differences of galaxy formation and evolution

Unlike the simulations described above, simulations which investigate the influence of the large-scale environment on the formation and evolution of galaxies have presented a more uniform picture. Simulations by Jung et al. (2014); Xie et al. (2014) and Tonnesen & Cen (2015) show that dark matter halos assembled later in underdense regions for a given halo mass. For central galaxies, Jung et al. (2014) and Tonnesen & Cen (2015) find that the ratio of stellar mass to halo mass is larger in overdense regions because star formation rates were higher in these denser regions.

Cen (2011) studied cosmic downsizing with high-resolution large-scale hydrodynamic galaxy formation simulations based on the Λ CDM cosmology. He finds that cosmic downsizing is part of a trend where the sSFR is a function of halo mass such that lower-mass galaxies have higher sSFRs. The formation of large halos (groups and clusters) and the large-scale structure causes cosmic gas to heat beyond a critical temperature at which the gas's entropy is too high to cool to continue feeding the galaxies and their star formation. As the surrounding gas in the dense regions becomes heated

beyond the critical limit, the sSFR of the affected galaxies decreases and the galaxies transition from the blue sequence to the red cloud. In the void environment, this heating does not occur, and so galaxies in the voids maintain a high sSFR in the present epoch. While this is the overall trend, there still exists some galaxies at $z = 0$ which have a high sSFR but reside in the more dense environments.

Vita

Kelly A. Douglass

EDUCATION

Drexel University Philadelphia, Pennsylvania USA

Ph.D., Physics, July 2017
M.S., Physics, June 2013

Cornell University Ithaca, New York USA

B.A., Physics, May 2011

PUBLICATIONS

- Douglass, K.A., Vogeley, M.S., & Cen, R. “Large-scale environmental dependence of chemical abundances in dwarf galaxies and implications for connecting star formation and halo mass”. submitted to ApJ, 2017
- Douglass, K.A. & Vogeley, M.S. “Large-scale environmental dependence of the abundance ratio of nitrogen to oxygen in blue, star-forming galaxies fainter than L_* ”. ApJ, 837: 42–55, 2017
- Douglass, K.A. & Vogeley, M.S. “Determining the large-scale environmental dependence of gas-phase metallicity in dwarf galaxies”. ApJ, 834: 186–198, 2017

AWARDS

- Drexel University College of Arts & Sciences Outstanding Dissertation Award, 2017
- AAS Chambliss Astronomy Achievement Student Award, 2014
- Drexel University Continuing Teaching Excellence Award, 2014
- Drexel University Teaching Excellence Award, 2013
- Drexel University Teaching Excellence Award — Highly Commended, 2012
- Drexel University Department of Physics First Year Graduate Student Award, 2012
- Drexel University College of Arts & Sciences Dean’s Scholarship, 2011–13

TEACHING EXPERIENCE

Teaching Assistant Physics 135: How Things Work, Drexel University

Teaching Assistant Physics 113, 114, 115: Contemporary Physics I, II, III, Drexel University

Teaching Assistant Physics 102, 201: Fundamentals of Physics II, III, Drexel University

Teaching Assistant Education T580: TA Orientation and Preparation, Drexel University

Teaching Assistant & Consultant Computer Science 1112: Introduction to MATLAB, Cornell University

Grader Honors 301: Special Theory of Relativity, Drexel University

Grader Physics 428: Quantum Mechanics III, Drexel University

PUBLIC OUTREACH

- Professor Bob’s Hands-On Science
- Volunteer at the Lynch Observatory

June 2015 to July 2017
September 2011 to June 2017

